Extraction of Heavy-Flavor Transport Coefficients in QCD Matter

R. Rapp*[1], P.B. Gossiaux*[2], A. Andronic*[3,4], R. Averbeck*[3], S. Masciocchi*[3], A. Beraudo[5], E. Bratkovskaya[3,6], P. Braun-Munzinger[3,7], S. Cao[8], A. Dainese[9], S.K. Das[10,11], M. Djordjevic[12], V. Greco[11,13], M. He[14], H. van Hees[6], G. Inghirami[3,6,15,16], O. Kaczmarek[17,18], Y.-J. Lee[19], J. Liao[20], S.Y.F. Liu[1], G. Moore[21], M. Nahrgang[2], J. Pawlowski[22], P. Petreczky[23], S. Plumari[11], F. Prino[5], S. Shi[20], T. Song[24], J. Stachel[7], I. Vitev[25], and X.-N. Wang[26,18]

[1] *Cyclotron Institute and Department of Physics and Astronomy, Texas A&M University, College Station, USA*
[2] *SUBATECH, IMT Atlantique, Université de Nantes, CNRS-IN2P3, Nantes, France*
[3] *Research Division and EMMI, GSI Helmholtzzentrum für Schwerionenforschung, Darmstadt, Germany*
[4] *Institut für Kernphysik, Westfälische Wilhelms-Universität Münster, Münster, Germany*
[5] *INFN, Sezione di Torino, Torino, Italy*
[6] *Institut für Theoretische Physik, J.W. Goethe-Universität, Frankfurt am Main, Germany*
[7] *Physikalisches Institut, Ruprecht-Karls-Universität Heidelberg, Heidelberg, Germany*
[8] *Department of Physics and Astronomy, Wayne State University, Detroit, USA*
[9] *INFN, Sezione di Padova, Padova, Italy*
[10] *School of Nuclear Science and Technology, Lanzhou University, Lanzhou, China*
[11] *Department of Physics and Astronomy, University of Catania, Italy*
[12] *Institute of Physics, University of Belgrade, Belgrade, Serbia*
[13] *Laboratori Nazionali del Sud, INFN-LNS, Catania, Italy*
[14] *Department of Applied Physics, Nanjing University of Science and Technology, Nanjing, China*
[15] *Frankfurt Institute for Advanced Studies, Frankfurt am Main, Germany*
[16] *J. von Neumann Institute for Computing, Jülich, Germany*
[17] *Fakultät für Physik, Universität Bielefeld, Bielefeld, Germany*
[18] *Key Laboratory of Quark and Lepton Physics and IPP, Central China Normal University, Wuhan, China*
[19] *Department of Physics, Massachusetts Institute of Technology, Cambridge, USA*
[20] *Department of Physics, Indiana University, Bloomington, USA*
[21] *Technische Universität Darmstadt, Darmstadt, Germany*
[22] *Institut für Theoretische Physik, Ruprecht-Karls-Universität Heidelberg, Heidelberg, Germany*
[23] *Physics Department, Brookhaven National Laboratory, Upton, USA*
[24] *Institut für Theoretische Physik, Universität Gießen, Gießen, Germany*
[25] *Theoretical Division, Los Alamos National Laboratory, Los Alamos, USA*
[26] *Nuclear Science Division, Lawrence Berkeley National Laboratory, Berkeley, USA*

September 17, 2018

*Editor

Abstract

We report on broadly based systematic investigations of the modeling components for open heavy-flavor diffusion and energy loss in strongly interacting matter in their application to heavy-flavor observables in high-energy heavy-ion collisions, conducted within an EMMI Rapid Reaction Task Force framework. Initial spectra including cold-nuclear-matter effects, a wide variety of space-time evolution models, heavy-flavor transport coefficients, and hadronization mechanisms are scrutinized in an effort to quantify pertinent uncertainties in the calculations of nuclear modification factors and elliptic flow of open heavy-flavor particles. We develop procedures for error assessments and criteria for common model components to improve quantitative estimates for the (low-momentum) heavy-flavor diffusion coefficient as a long-wavelength characteristic of QCD matter as a function of temperature, and for energy loss coefficients of high-momentum heavy-flavor particles.
arxiv: 1803.03824 [nucl-th]

Task Force Formation and Acknowledgment:

The article presents calculations done in the context of the Heavy-Flavor EMMI RRTF effort, as agreed among the participants. The publication is signed by the people who actively participated in the RRTF meetings and by those who contributed explicitly to the follow-up activities leading to this article. We acknowledge that the results presented here would not have been possible without the work by all authors of the models and computation approaches utilized in this comparison. Therefore we explicitly thank all colleagues who contributed to the creation of the different models, independently from the RRTF effort; these are, in alphabetical order of the model acronyms: Catania: F. Scardina; CUJET: M. Gyulassy and J. Xu; Duke: S.A. Bass and Y. Xu; LBL/CCNU: G.-Y. Qin and T. Luo; Nantes: J. Aichelin and K. Werner; PHSD: H. Berrehrah, D. Cabrera, W. Cassing, L. Tolos and J.M. Torres-Rincon; POWLANG: A. De Pace, M. Monteno and M. Nardi; TAMU: R.J. Fries, K. Huggins and F. Riek; UrQMD: M. Bleicher, T. Lang and J. Steinheimer.

We also thank Z. Conesa del Valle for providing the software used to compare D meson cross sections with FONLL, G.E. Bruno for providing the calculation of the c- quark R_{AA} with FONLL+EPPS16, and C. Shen for information on the OSU hydro code; we also thank E. Bruna, C. Greiner, and J. Bielcik for discussions in the early stages of the task force activities.

Contents

1 Introduction **5**

2 Initial Heavy-Flavor Spectra **8**
- 2.1 Baseline for p_t distributions of c quarks and fragmentation functions to D mesons . . . 8
- 2.2 Cold Nuclear Matter Effects . . . 12
- 2.3 Exploration of Uncertainty on $R_{\rm AA}$ and v_2 in Pb-Pb(2.76 TeV) . . . 14

3 Bulk Evolution Models **17**
- 3.1 Bulk Comparisons . . . 18
- 3.2 Charm-Quark Spectra with Common Transport Coefficient . . . 21

4 Hadronization **24**
- 4.1 Comparison of D-Meson Spectra from Common Transport Coefficients . . . 25
- 4.2 Recombination in Thermal Medium . . . 29
- 4.3 In-Medium Fragmentation . . . 31

5 Transport Coefficients and Implementation **33**
- 5.1 Comparison of Existing Coefficients . . . 33
- 5.2 Different Transport Coefficients in a Common Hydrodynamic Medium . . . 35
- 5.3 Perturbative Analysis . . . 37
- 5.4 Functional Renormalization Group . . . 38
- 5.5 Information and Constraints from Lattice QCD . . . 39
  - 5.5.1 Heavy-quark diffusion coefficient . . . 39
  - 5.5.2 Charm fluctuations and correlations and charm degrees of freedom in hot matter 41
  - 5.5.3 Charm meson correlators . . . 42
- 5.6 Boltzmann vs. Langevin . . . 43
  - 5.6.1 Fokker-Planck and Boltzmann transport equations . . . 43
  - 5.6.2 Numerical Results Comparing Boltzmann and Langevin Simulations . . . 44

6 High-p_T Energy Loss and $\hat{q}$ **47**
- 6.1 Transverse momentum broadening and QGP properties . . . 47
- 6.2 Energy dependence of the transport coefficient . . . 49
- 6.3 Dynamical energy loss formalism . . . 49
- 6.4 Next-to-leading order calculation of heavy-flavor spectra in heavy-ion collisions . . . 52
- 6.5 Reference Results in an Infinite and Finite QGP . . . 56

7 Summary and Perspectives **60**

A Overview of Model Approaches Employed in this Work **64**

1 Introduction

The characterization of the properties of matter can be carried out at various levels, utilizing different ways of testing its response to external excitations. Bulk properties are encoded in the equation of state, $\epsilon(P)$, which characterizes how a system responds to changes in its pressure. Transport coefficients characterize how small perturbations from equilibrium, often associated with conserved quantities, are transmitted through the medium. In quantum field theory, transport coefficients can be formulated as the zero-energy and long-wavelength limit of correlation functions. This, in particular, allows to establish connections between microscopic calculations of spectral (or correlation) functions and their underlying transport coefficients.

High-energy collisions of atomic nuclei have revealed remarkable properties of strongly interacting matter at high temperature. For example, the ratio of shear viscosity to the entropy density, η/s, of the medium has been inferred to be the smallest of any known substance [1]. However, the extraction of this quantity, including its temperature dependence, from fitting viscous hydrodynamic simulations of the fireball to final-state hadron spectra, is rather indirect, involving the entire system evolution. Progress has been made in controlling basic features of the fireball evolution [2], but significant uncertainties persist, *e.g.*, in the initial conditions and pre-equilibrium evolution of the quark-gluon plasma (QGP). Furthermore, the microscopic origin of the small η/s, *i.e.*, how it emerges from the fundamental interactions of Quantum Chromodynamics (QCD) in the medium, remains a central question that calls for additional observables and methods. In particular, non-monotonic features of transport coefficients in the vicinity of the (pseudo-) critical transition temperature are of key relevance to our understanding of the phase structure of QCD.

The diffusion of heavy quarks in QCD matter at not too high temperatures has long been recognized as a promising concept and phenomenological tool to diagnose the medium produced in heavy-ion collisions (HICs) [3]. The basic realization is that the heavy-quark (HQ) mass, m_Q, is parametrically large compared to the scales that characterize the QCD medium produced in experiment, *i.e.*, its typical temperature, including the pseudo-critical transition temperature, $T_{\rm pc}$, which is ultimately related to the QCD scale parameter, $\Lambda_{\rm QCD}$ and, to a lesser extent, to the precise values of the light-quark masses. This realization entails a sequence of benefits, both phenomenologically and theoretically, for using heavy-flavor (HF) particles as a probe of the medium, namely that (a) the production of heavy quarks is reasonably well controlled as a hard initial-state process, (b) the propagation of HF particles through the medium is, at low momenta, of a diffusive "Brownian motion" type and thus characterized by well-defined transport coefficients, most notably the spatial diffusion coefficient $\mathcal{D}_s$, (c) heavy quarks can remain good quasi-particles (*i.e.*, their collisional width is much smaller than their energy, $\Gamma_Q \ll E_Q$) in a QGP with large interaction strength where light partons are already dissolved (*i.e.*, their widths are comparable or larger then their energies, $\Gamma_q \gtrsim E_q$); (d) the ''identity" of heavy quarks is preserved in the hadronization process thus providing tests of it's microscopic mechanisms, (e) interactions of low-momentum heavy quarks with the medium are of potential-type, *i.e.*, elastic collisions with small energy transfer. Furthermore, the thermalization time of heavy quarks is delayed relative to the light partons of the bulk medium, parametrically by a factor of order $\sim M_Q/T$, which renders it comparable to the lifetime of the QGP fireballs in HICs. Thus, HF particles are not expected to fully thermalize and therefore preserve a memory of their interaction history which can serve as a gauge of their interaction strength with the medium. The HF diffusion coefficient, $\mathcal{D}_s$, arguably provides

the most direct window on the in-medium QCD force in HICs, and thus on the coupling strength of the medium. To the extent that the same in-medium interactions are operative in the transport of different quantities, *e.g.*, energy-momentum or electric charge, one expects the pertinent transport coefficients, scaled to dimensionless units, to relate to each other, *e.g.*, $\eta/s \sim \mathcal{D}_s(2\pi T) \sim \sigma_{\rm EM}/T$ (where $\sigma_{\rm EM}$ denotes the electric conductivity).

At high momentum HQ production in heavy-ion collisions can be understood as a part of the in-medium parton shower evolution. The large HQ mass affects the splitting functions which encode the many-body physics of parton branching in the QGP, including the suppression of forward radiation and interference effects. The HQ soft-gluon emission energy loss limit, extensively used in jet quenching phenomenology, is connected to the general high-energy parton shower picture. The scale separation $T \ll M_Q \ll E$ allows for the use of heavy quarks as independent probes of, *e.g.*, the Debye screening mass (m_D) or the parton mean-free-path (λ), encoded in transport parameters such as $\hat{q} \sim m_D^2/\lambda$.

Over the last decade, open HF observables, *i.e.*, transverse-momentum (p_T) spectra and elliptic flow (v_2) of particles containing a single charm (c) or bottom (b) quark (or their decay products), have much advanced and are now at the verge of becoming a precision probe of QCD matter. This has triggered intense theoretical activity aimed at understanding the intriguing experimental results on how HF spectra are modified when going from elementary proton-proton collisions to reactions with heavy nuclei, see, *e.g.*, Refs. [4–6] for recent reviews. The modeling efforts have reached a critical stage. Several approaches have accomplished a qualitative or semi-quantitative agreement with (some of the) existing data, but it seems fair to say that no single approach is yet able to quantitatively describe all available HF measurements from the Relativistic Heavy-Ion Collider (RHIC) and the Large Hadron Collider (LHC), from low to high p_T. At the same time, a fundamental understanding of the underlying processes employed in the phenomenological modeling efforts requires the latter to be firmly rooted in QCD. The complexity of the problem likely involves different prevalent mechanisms not only as a function of p_T (*e.g.*, collisional vs. radiative and/or perturbative vs. non-perturbative interactions), but also as a function of temperature. In addition, the accuracy of the information extracted from HF observables also hinges on a realistic space-time evolution for the bulk medium, *e.g.*, hydrodynamic or transport models, as well as initial conditions for the HQ spectra, presumably modified by "cold-nuclear-matter" (CNM) effects in the incoming nuclei prior to the collision. Indeed, the individual models currently in use employ rather different ingredients for each of the modeling components, including a varying degree of fit parameters (*e.g.*, K factors for the transport coefficients). At this point, it becomes compelling to go beyond incremental improvements of individual approaches and launch a broader effort supported by active researchers in the field. For this purpose an EMMI Rapid Reaction Task Force was initiated, approved and formed, and two onsite meetings convened at GSI Darmstadt (Germany) in July and December of 2016 [7]. The key open questions and objectives in the open HF problem that were identified and addressed during the meeting are:

1) How do the conceptual underpinnings of the current theoretical models compare and constrain their applicability in various regions of phase space and temperature? Do these uncertainties provide a sufficiently robust basis for systematic uncertainty evaluations of the extracted transport coefficients? Can quantitative connections to jet quenching in the light-flavor sector be made?

2) What is the impact of the available implementations of hadronization, in particular HQ coales-

cence, on D-meson spectra, and how can they be seamlessly connected to the QGP and hadronic diffusion processes?

3) What are the benefits and limitations for Boltzmann vs. Langevin implementations of the HF transport in an evolving medium?

4) What is the role of the different medium evolution models, and how do different predictions for the temperature- and momentum-dependent transport coefficients in current model calculations manifest themselves in observables?

5) What are future precision requirements on existing observables, and are there other ways to analyze data (new observables), to improve current accuracies, and to what extent? In particular, in what ways are the upcoming data from RHIC and the LHC instrumental in extending our knowledge of deconfined matter?

The present effort is a first step in these directions by scrutinizing the different components in the modeling efforts of various research groups and performing targeted calculations to unravel, and ultimately quantify, how pertinent uncertainties impact the extraction of HF transport coefficients. This document is organized as follows. In Sec. 2, we start by developing a common baseline for the initial HQ and D-meson transverse-momentum spectra from pp collisions, explore uncertainties in the implementation of CNM effects and suggest a standardized approach to account for them. In Sec. 3 we investigate the role of bulk evolution models, by evaluating the outcomes for the nuclear modification factor and elliptic flow of charm quarks in Pb-Pb(2.76 TeV) collisions by using a common pre-defined HQ interaction in the QGP within various hydrodynamic and transport simulations as used in current phenomenological applications. In Sec. 4 we study the differences in the treatment of HQ hadronization, in particular different schemes of HQ recombination with light partons in the quark-hadron transition of the bulk medium, as well as fragmentation mechanisms. In Sec. 5 we focus on the interactions of heavy quarks at low and intermediate momenta in the QGP and their transport implementation; transport coefficients as used by different groups are scrutinized, a publicly accessible repository of transport coefficients [8] is provided, the outcome of different charm-quark transport coefficients from Langevin simulations in a common hydrodynamic evolution is studied, insights from perturbative QCD (pQCD) and lattice QCD (lQCD) are discussed and put into context, and two common schemes (Boltzmann and Fokker-Planck Langevin) for implementing HF transport into bulk evolution models are compared. In Sec. 6 the transport of high-momentum heavy quarks is discussed, starting with basic definitions of momentum broadening and the pertinent transport coefficient ($\hat{q}$), its dependence on jet energy, dynamical effects in energy loss, next-to-leading order calculations and the problem of non-locality in radiative processes. A summary with an outlook for future developments is given in Sec. 7.

Concerning notation, we will use $Q = c, b$ as a generic for the heavy quarks charm and bottom, $q = u, d, s$ for light quarks, p_t for quark and p_T for hadron transverse-momenta. A listing of the model approaches involved in the studies reported in the following is given in App. A.

2 Initial Heavy-Flavor Spectra

2.1 Baseline for p_t distributions of c quarks and fragmentation functions to D mesons

In this section we describe the construction of a common baseline for the initial p_t-differential cross sections of c quarks which are required as an input to simulations for their transport through a QGP formed in ultrarelativistic heavy-ion collisions (we will use the notation p_t and p_T for quark and hadron transverse momenta, respectively). The initial p_t spectra will be based on FONLL calculations [9, 10] and will be supplemented by fragmentation functions to D mesons based on the BCFY framework [11], also used by the FONLL authors, to enable quantitative constraints from experimental measurements in proton-proton (pp) collisions and also to serve as a baseline for hadronization (at least at high p_t) in the heavy-ion environment. A common baseline for the input to transport calculations will reduce uncertainties in the comparison of results obtained with various transport for heavy-ion observables such as the nuclear modification factor, R_{AA}, and elliptic flow, v_2, of heavy-flavor (HF) particles (or their decay products). Indeed, different shapes of the initial p_t distribution lead to different values of R_{AA} and v_2 for the same QGP parameters (energy loss or diffusion coefficients), as will be discussed in Sec. 2.3. This can be easily seen for the simple case of a power-law p_t distribution $\propto 1/p_t^n$ and constant energy loss ΔE, giving a quark-level $R_{AA} \sim p_t^n/(p_t + \Delta E)^n$, which clearly depends on n. In the same way, different fragmentation functions can lead to different values for the hadron-level $R_{AA}(p_T)$ for the same quark-level $R_{AA}(p_t)$. Similar arguments apply for v_2.

Fixed-Order Next-to-Leading-Log (FONLL) calculations are widely used to obtain the initial heavy-quark (HQ) p_t-differential cross sections that serve as an input for the transport and energy loss models. This is a perturbative-QCD (pQCD) calculation in which the HQ production cross section, also denoted as partonic cross section $\hat{\sigma}$, is obtained through an expansion in powers of the strong coupling constant, α_s. In particular, in FONLL the partonic cross section is calculated to next-to-leading order (NLO) in α_s (with the terms proportional to α_s^2 and α_s^3) and with an all-order resummation of logarithms of p_t/m_Q, where p_t and m_Q are the HQ transverse momentum and mass, respectively. The HF hadron cross section is factorized as a convolution of the parton distribution functions (PDFs) of the incoming partons, of the partonic cross sections and of a nonperturbative fragmentation function that encodes the probability for a heavy quark with momentum p to fragment into a HF hadron with momentum $z \cdot p$, with $0 < z < 1$. FONLL uses the collinear factorization scheme, in which the factorization variable is related to the squared momentum transfer in the hard process, Q^2. In particular, the PDFs, the partonic cross section and the fragmentation function are evaluated at the same scale μ_F (factorization scale), which is taken to be proportional to the transverse mass of the produced heavy quark $\mu_0 = \sqrt{m_Q^2 + p_t^2}$. The strong coupling constant α_s is evaluated at the renormalization scale, μ_R, also taken to be proportional to μ_0. The central values of the perturbative scales are taken as $\mu_F = \mu_R = \mu_0$. The uncertainties of the c-quark cross section are estimated using three values of m_c, 1.3, 1.5 and 1.7 GeV/c^2, and, for the central value of m_c, seven sets of values of μ_F and μ_R defined by $(\mu_F/\mu_0, \mu_R/\mu_0) = (1,1)$, (0.5,0.5), (0.5,1), (1,0.5), (2,2), (1,2), (2,1). The bands defined by the envelope of the minimum and maximum cross sections obtained from the mass variation and from the scale variations are summed in quadrature. In addition, the envelope obtained by varying the PDFs within their uncertainties is also added in quadrature. The PDF set used in recent FONLL calculations is CTEQ6.6 [12].

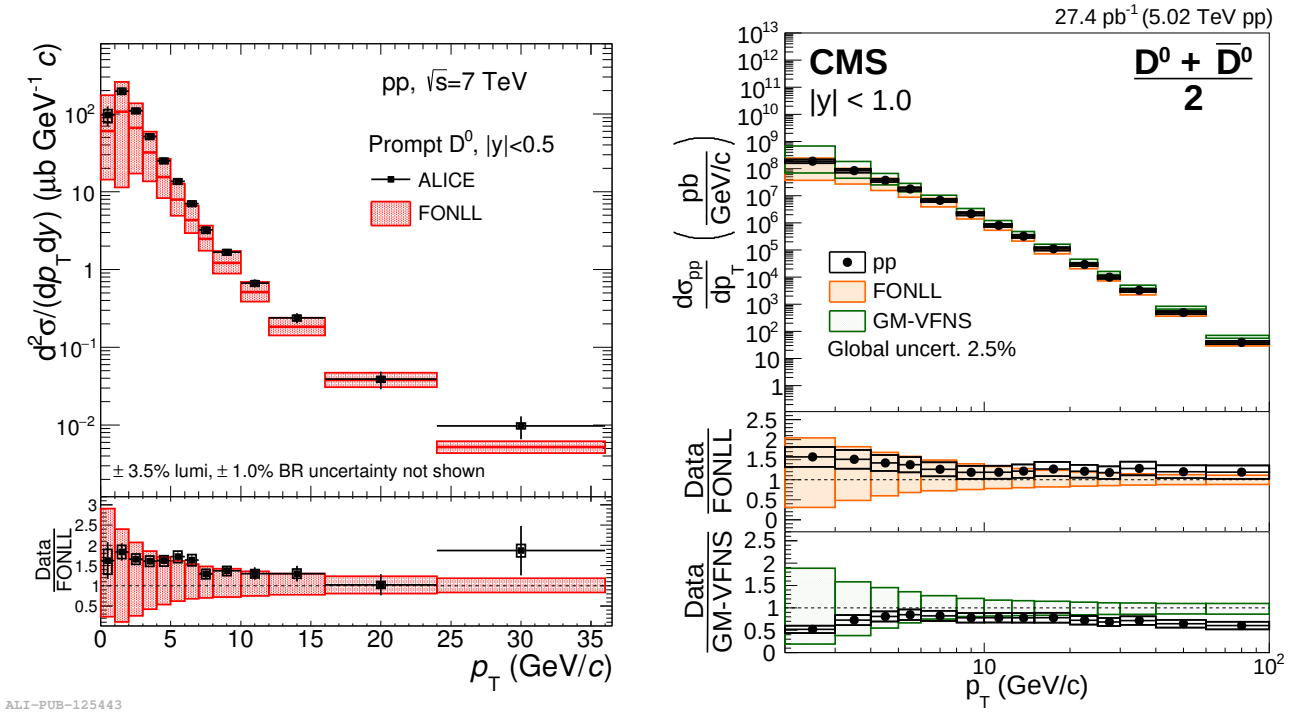

Figure 1: Cross sections for D^0 meson production at central rapidity in pp collisions at $\sqrt{s} = 7$ and 5.02 TeV, measured by ALICE [13] and CMS [14], respectively, compared with the FONLL and GM-VFNS calculations.

The FONLL calculation provides a good description of the production cross sections of D and B mesons in pp (and $p\bar{p}$) collisions at center-of-mass energies from 0.2 to 13 TeV over a wide p_T range at both central and forward rapidities (see, *e.g.*Ref. [5] and references therein). In the case of D-meson production, two general observations can be made, which are clearly illustrated by the D^0-meson cross sections at $\sqrt{s} = 7$ TeV and 5.02 TeV measured by ALICE [13] and CMS [14], respectively, and shown in Fig. 1:

- the central value of the FONLL calculation ($m_c = 1.5$ GeV/c^2, $\mu_F = \mu_R = \mu_0$) yields spectra that lie below the experimental data, and the ratio data/FONLL depends on p_T, increasing a bit towards low p_T; therefore, the central value of FONLL does not provide an optimal description of the shape of the p_T distribution of D mesons (we recall that it is the shape of the p_T distribution that affects R_{AA} and v_2);

- the uncertainties of the theoretical calculation, dominated by the perturbative scale setting, are significantly larger than the experimental ones [13–24], especially for transverse momenta smaller than 10-15 GeV/c; therefore, considering the total FONLL uncertainties is not the best approach.

We therefore choose to define the baseline p_t distribution using the FONLL cross section that best describes the shape of the D^0 cross sections at both energies, $\sqrt{s} = 5$ TeV and 7 TeV (shown in Fig. 1), among the nine FONLL cross section obtained by the aforementioned seven scale sets and three m_c values. The uncertainty introduced by the choice of the p_T shape can be studied by using the two FONLL cross sections that span the maximum shape variation but are still consistent with the shape

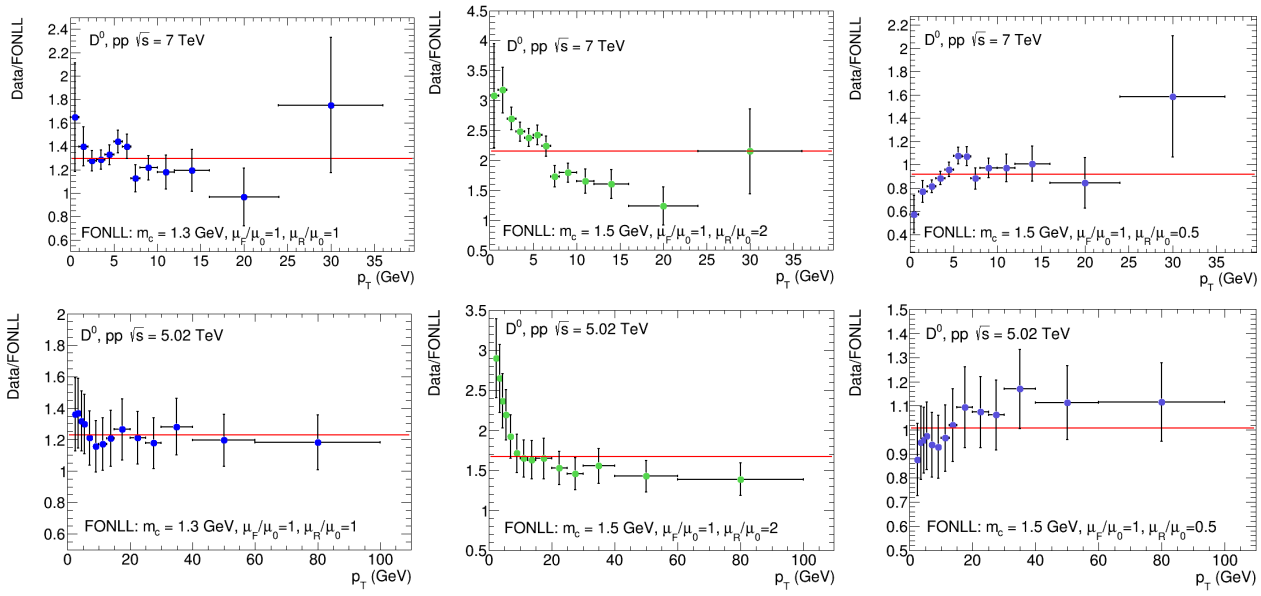

Figure 2: Ratios of the cross sections for D^0 meson production at central rapidity in pp collisions at $\sqrt{s} = 7$ (upper rows) and 5.02 TeV (lower rows), measured by ALICE [13] and CMS [14], respectively, with FONLL cross sections for the best-fitting (left) and the two extreme parameter sets (central and right).

of the data. We propose to use the cross sections with these three sets of parameters for all LHC energies, in particular $\sqrt{s_{NN}} = 2.76$ and 5.02 TeV for Pb–Pb collisions. We did not use pp data at $\sqrt{s} = 2.76$ TeV, because the available D-meson cross section measurements at this energy at central rapidity [19] have much larger experimental uncertainties than the data at the higher energies.

More concretely, we adopt the following procedure.

1. For the two energies, $\sqrt{s} = 5.02$ and 7 TeV, we constructed a ratio data/FONLL for each of the nine parameter sets. The uncertainties on this ratio are the uncertainties of the ALICE and CMS data, were we removed the global uncertainties that do not change the shape of the cross section.

2. We fitted each ratio with a constant.

3. We defined the 'best-fitting' FONLL cross section as the one having the minimum value of $(\chi^2/ndf)_{5.02\,\mathrm{TeV}} + (\chi^2/ndf)_{7\,\mathrm{TeV}}$ and the two 'extreme' cross sections as those with opposite slope in the data/FONLL ratio, largest values of the χ^2 sum, but both $(\chi^2/ndf)_{5.02\,\mathrm{TeV}}$ and $(\chi^2/ndf)_{7\,\mathrm{TeV}}$ smaller than 2.

The resulting cross sections are:

- 'best fitting' set: $m_c = 1.3$ GeV/c^2, $\mu_F = \mu_R = \mu_0$, with $(\chi^2/ndf)_{5.02\,\mathrm{TeV}} = 0.13$ and fitted constant value of 1.23 ± 0.05 at 5.02 TeV, $(\chi^2/ndf)_{7\,\mathrm{TeV}} = 0.88$ and fitted constant value of 1.29 ± 0.03 at 7 TeV;

- 'extreme' sets: $m_c = 1.5$ GeV/c^2, $\mu_F = \mu_0$, $\mu_R = 0.5\,\mu_0$ and $m_c = 1.5$ GeV/c^2, $\mu_F = \mu_0$, $\mu_R = 2\,\mu_0$.

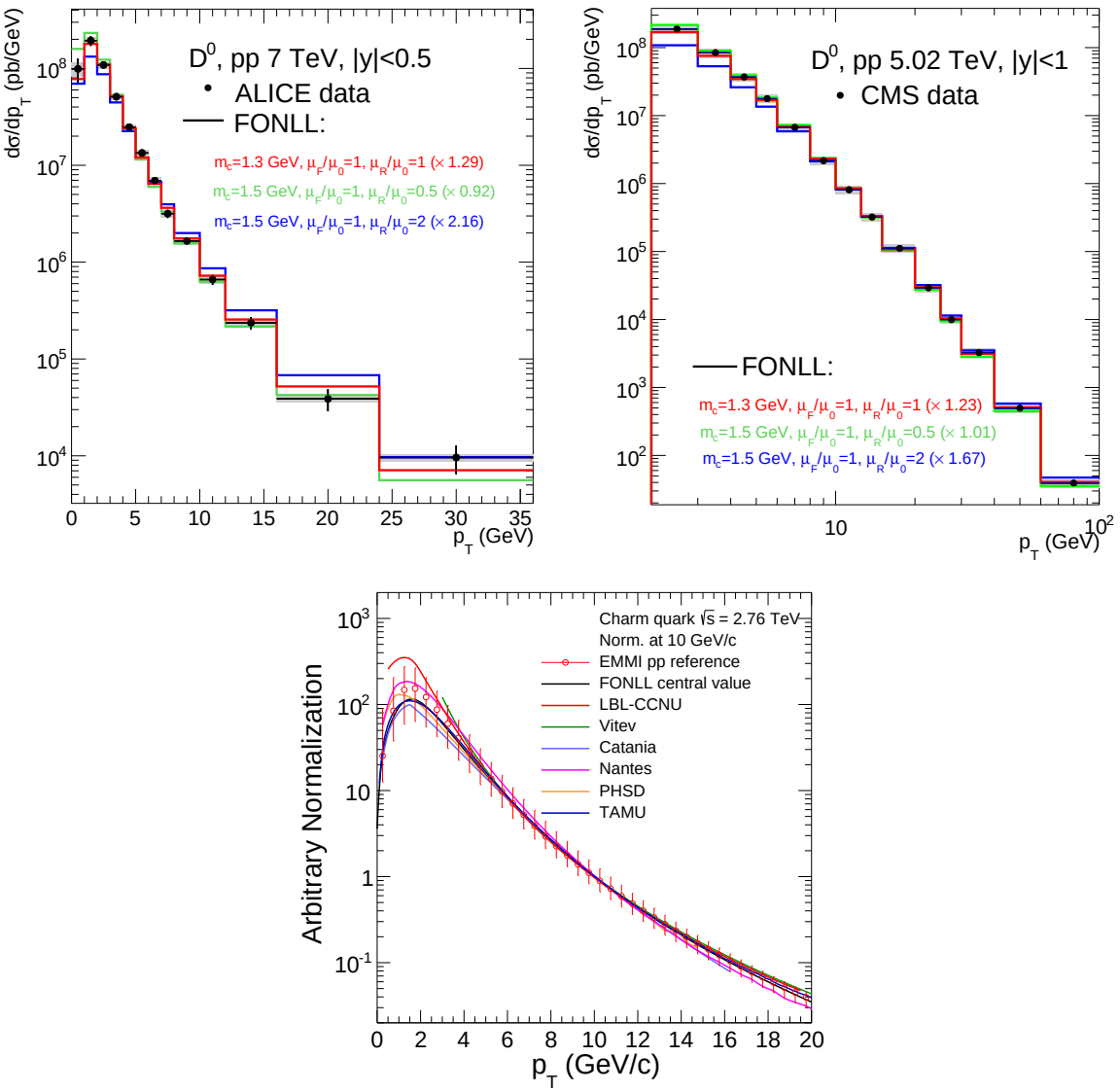

Figure 3: Top-left: cross section for D^0-meson production at central rapidity in pp collisions at $\sqrt{s}$ = 7 TeV, measured by ALICE [13], compared with the best-fitting and extreme FONLL cross sections scaled to match the data. Top-right: cross section for D^0-meson production at central rapidity in pp collisions at $\sqrt{s}$ = 5.02 TeV, measured by CMS [14], compared with the best-fitting and extreme FONLL cross sections scaled to match the data. Lower panel: our proposed reference for the shape of the c-quark p_t distribution in pp collisions at $\sqrt{s}$ = 2.76 TeV, compared with those used in some of the heavy-ion models; to readily compare their shapes, all curves are normalized to p_t=10 GeV.

The best-fitting cross section uses the minimum value of m_c (1.3 GeV/c^2), which is consistent with the fact that for m_c = 1.5 GeV/c^2 the ratio data/FONLL increases at low p_T, where the value of the quark mass has the largest influence on the cross section, and a smaller mass value increases the cross section. The sets with the largest χ^2/ndf values (up to 4-5) are those with $\mu_F = 0.5\,\mu_0$.

Figure 2 shows the data/FONLL ratios and fits for the best-fitting (left) and extreme sets (center and right), at 7 (upper row) and 5.02 TeV (lower row). Figure 3 (upper panels) shows the comparison of the three cross sections, scaled by the fitted constants, with the data at $\sqrt{s}$ = 7 and 5.02 TeV. The

lower panel of the same figure compares our proposed reference for c quarks at $\sqrt{s} = 2.76$ TeV with those used as initial conditions in several transport calculations in heavy-ion collisions.

The FONLL c-quark p_t-differential cross sections, $d\sigma/dp_t$, integrated over $|y| < 1$ for the three parameters sets at $\sqrt{s} = 2.76$ and 5.02 TeV, are provided in an online repository [8]. For the Pb-Pb input p_t distributions, these cross sections can be multiplied by a nuclear modification factor R_{AA} for c quarks obtained from nuclear shadowing according to the EPS09NLO PDF modifications [25], which is discussed in more detail in the following section.

In order to obtain the D-meson p_T distributions, c quarks are fragmented using the BCFY function [11] to convert them into pseudoscalar ($D_{Q\to P}(z)$) and vector ($D_{Q\to V}(z)$) mesons:

$$\begin{aligned} D_{Q\to P}(z) &= N\,\frac{rz(1-z)^2}{(1-(1-r)z)^6}\left[6-18(1-2r)z+(21-74r+68r^2)z^2\right. \\ &\quad \left.-2(1-r)(6-19r+18r^2)z^3+3(1-r)^2(1-2r+2r^2)z^4\right]\,, \qquad (1) \\ D_{Q\to V}(z) &= 3N\,\frac{rz(1-z)^2}{(1-(1-r)z)^6}\left[2-2(3-2r)z+3(3-2r+4r^2)z^2\right. \\ &\quad \left.-2(1-r)(4-r+2r^2)z^3+(1-r)^2(3-2r+2r^2)z^4\right]\,. \qquad (2) \end{aligned}$$

These functions are the same as used in FONLL calculations. The only parameter (apart from the normalization N) is r, which can be set to the same values used in FONLL, which were obtained by fitting the analytical forms reported above to the $D^\star$ fragmentation function measured by ALEPH (see Ref. [26] for details). The resulting values are $r = 0.06$ for $m_c = 1.3$ GeV/c^2, which is the mass used for the best-fitting cross section, and $r = 0.10$ for $m_c = 1.5$ GeV/c^2. These functions should be used for both the Pb-Pb spectra (when considering independent fragmentation outside the QGP), *i.e.*, the numerator of the R_{AA}, and the pp spectra figuring into the denominator of the R_{AA}.

2.2 Cold Nuclear Matter Effects

Cold-nuclear-matter (CNM) effects modify the yields and kinematic distributions of hadrons produced in hard scattering processes in the case of pA and AA collisions, see, *e.g.*, Refs. [27, 28] for recent analyses at the LHC. The largest CNM effect at LHC energies is the nuclear modification of parton distribution functions, *i.e.*, the fact that the PDFs of nucleons within nuclei are different from the PDFs of free protons. We report the expected effects using the EPS09NLO [25] and EPPS16 [29] parameterizations of the nuclear PDF modifications, which both depend on x, Q^2 and the mass number A, and are defined as $R_i^A(x,Q^2) = f_i^A(x,Q^2)/f_i^p(x,Q^2)$, where i denotes the parton type (gluon, valence quark or sea quark) and f^A, f^p are the PDFs of the nucleon in a nucleus of mass A and of the free proton, respectively. The features of the modifications that are most relevant for HQ production up to momenta of a few tens of GeV/c are the reduction of R_i^A below unity for x lower than about $3\cdot10^{-2}$, namely nuclear shadowing, and the increase above unity for $x > 3\cdot10^{-2}$, namely anti-shadowing. These modifications are larger for small values of Q^2.

Figure 4 shows the CNM modification of R_{AA} for the c-quark p_t distribution in Pb-Pb collisions at LHC energies. The upper panels show the results for $\sqrt{s_{NN}} = 2.76$ and 5.02 TeV as obtained with the HVQMNR NLO calculation [30], the CTEQ6M PDFs [12] and the EPS09NLO nuclear modification. The lower panel shows the result for $\sqrt{s_{NN}} = 5.02$ TeV as obtained with the FONLL calculation [9, 10], the CTEQ10 PDFs [31] and the EPPS16 nuclear modification. The uncertainty bands are obtained according to the EPS09 and EPPS16 prescriptions, thus representing the uncertainty on the nuclear

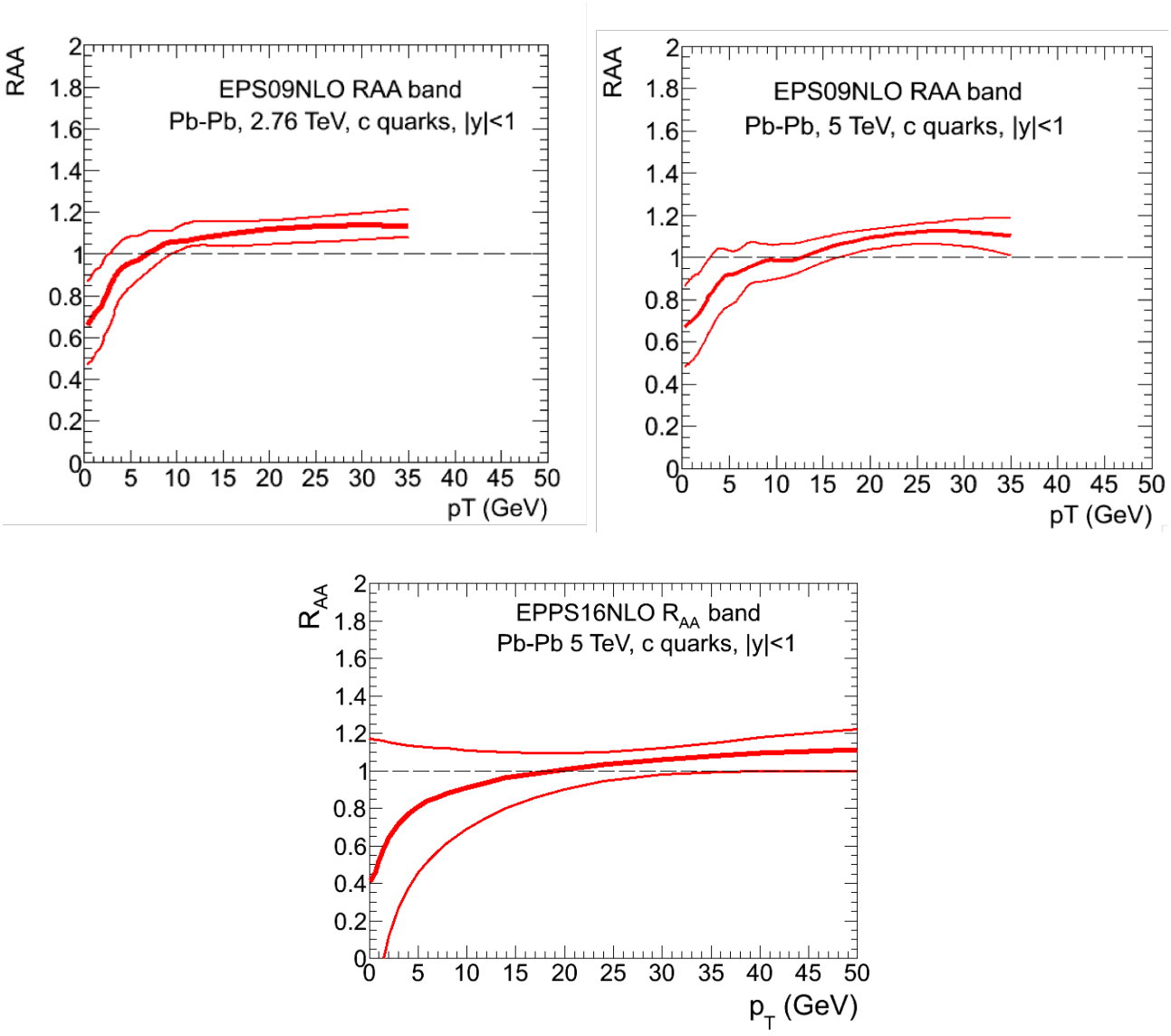

Figure 4: Nuclear modification factor of the c-quark p_t distribution as obtained using, in the two upper panels, the HVQMNR NLO calculation [30] with CTEQ6M PDFs [12] and EPS09NLO nuclear modification [25], and, in the lower panel, the FONLL calculation [9, 10] with CTEQ10 PDFs [31] and EPPS16 nuclear modification [29]. The uncertainty bands correspond to the EPS09 and EPPS16 uncertainties.

modification of the PDFs. The central values of the R_{AA} values at the two energies are similar, with the result given by the EPPS16 set being slightly lower than that of the EPS09 set. The uncertainties are significantly larger with the more recent EPPS16 set compared to the EPS09 set, because in the EPPS16 analysis the authors allow for additional parameters (which are not constrained by the existing data) in the functional form that regulates the x and Q^2 dependence of R_i^A [29]. While we report here results with both sets, we note that the nuclear modification factor of D mesons in pPb collisions at the LHC as measured by the ALICE [21] and LHCb [32] experiments at central and forward rapidity, respectively, is described within uncertainties using the EPS09 set. Therefore, EPS09 could be considered as an acceptable effective implementation of the shadowing effects for

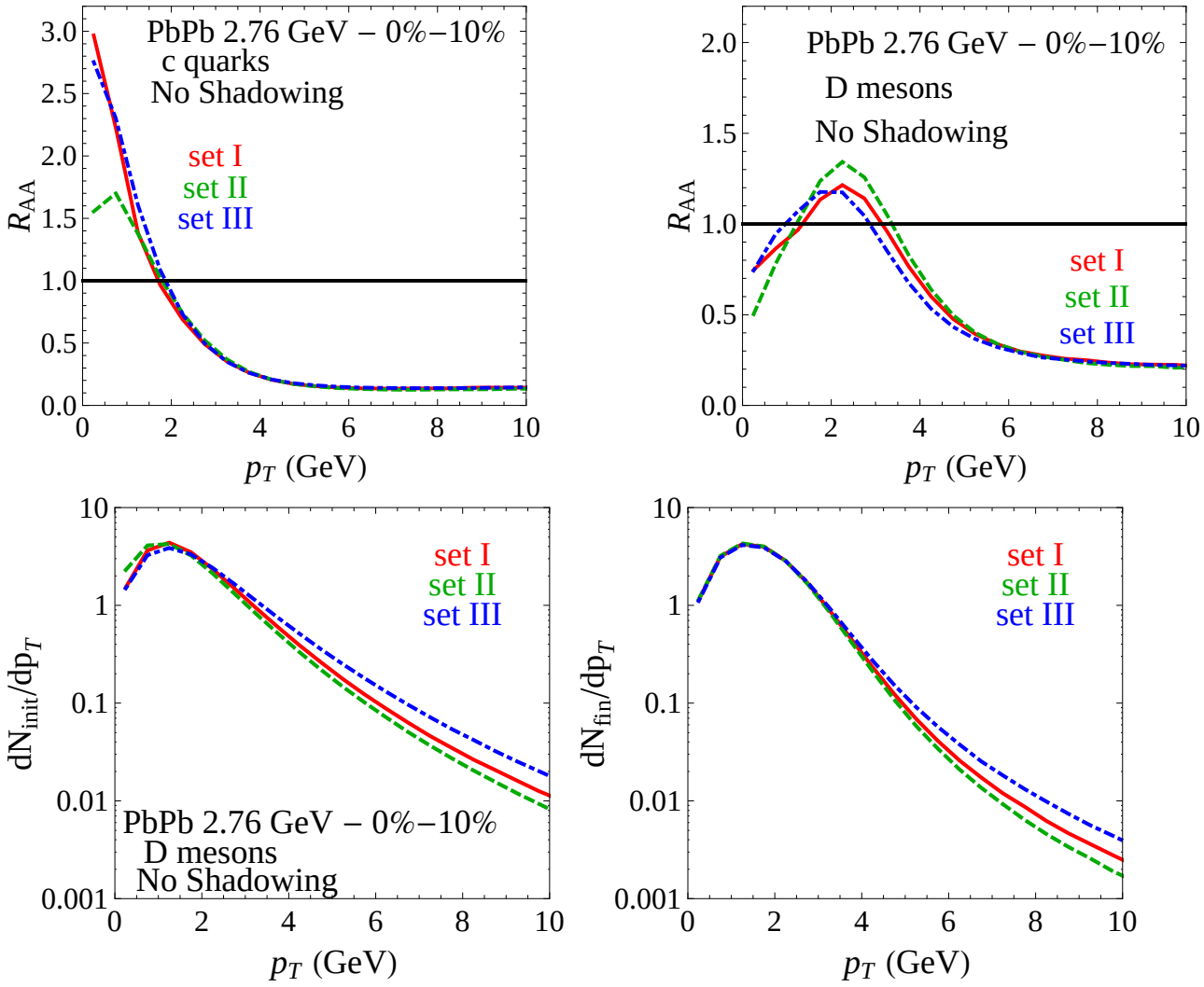

Figure 5: Impact of the variation in the initial c-quark spectrum from pp collisions on the R_{AA} (top row) and transverse-momentum spectra (bottom row) of c quarks and D mesons. Upper left: R_{AA} of c quarks stemming from the three sets for the initial spectrum, transported through the QGP in the Nantes model; upper right: same for D mesons; lower left: spectra of "initial" D mesons, obtained from the hadronization of initial c quarks; lower right: spectra of final D mesons.

charm quarks, while EPPS16 could be considered as the most up-to-date implementation of nuclear PDFs and their uncertainties.

The R_{AA} values for both sets can be downloaded in numerical format and used as multiplicative factor, depending on the c-quark p_t, to obtain an input c-quark p_t distribution for transport simulation in Pb-Pb collisions.

2.3 Exploration of Uncertainty on $R_{\rm AA}$ and v_2 in Pb-Pb(2.76 TeV)

In this section we address the consequences of an imprecise knowledge of the initial c-quark spectrum on the nuclear modification factor in heavy-ion collisions, thereby focusing on the impact on the final spectra of c quarks just before hadronization and D mesons just after hadronization. We conduct

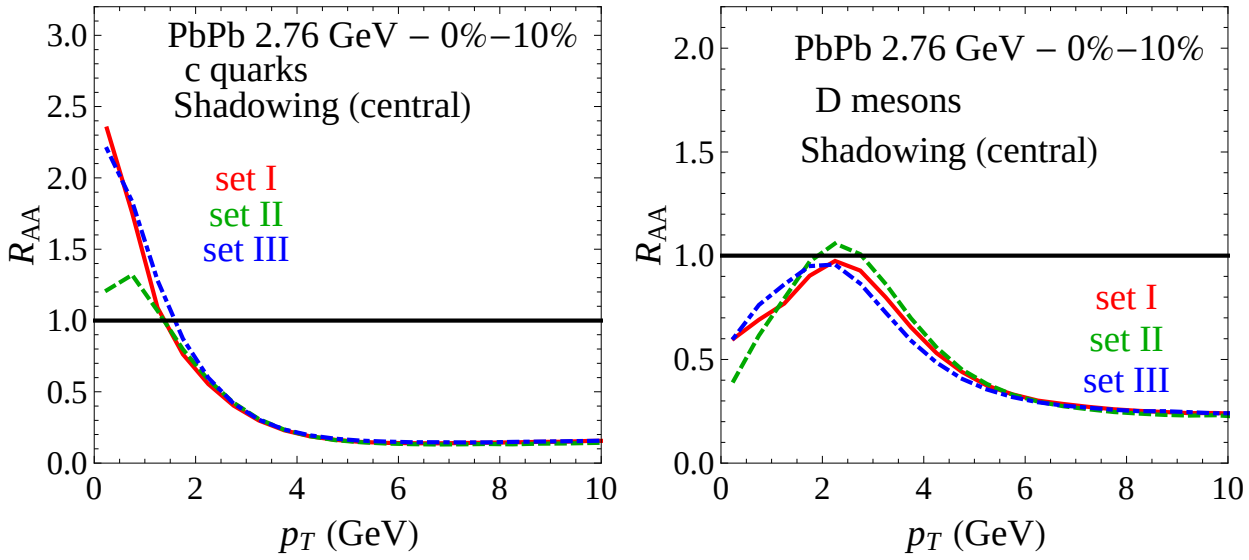

Figure 6: Same as upper panels in Fig. 5 with CNM effects included in the initial c-quark p_t spectrum (see text for details).

this study within the Nantes transport model [33][1] with elastic energy loss only (with a K factor of $K = 1.5$ for the pQCD* HQ-medium interaction, and a coalescence/BCFY fragmentation scheme) in 0-10 % Pb-Pb($\sqrt{s_{NN}}$=2.76 TeV) collisions.

We start by focusing on the effects of the c-quark spectrum produced in pp (*i.e.*, without CNM effects) taken as the initial condition for the transport. This is carried out by considering the FONLL approach with the 3 parameter sets resulting from the study performed in Sec. 2.1:

- set I: $m_c = 1.3$ GeV, $\mu_F/\mu_0 = 1$, $\mu_R/\mu_0 = 1$, scaled by 1.33
- set II: $m_c = 1.5$ GeV, $\mu_F/\mu_0 = 1$, $\mu_R/\mu_0 = 0.5$, scaled by 0.93
- set III: $m_c = 1.5$ GeV, $\mu_F/\mu_0 = 1$, $\mu_R/\mu_0 = 2$, scaled by 2.21

In the upper panels of Fig. 5, we show the R_{AA} of c quarks (left) and the R_{AA} of D mesons after hadronization (right). We find a clear separation between a high-p_T regime ($p_T \gtrsim 3$ GeV), for which the R_{AA} is essentially independent of the chosen set, and a low-p_T regime ($p_T \lesssim 3$ GeV), for which significant differences are found in the c-quark R_{AA}, which are somewhat tempered in the D-meson R_{AA}.

In order to clarify these observations, we display in the lower panels of Fig. 5 the spectra of "initial" D mesons (left; obtained from the distributions of initial c-quarks through fragmentation) as well as the spectra of final D mesons (right). In the high-p_T regime, we see that the hierarchy between the 3 sets is preserved through the HQ transport, as energy loss is the dominant process. This explains the overlaps observed at the R_{AA} level. In the low-p_T regime, distributions ensuing from the transport of various sets converge towards a unique profile, a feature arising from the rather large degree of thermalization of c quarks in the QGP phase[2]. Hence, one concludes that the differences seen for the R_{AA} in this regime merely result from the choice of the initial distribution adopted in the

[1] We expect that the conclusions do not strongly depend on the specific transport model used for this study.
[2] The degree of c-quark thermalization in the QGP can of course vary in different transport models.

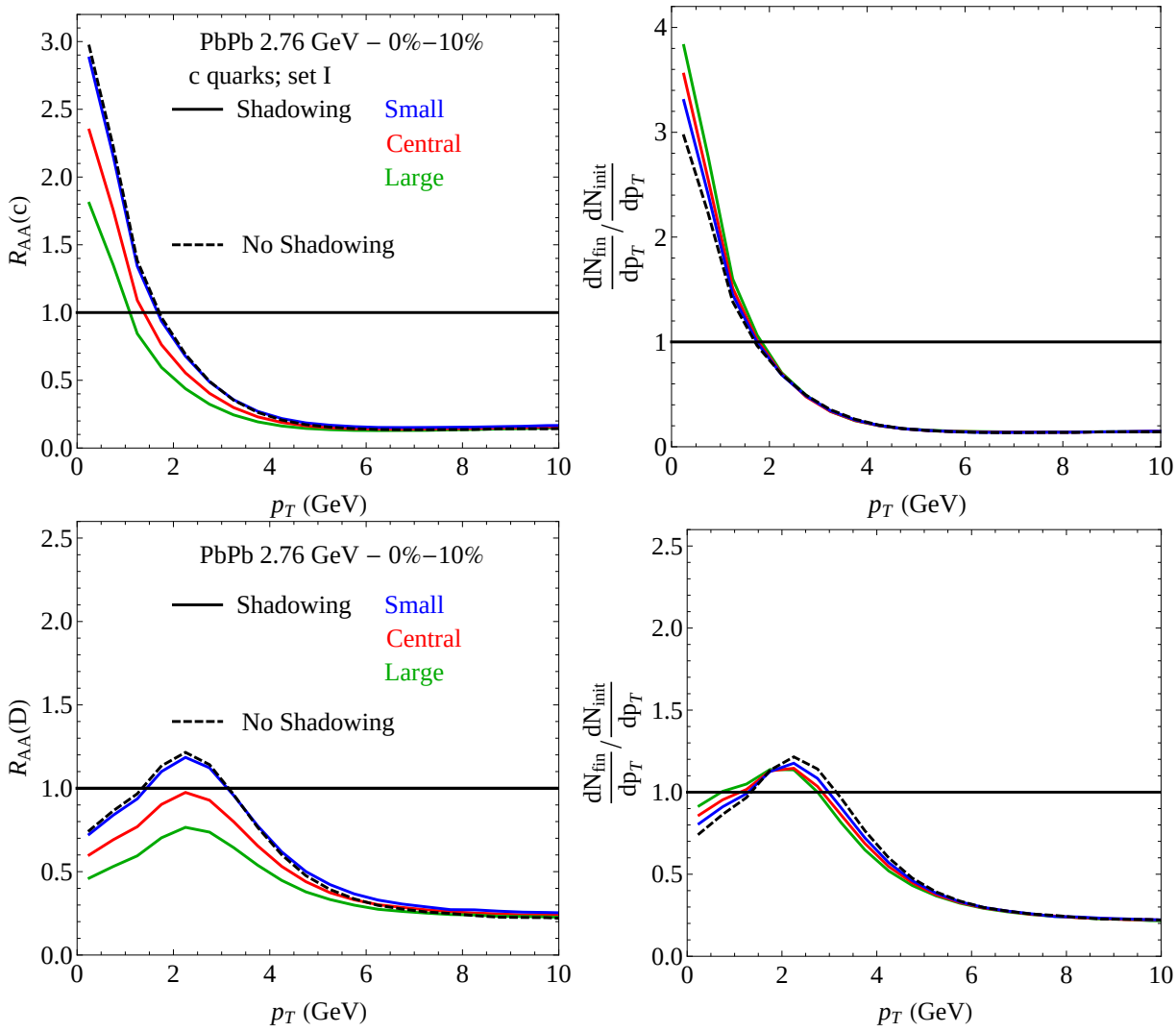

Figure 7: Top row: R_{AA} of c quarks (left panel) resulting from initial-set I without (dashed line) and with (solid line) multiplication by various CNM prescriptions for the initial c-quark spectrum as shown in Fig. 4; right panel: ratio of final c-quark p_t-spectrum to the initial input spectrum (including CNM effects) to the transport simulation. Bottom row: same as top row but for D mesons.

denominator. This could lead to systematic differences between various groups that could be easily corrected by adopting a common baseline of the type suggested in Sec. 2.1.

Next we investigate the consequences resulting from the CNM effects described in Sec. 2.2. In Fig. 6, we display the same quantities, but with CNM effects taken into account by multiplying the various sets evaluated for pp collisions by a reduction factor chosen as the central line of Fig. 4. All curves in Fig. 6 follow the same trend as the corresponding ones in the upper row of Fig. 5, with an expected additional suppression at low p_t.

In upper left panel of Fig. 7, we explore more systematically the CNM effects on the c-quark R_{AA} by considering various input distributions for the transport obtained from set I multiplied by the initial "R_{AA}" corresponding to the various prescriptions shown in Fig. 4. The case without CNM effect is also shown. It nearly overlaps with the "small" shadowing case, while prescriptions corresponding to larger shadowing naturally lead to a stronger suppression at small p_t ($p_t \lesssim 4\,\mathrm{GeV}$).

In the upper right panel of Fig. 7, we display the ratios between the final and the initial spectra (where the latter also *include* CNM effects). These ratios reflect the genuine modifications in the QGP phase and are seen to be not much affected by the precise shape of the initial distribution. Thermalization of c quarks at small p_t has the tendency to compensate the depletion in the initial distribution and is the reason for the reversal of the hierarchy observed in this range.

In the bottom row of Fig. 7, we show the same quantities as in the top row but for the D mesons; the same observations as for c quarks apply. In the low-p_T regime, we find differences of the order of $\pm 25\%$ for small/large CNM effects as compared to the intermediate case. Comparing with Fig. 5, we conclude from this study that the uncertainties on the CNM effects dominate by far over those on the c-quark spectra from pp collisions.

3 Bulk Evolution Models

The evolution of the bulk medium in HICs, characterized by the space-time dependence of temperature and local flow velocity, provides the link between the interactions of HF particles with the medium and the time evolution of their spectra. It is therefore mandatory to carefully compare the different medium evolutions as employed in HF phenomenology in the current literature.

In the following comparison, we have focused on approaches which were primarily designed to work at low and intermediate charm-quark momenta. Specifically, and very briefly, these are:

- UrQMD: HQ Langevin transport in a 3+1D ideal hydrodynamic evolution, initialized by smeared UrQMD string/energy density configurations at a starting time of τ_0=0.5 fm, with a Polyakov-loop model-based QGP EoS fitted to lQCD with final QGP temperature of T_c=160 MeV [34, 35];
- TAMU: HQ Langevin transport in a 2+1D ideal hydrodynamic evolution with smooth initial conditions, starting time τ_0=0.4 fm, with lQCD-fitted EoS and final QGP temperature of T_c=170 MeV [36];
- Nantes: HQ Boltzmann transport using the EPOS-2 event generator with fluctuating initial conditions and 3+1D ideal hydro starting at τ_0=0.3 fm, with lQCD-based EoS [37] and final QGP temperature T_c=166 MeV [38];
- Catania: HQ Langevin transport using Boltzmann simulations for the bulk evolution with massive quasiparticles, coarse-grained to obtain local temperatures, starting time τ_0=0.3 fm and final QGP temperature of T_c=170 MeV [39];
- LBL-CCNU: HQ Boltzmann transport assuming massless thermal partons in the VISHNU 2+1D viscous hydrodynamic evolution (OSU hydro) including event-by-event initial conditions, starting at τ_0=0.6 fm, with lQCD-fitted EoS [40] and final QGP temperature of T_c=165 MeV [41–43]
- Duke: HQ Langevin transport with the same hydrodynamic evolution as in LBL-CCNU.
- CUJET: HQ energy loss calculation (limited to p_T>6 GeV) [44–46] with elastic-only friction coefficient from pQCD*5 using the VISHNU 2+1D viscous hydrodynamic model with T_c=160 MeV (the radiative processes included in the default CUJET framework have been switched off).
- POWLANG: HQ Langevin transport in the ECHO-QGP 3+1D viscous hydrodynamic evolution with lQCD-based EoS, starting time τ_0=0.6 fm and final QGP temperature of T_c=155 MeV [47].

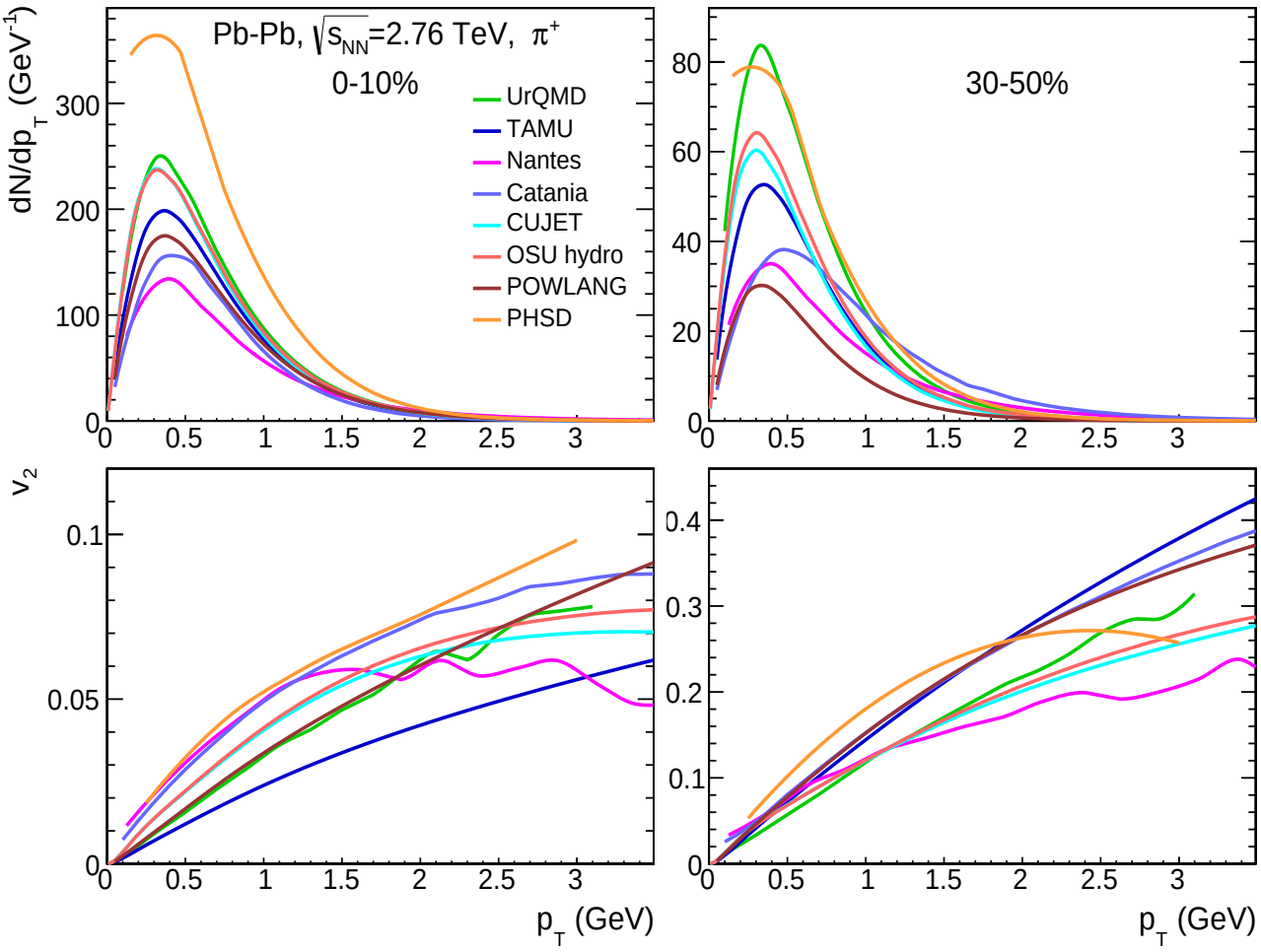

Figure 8: Comparison of the p_T spectra (upper panels) and elliptic flow (lower panels) of direct pions (no feeddown) right after hadronization in 0-10% (left panels) and 30-50% (right panels) Pb-Pb(2.76 TeV) collisions within the different fireball evolution models used for HF transport (as identified in the legends).

- PHSD: HQ Boltzmann transport in a microscopic off-shell transport model utilizing a dynamical quasiparticle model for the QGP EoS fitted to lQCD data with a final QGP energy density of 0.5 GeV/fm^3 corresponding to a would-be equilibrium temperature of $T_c \simeq 160$ MeV [48–50].

We note that for the purpose of the present discussion the notion of T_c pertains to the temperature where the hadronization of heavy quarks into HF hadrons is carried out, which also delineates the partonic and hadronic treatment of the HQ and HF-hadron interactions in the bulk medium (the latter are not discussed in this section).

3.1 Bulk Comparisons

To prepare for the interpretation of the resulting charm-quark (and later D-meson) spectra with a common QGP transport interaction, we start by inspecting the results of the bulk evolution for their radial and elliptic flow in terms of light-hadron production at T_c. While this does not give a complete picture of the space-time history of the medium expansion as experienced by the propagating c-quarks, it should nevertheless provide a useful benchmark. To reduce ambiguities in the comparison of the

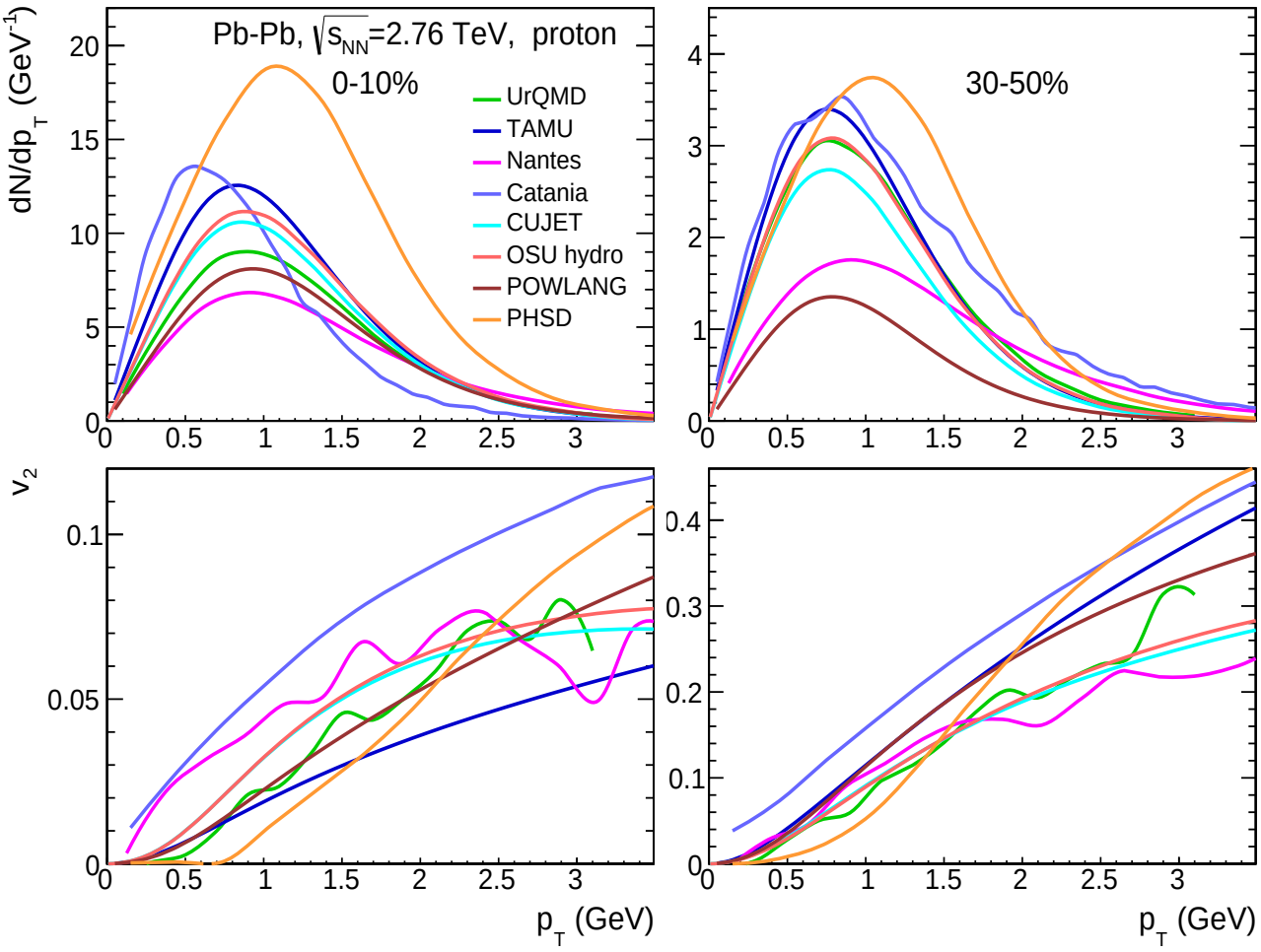

Figure 9: Comparison of the p_T spectra (upper panels) and elliptic flow (lower panels) of direct protons (no feeddown) right after hadronization in 0-10% (left panels) and 30-50% (right panels) Pb-Pb(2.76 TeV) collisions within the different fireball evolution models used for HF transport (as identified in the legends).

collective properties of the bulk across the different evolution models, we perform the comparison of p_T-spectra and v_2 at the hadron level, specifically for direct pions and protons, *i.e.*, without any feeddown from resonance decays. This avoids, *e.g.*, complications associated with different quark masses in the description of the QGP or issues related with gluonic degrees of freedom.

Direct-pion and -proton p_T spectra and v_2 at hadronization are summarized in Figs. 8 and 9, respectively, for 0-10% and 30-50% Pb-Pb(2.76 TeV) collisions. For both pions and protons all evolution models give maximum structures in the p_T spectra whose locations are indicative for the size of the transverse flow at hadronization. There is an approximate agreement within about 20% in both magnitude and shape of the pion and proton spectra for the hydrodynamic models used by TAMU, CUJET and the OSU hydro (used by LBNL/CCNU and Duke). The ECHO-QGP model used by the Torino group and the EPOS-2 model used by the Nantes group tend to fall somewhat off in both the pion and proton multiplicities, especially for the 30-50% centrality class. The PHSD model, where the direct contributions to pions and protons are not readily extracted from the underlying off-shell hadronization scheme, shows somewhat larger yields. They differ from those of hydro-based models since the

Model	dN_{π^+}/dy ($dS/d\eta$)		dN_p/dy	
	0-10%	30-50%	0-10%	30-50%
UrQMD	495	152	34	11
TAMU	682 (12400)	170 (3080)	58	15
Nantes	478	129	38	10
Catania	(14000)	(3700)		
LBL-CCNU/Duke	653 (12600)	160 (3080)		
CUJET	610 (10820)	142 (2610)	45	11
POWLANG	(9100)	(1450)		
PHSD	722	148	31	6
exp.	670±68	163±15	31±4	8±1

Table 1: Inclusive π^+ and proton numbers (*i.e.*, including strong and electromagnetic feeddown) per unit momentum-space rapidity in Pb-Pb(2.76 TeV) collisions in the various bulk evolution models. Also shown in parentheses are the values for the total entropy per unit space-time rapidity at the end of the QGP phase (as available). As a reference the last row shows experimental values from Ref. [51].

hadronization of massive quasiparticles in the PHSD goes via the production of resonances/strings, which includes feeddown from resonance and string decays.

The shape of the pion spectra, *i.e.*, the maximum structure and its location in p_T, generally agrees quite well across the models. The sensitivity to the transverse flow is enhanced in the spectra of protons due to their larger sensitivity to blue shift effects. In this regard, all hydro models, as well as the UrQMD model, show satisfactory agreement. The maximum in the proton spectra in PHSD is at slightly higher p_T than in the other models, indicative for a stronger radial flow at hadronization, while it is at slightly lower p_T in the Catania transport model for 0-10% centrality.

To shed more light on the somewhat unexpected range in the yields of the direct pions (and, to a lesser degree, of the direct protons), we collect in Tab. 1 information on the inclusive yields, *i.e.*, including strong and electromagnetic decay feeddowns, and/or on the total entropy per unit rapidity as available, at the respective ends of the QGP phase in the various bulk evolution models. In the table we also quote the experimentally measured values, which are, however, not necessarily to be understood as a precise benchmark for the model yields at T_c since further chemistry-changing processes (*e.g.*, entropy production in both viscous-hydro and transport models, inelastic reactions in transport models), or a later chemical freezeout (*e.g.*, T_c=170 MeV vs. T_{ch}=160 MeV in the TAMU model) can affect the finally observable yields. The TAMU, OSU (used by LBL-CCNU and Duke) and CUJET hydro models are within a 10% range of the inclusive pion numbers, while the POWLANG and Nantes models come out on the low end, with a ∼25% smaller total entropy / inclusive pion number, respectively; this range is approximately consistent with the comparisons of the direct-pion spectra discussed in Fig. 8, although the TAMU results for the latter are trending somewhat lower given that is has the largest inclusive-pion numbers of the hydro models. For the transport models Catania and PHSD, where the direct-pion numbers in 0-10% defined the upper and lower ends of the range, the total entropy (∼14000) and inclusive pion number (722), respectively, are better aligned with the range defined by the hydro models. This reiterates that direct-pion numbers in transport models may not be a good bulk measure, due to different hadronization mechanisms (*e.g.*, coalescence

or string fragmentation) which generally do not result in chemical equilibrium abundances as implied by hydrodynamic models. In addition, inelastic processes in the transport through the hadronic phase may further modify the hadro-chemistry prior to kinetic freezeout. These considerations suggest that the overall discrepancies in the direct-pion numbers are reduced when comparing more inclusive measures; the spread in the hydro models mostly originates from the different entropy inputs (which may be the most relevant quantity thus far for characterizing the matter content of the QGP), while differences in the hadro-chemistry (which is also affected by the resonance content of the hadron gas EoS) indice some variations when going from direct to inclusive pions. Further studies are required to further resolve these discrepancies and reduce the uncertainties related to the bulk evolution models.

The linear y-scale in the p_T spectra emphasizes that more than 90% of the pion (proton) yields are concentrated at rather low momenta, $p_T \lesssim 1.5(2.5)\,\mathrm{GeV}$. The low-$p_T$ particles are the relevant scattering partners for HF diffusion, and for the interpretation of the bulk v_2 that we turn to next.

For the v_2 (lower panels in Figs. 8 and 9), the pion and proton curves are reasonably well collimated for semicentral collisions for $p_T < 2\,\mathrm{GeV}$; the spread is larger for central collisions where the treatment of initial-geometry fluctuations and initial-flow fields have a more significant impact on the evolution of the overall smaller (and thus less robust) spatial eccentricity and its conversion into momentum eccentricity. At higher p_T, transport calculations and hydro models with viscosity exhibit a more pronounced levelling off than ideal hydrodynamic models; However, as mentioned above, at these momenta the phase space density of the medium is suppressed by more than an order of magnitude and thus not expected to play a significant role for interactions with heavy quarks.

3.2 Charm-Quark Spectra with Common Transport Coefficient

As an initial test of how different bulk medium evolution models as employed by the various research groups affect the results for HF observables, calculations were carried out by the groups using their own evolution model but with a common pre-defined transport coefficient (for Langevin approaches) or pertinent cross section (for Boltzmann approaches). Specifically, pQCD Born diagrams for elastic charm-quark scattering off thermal quarks, anti-quarks and gluons were used, where, for example, the basic matrix element of t-channel gluon exchange is given by

$$\mathcal{M}_t \propto \frac{\alpha_s}{t - m_D^2} \ . \tag{3}$$

The coupling constant has been fixed at $\alpha_s = 0.4$ (corresponding to g=2.24), the Debye mass at $m_D = gT$, and thermal parton masses in the heat bath at $m_{\mathrm{th}} = gT$, assuming 3 light-quark flavors. For the charm-quark mass a constant value of m_{c}=1.5 GeV has been used, and an overall K factor of 5 was applied to the squared matrix elements (numerical tables for the pertinent HQ transport coefficients are available from the HF-RRTF repository [8]). in the following, we refer to this interaction as "pQCD*5". The resulting spatial HQ diffusion coefficient amounts to $\mathcal{D}_s(2\pi T) \simeq 6$ at T=300 MeV, with a weak temperature dependence. Furthermore, in the Langevin approaches, a uniform implementation of the Einstein relation was adopted, with friction (A) and transverse diffusion (B_0) coefficients as calculated from the pQCD scattering matrix elements and the longitudinal one adjusted to $B_1 = TEA$ to ensure the correct equilibrium limit ($E = \sqrt{m_c^2 + p^2}$ is the on-shell c-quark energy).

Within the above bulk models, the charm-quark R_{AA} and v_2 have been evolved through the QGP phase of 0-10% and 30-50% Pb-Pb(2.76 TeV) collisions, with initial charm-quark spectra from pp

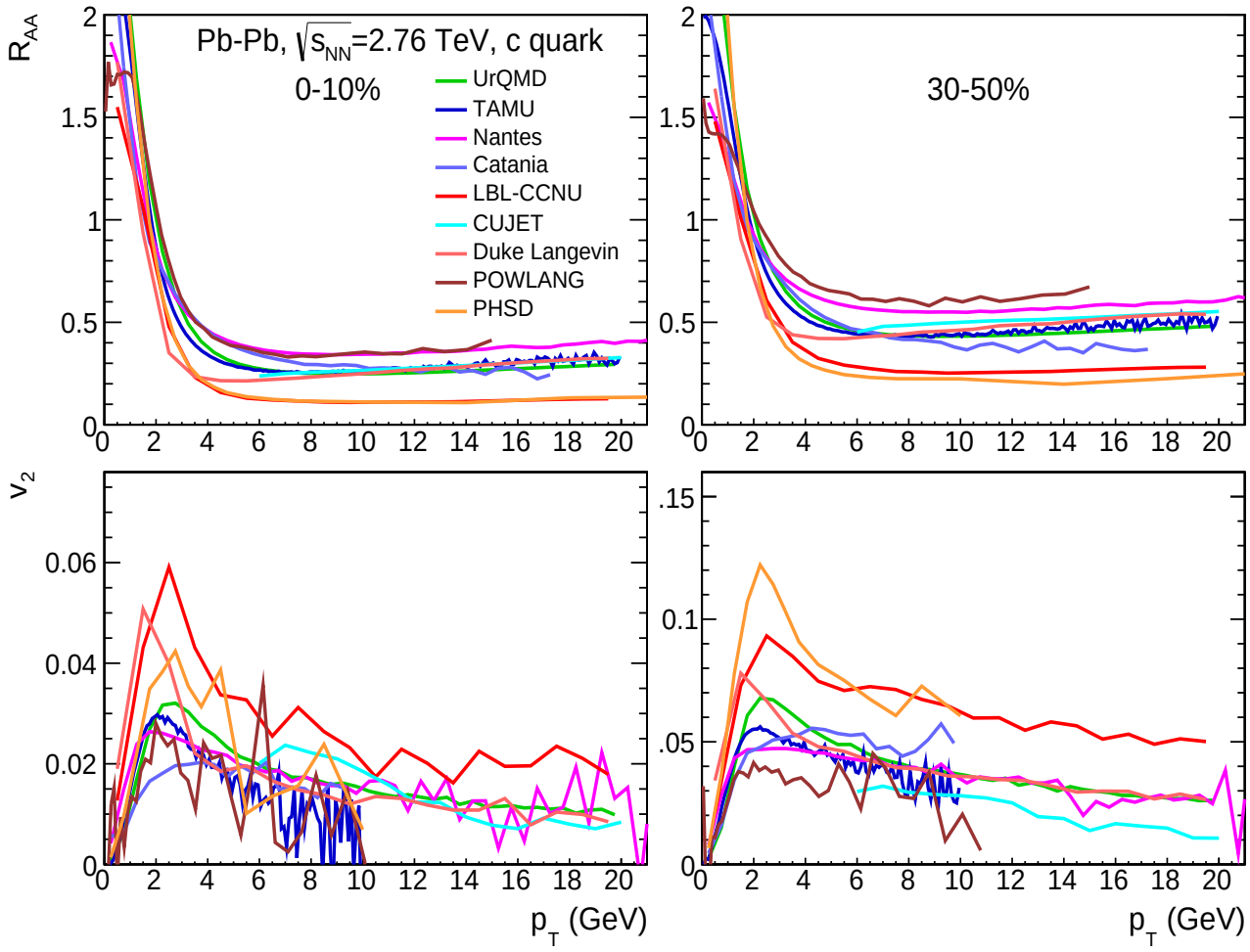

Figure 10: Comparison of the nuclear modification factor (upper panels) and elliptic flow (lower panels) of charm quarks in 0-10% (left panels) and 30-50% (right panels) Pb-Pb(2.76 TeV) collisions using a common charm-quark pQCD*5 interaction in the QGP (transport coefficient for Langevin diffusion or cross section for Boltzmann transport implementations). The different model approaches are identified in the legends and detailed in the text.

collisions without CNM effects (such as shadowing or Cronin effect). The results recorded at the end of the QGP phase are collected in Fig. 10.

All $R_{\rm AA}$'s (upper panels of Fig. 10) are reasonably well collimated in the fall-off region around $p_t \simeq 2$ GeV where they pass through one; this is largely a consequence of charm-quark number conservation, as the total yield is mostly concentrated around this value of transverse momentum. This somewhat limits the discrimination power of the low-p_t c-quark $R_{\rm AA}$ (this situation will much improve at the D-meson level). At higher p_t, all calculations level off for $p_t \gtrsim 6$ GeV, for most models in a reasonably collimated range of $R_{\rm AA} \simeq$0.3-0.4 and 0.4-0.6 for 0-10% and 30-50% centrality, respectively. Notable outliers are the LBL-CCNU Boltzmann transport model and the PHSD transport model. In the former case, this can be understood as being due to the use of massless thermal partons in the bulk evolution, which implies a significantly larger number of scatterers at a given temperature compared to the massive thermal partons used in the calculation of the pQCD*5 transport coefficients (conversely, if the transport coefficients are calculated with massless thermal partons it typically increases the low-

momentum thermalization rate a factor of up to ∼2). In the case of PHSD, we note that the pQCD*5 interaction is implemented via charm-quark Born scattering diagrams off the bulk partons as used in the transport model (which are not necessarily in chemical and thermal equilibrium and generally differ in mass from the value of gT [52]), with a momentum- and temperature-dependent K-factor to match the pQCD*5 friction coefficient in the equilibrium limit (which may also entail differences in the transverse and longitudinal diffusion coefficients). Also recall that the PHSD bulk evolution is the one with the largest inclusive pion number in central collisions. On the other hand, the POWLANG and Nantes results, which are among the ones with the weakest medium modifications (*i.e.*, relatively large c-quark $R_{\rm AA}$ and small v_2), are obtained from the hydro evolutions with the smallest entropy content; this qualitative consistency is quite encouraging. Also to be kept in mind are the varying treatments of the initial conditions (*e.g.*, with or without transverse flow, the initial transverse energy density distribution and its possible fluctuations), for which a more in-depth analysis is left to future work. For central collisions, the UrQMD, TAMU, Nantes, Catania, CUJET, Duke and POWLANG $R_{\rm AA}$'s for p_t=10-20 GeV, are all within a range of ±0.05 around 0.3-0.35, with a slight upward trend for most, which is quite encouraging. For semi-central collisions POWLANG and Nantes, on the one hand, and Catania, on the other hand, lie somewhat above and below, respectively, a ±0.05 range of the other models. These deviations can at least in part be understood by the factor of ∼2.5 difference of the total entropies in these calculations, being at the low (POWLANG, Nantes) and high (Catania) end of the various evolution models, recall Table 1.

For the v_2, displayed in the lower panels of Fig. 10, the sensitivity is somewhat limited for 0-10% centrality due to the relatively small signal and appreciable statistical fluctuations in the calculations. For the 30-50% centrality, the stronger impact found for the bulk media in the PHSD and LBL-CCNU models in the $R_{\rm AA}$ is also reflected in the larger v_2 within these approaches, reaching a maximum of more ≥9% while all other calculations mostly lie within a ∼4-6%, with DUKE and UrQMD exhibiting slightly more pronounced (*i.e.*, narrow) maxima near 7% but subsequently leveling off well within the common trend. These systematics proceed out to higher p_t, with the main band largely bracketed by Catania (upper part) and POWLANG (lower part), correlating well with the observations for the $R_{\rm AA}$.

One of the differences in the bulk evolution models relevant to HF observables is the temperature $T_{\rm c}$ where the QGP evolution is assumed to end. To illustrate this uncertainty, we show in Fig. 11 the impact of a variation of this quantity on the final c-quark spectra. Concretely, within the Catania transport approach, the results for the default value of T_c=155 MeV are compared to terminating the QGP evolution at $T_{\rm c}$=170 MeV, as used, *e.g.*, in the TAMU hydro evolution. It turns out that the $R_{\rm AA}$ is affected little, while the v_2 picks up an appreciable contribution of up to 20% when the evolution is run to the lower temperature. This result is consistent with previous studies [53, 54] where the suppression figuring in the $R_{\rm AA}$ is identified a density-driven effect which is most effective in the earliest phases of the fireball, while the transfer of v_2 from the medium to the heavy quark is most effective when the fireball v_2 is large which is primarily in the later phases of the evolution, closer to $T_{\rm c}$. This effect is further augmented when the coupling strength of the medium is largest near $T_{\rm c}$ (including coalescence processes), for which initial evidence was already deduced from the first PHENIX HF electron data [55, 56]. The pQCD*5 interaction underlying the studies in this section does not feature an enhanced strength near $T_{\rm c}$, and therefore the increase of the HQ v_2 near $T_{\rm c}$ is expected to be more pronounced for nonperturbative interactions.

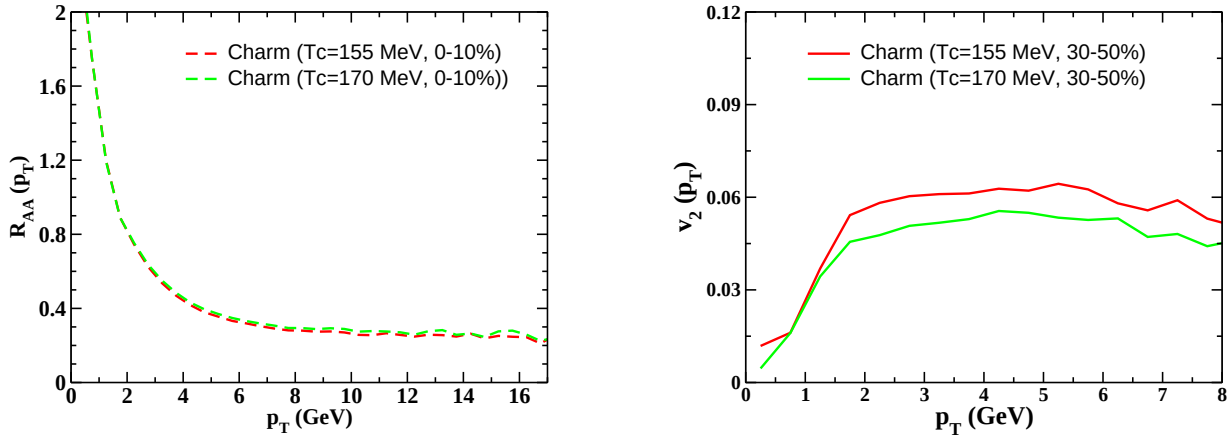

Figure 11: Comparison of the charm-quark nuclear modification factor in 0-10% (left panel) and elliptic flow in 30-50% (right panel) Pb-Pb(2.76 TeV) collisions computed with the pQCD*5 interaction within the Catania Langevin transport approach when varying the final temperature of the QGP evolution from the default value of T_c=155 MeV (red lines) to T_c=170 MeV (green lines).

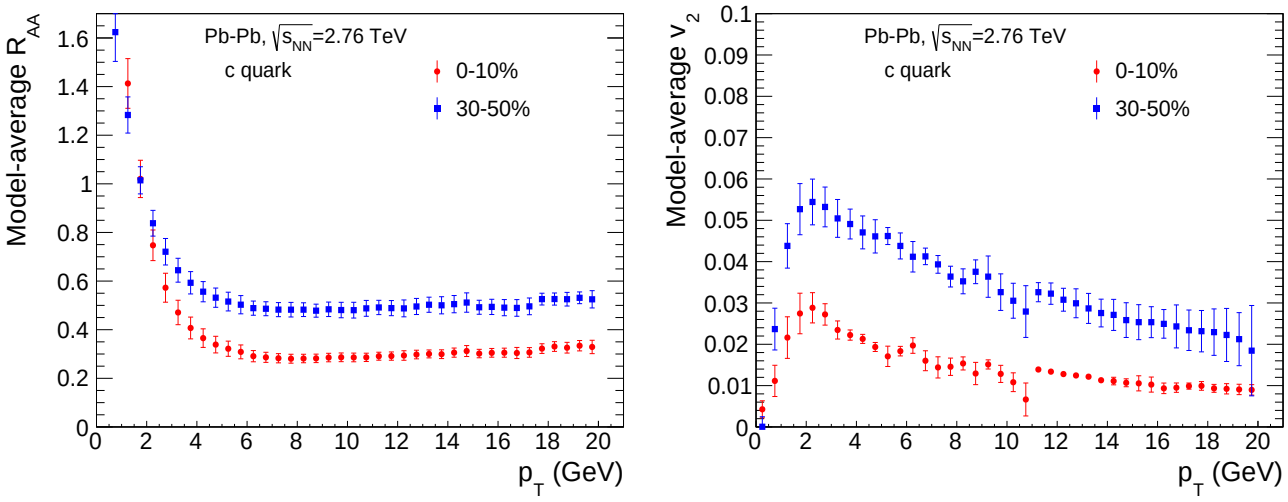

Figure 12: Statistical average of the transport models calculations using the (elastic) pQCD*5 interaction for charm-quark nuclear modification factor (left panel) and elliptic flow (right panel) at the end of the QGP phase in 0-10% (red dots) and 30-50% (blue squares) Pb-Pb(2.76 TeV) collisions.

We finish this section by performing a statistical average of the above discussed model calculations for the c-quark $R_{\rm AA}$ and v_2, cf. Fig. 12 (for reasons mentioned earlier we do not include the LBL-CCNU and PHSD results in the averages). The result of this procedure suggests a roughly $\pm$10% uncertainty due to the different bulk evolution models for the QGP phase (somewhat larger for the high-p_T v_2).

4 Hadronization

The hadronization mechanism of heavy quarks into heavy mesons and baryons [57, 58] in heavy-ion collisions has been established as an important ingredient to the phenomenology of the observed heavy-

flavor $R_{\rm AA}$ and v_2 at both RHIC [55, 56] and the LHC [59, 60]. As such it is critical to scrutinize the different theoretical treatments of this modeling component. In the following section (4.1) we first compare the impact of the various hadronization mechanisms from the literature as applied in current model approaches to the charm-quark spectra in Pb-Pb(2.76 TeV) collisions as computed with the common pQCD*5 transport coefficient in Sec. 3.2. We then elaborate on different ways of implementing heavy-light quark coalescence by directly comparing several approaches applied to the same input charm-quark spectrum within the same bulk medium background (temperature and flow field) and critically inspect the effects on the resulting D-meson p_T spectra and v_2 in Sec. 4.2). Finally we discuss an alternative for in-medium hadronization based on a fragmentation scheme with surrounding medium partons in Sec. 4.3).

4.1 Comparison of D-Meson Spectra from Common Transport Coefficients

Let us start the discussion of charm-quark hadronization by briefly outlining its implementation by the various groups.

- UrQMD: Instantaneous coalescence model (ICM) in momentum space [58] with massive light quarks (m_q=0.37 GeV), with spatially uniform light-quark distributions but including their collective flow, supplemented with Peterson fragmentation for left-over c-quarks.

- TAMU: Resonance recombination model (RRM) [61], based on a rate from the Boltzmann equation with resonant $c+q \to D$ interaction on the hydrodynamic hypersurface (including the spatial dependence of flow fields) at $T_{\rm c}$ [62] with massive light quarks (m_q=0.3 GeV) including effects of hadro-chemistry, supplemented by FONLL fragmentation.

- Nantes: ICM with light quarks of mass m_q=0.1 GeV including spatial dependence of local flow fields, supplemented with fragmentation [63].

- Catania: ICM in momentum space [58] with massive light quarks (m_q=0.33 GeV) including global transverse flow, with spatially uniform light-quark distributions, supplemented with Peterson fragmentation.

- LBL-CCNU and Duke: ICM in momentum space [58] with thermal light-quark distributions with mass m_q=0.3 GeV and transverse-flow effects simulated through an effective temperature, including effects of hadro-chemistry, supplemented with PYTHIA fragmentation [64].

- CUJET: Fragmentation only using the perturbative BCFY scheme [11], cf. eq. (1), with the input c-quark constructed in Sec. 2.1 (in the original CUJET, harder input spectra [65] are combined with softer Peterson fragmentation (ϵ=0.06), resulting, however, in very similar D-meson spectra in pp).

- POWLANG: In-medium fragmentation which includes string formation with thermal partons in local restframe of the expanding medium, followed by PYTHIA fragmentation (cf. also Sec.4.3 for further details) [66, 67].

- PHSD: ICM Wigner functions in coordinate and momentum space, gradually hadronized in time based on a classical diffusion argument [68], with stochastic sampling of the local bulk en-

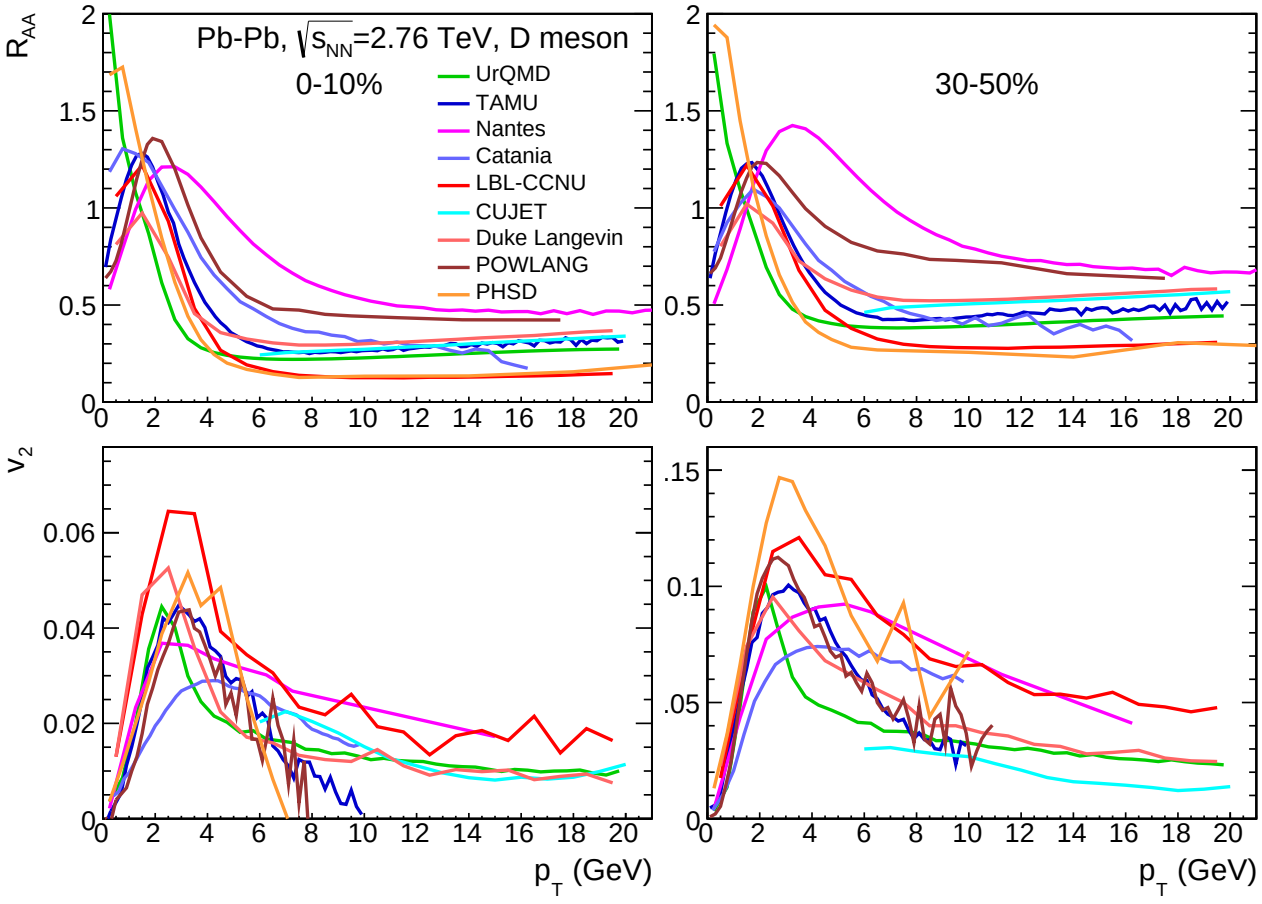

Figure 13: Comparison of the nuclear modification factor (upper panels) and elliptic flow (lower panels) of D mesons right after the hadronization transition, as obtained from the c-quark spectra from the different evolution models with the elastic pQCD*5 transport coefficient (displayed in Fig. 10) for 0-10% (left panels) and 30-50% (right panels) Pb-Pb(2.76 TeV) collisions.

vironment with thermal parton masses ($m_q \simeq 0.31$ GeV) and including higher D-meson resonance excitations, supplemented by fragmentation [49, 50].

In Fig. 13 we summarize the results of the D-meson $R_{\rm AA}$ (upper panels) and v_2 (lower panels) as they follow from the hadronization schemes described above applied to their respective charm-quark outputs with the pQCD*5 interaction (shown in Fig. 10). For the implementations within UrQMD (ICM Wigner functions with thermal quark masses of 370 MeV or more) and PHSD (ICM Wigner functions with finite times estimated from momentum diffusion), the D-meson $R_{\rm AA}$'s do not develop significant maximum structures at low p_T ("flow bumps"). A flow bump does develop for the Duke/LBL-CCNU coalescence model, for the POWLANG in-medium fragmentation scheme, for the RRM in TAMU, and most prominently for the Nantes implementation with comparatively small light-quark masses and space-momentum correlations accounted for. In the latter scheme the coalescence contribution penetrates out to rather high $p_T \simeq$12-14 GeV, notable as an enhancement over the pertinent c-quark $R_{\rm AA}$. This is significantly further out in p_T than in other implementations where coalescence effects cease above $p_T \simeq 6$ GeV, and thus their ordering in suppression at the c-quark level is preserved at the D-meson level (*i.e.*, it is little affected by independent fragmentation). We also remark that the D-meson $R_{\rm AA}$'s are not necessarily norm-conserving, even though the c-quark

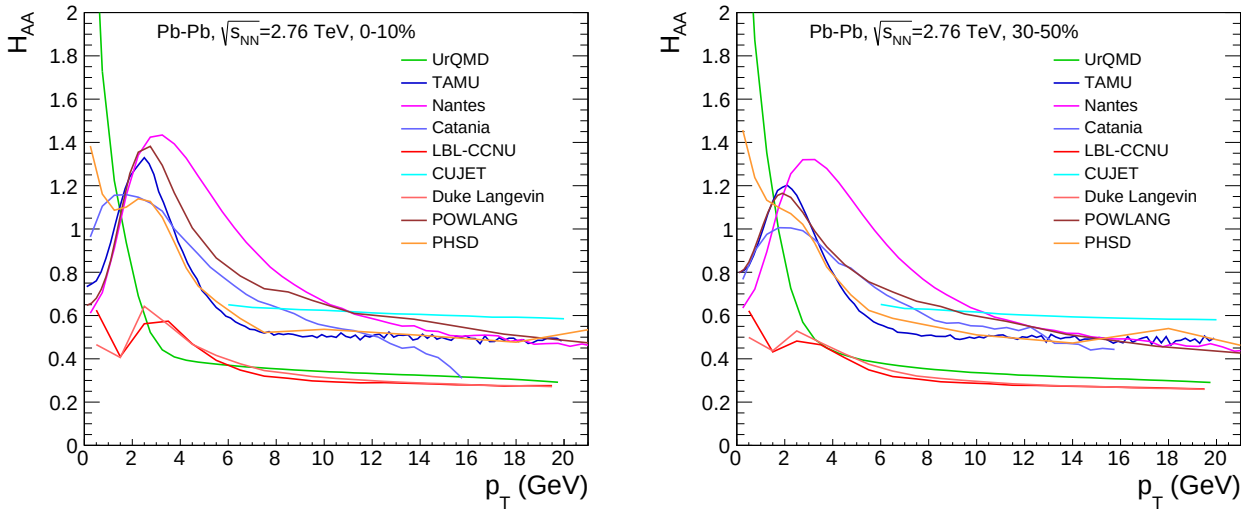

Figure 14: Comparison of the ratio of D-meson to charm-quark p_T spectra, $H_{\rm AA}(p_T = p_t)$, just after and before hadronization, respectively, in central (left panel) and semi-central (right panel) Pb-Pb(2.76 TeV) collisions for the results from the elastic pQCD*5 QGP transport simulations and individual hadronization procedures within the various bulk evolution models.

number is conserved; this is due to the "chemistry effect" as included by Duke/LBL-CCNU/PHSD (in principle also for TAMU, but for clarity not in the present calculation), where, *e.g.*, an increase in the D_s/D or Λ_c/D ratio in AA relative to pp collisions requires a decrease in other charm-hadron species.

The strong coalescence effect in the Nantes model also shows up in the D-meson v_2, roughly doubling the maximum value of the c-quark v_2 for 30-50% centrality while preserving a rather gradual decrease with p_T. The increase in the maximum D-meson v_2 over the c-quark one is comparable for the RRM employed by TAMU, but this enhancement fades away more rapidity in p_T recovering the c-quark values for $p_T \gtrsim 6\,$GeV, as is the case for the corresponding $R_{\rm AA}$. The low-p_T increase of the D-meson v_2 in the ICMs of UrQMD, LBL-CCNU and PHSD is up to 3% in absolute value, *i.e.*, 30-40% in relative magnitude; one also finds a broadening of the rather narrow maximum structure for the Duke c-quark v_2. The impact of coalescence on the D-meson v_2 in 0-10% central Pb-Pb collisions is relatively less pronounced, presumably due to the overall much smaller bulk-v_2 that can be imprinted on the forming D-meson.

In an attempt to more directly exhibit the effects of hadronization we introduce the quantity

$$H_{\rm AA}(p_T, p_t = p_T) = \frac{{\rm d}N_D/{\rm d}p_T}{{\rm d}N_c/{\rm d}p_t} = \frac{{\rm d}N_D^{\rm coal}/{\rm d}p_T + {\rm d}N_D^{\rm frag}/{\rm d}p_T}{{\rm d}N_c/{\rm d}p_t}\ , \tag{4}$$

evaluated at the same transverse momentum of the c-quark (p_t) and the D-meson (p_T); the pertinent ratios from Figs. 10 and 13 are plotted in Fig. 14. In the absence of coalescence effects this ratio simply characterizes the independent fragmentation function. Correspondingly, at high p_T one finds that the different approaches essentially level off in two regimes representing the different fragmentation functions, *i.e.*, CUJET (FONLL/BCFY), Nantes ($p_T = zp_t$), Catania (Peterson with ϵ_c=0.04), PHSD (PYTHIA tuned to FONLL) and TAMU (FONLL) vs. LBL-CCNU/Duke (PYTHIA6.4) and UrQMD (Peterson with ϵ_c=0.05). The $H_{\rm AA}$ more clearly exhibits shifts of c-quarks to higher p_T in the low- and intermediate-p_T regime, with marked "flow bumps" developing for TAMU, Nantes and POWLANG

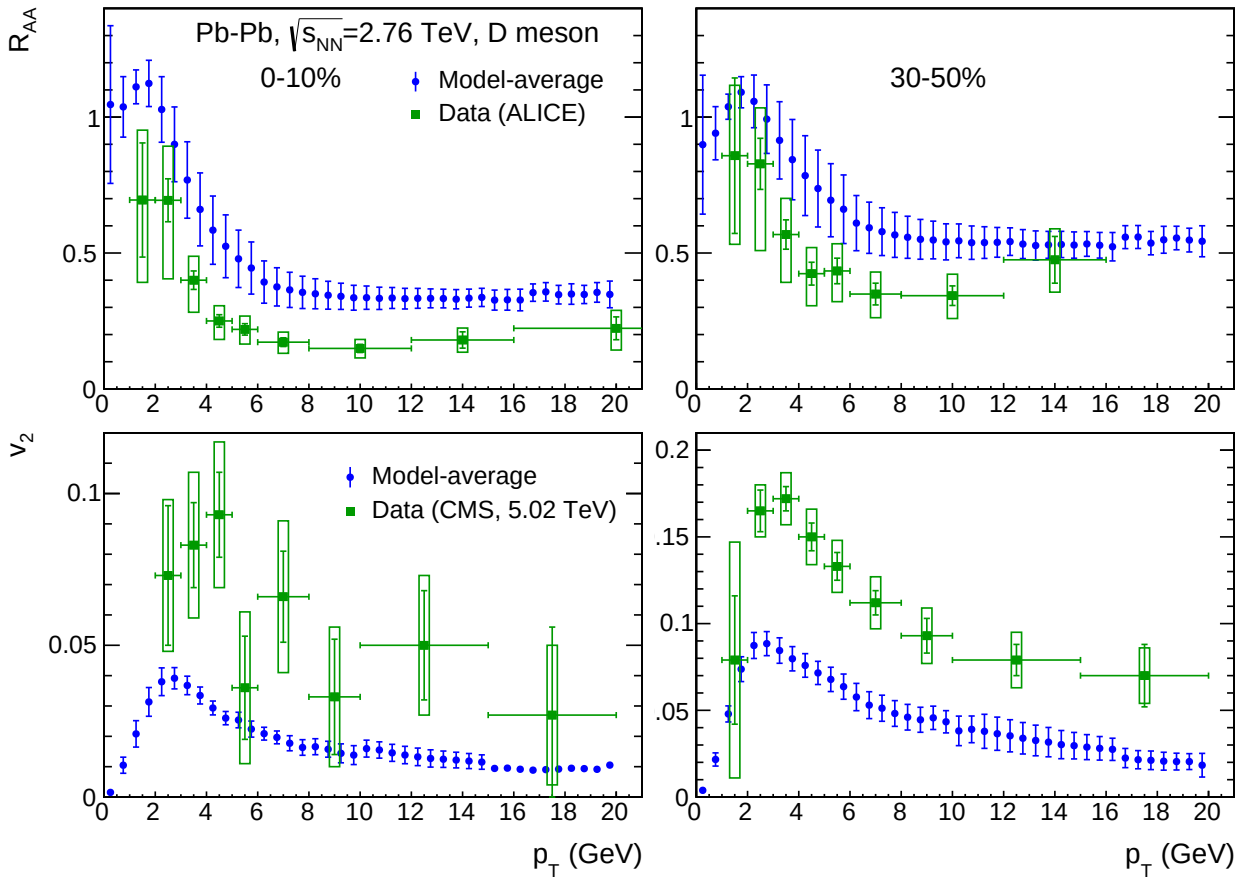

Figure 15: Statistical average of the transport models calculations for D-meson nuclear modification factor (upper panels) and elliptic flow (lower panels) after c-quark diffusion through the QGP with the elastic pQCD*5 interaction and subsequent hadronization in 0-10% (left column) and 30-50% (right column) Pb-Pb(2.76 TeV) collisions. The theoretical "averages" are compared to ALICE data [69] for the $R_{\rm AA}$ and CMS data[70] for the elliptic flow (the latter are for Pb-Pb(5.02 TeV) collisions).

(as seen before in the D-meson $R_{\rm AA}$), and smaller ones for LBL-CCNU/Duke and PHSD. All of them are more pronounced for central collisions, as expected.

Paralleling the charm-quark case, we finish this section by performing a statistical average over the D-meson $R_{\rm AA}$'s and v_2 resulting from the pQCD*5 diffusion calculations with different bulk and hadronization models, cf. Fig. 15 (as before, LBL-CCNU and PHSD results are not included in the averages). Relative to the c-quark case in Fig. 12, the most significant increase in the percentage uncertainty occurred in the low- and intermediate-p_T region of the D-meson $R_{\rm AA}$ where the radial flow effect from coalescence processes is most prominent. The absolute error also increases in the low- and intermediate-p_T elliptic flow, but since the overall signal increases substantially (by ∼50% or more), the relative error did not change much. At high p_T where fragmentation prevails, the values and uncertainty in the $R_{\rm AA}$ are little affected, while an additional spread is added to the small signal in the v_2, in part also due to the statistical fluctuations in (some of) the individual calculations.

Let us use the results shown in Fig. 15 for a preliminary comparison to pertinent experimental data [69, 70][3], in an attempt to assess the heavy-quark transport coefficient. For the nuclear mod-

[3]Note that the CMS v_2 data are for a collision energy of 5.02 TeV while the calculations are for 2.76 TeV. This choice

ification factor, especially for central collisions, the calculations overestimate the experimental $R_{\rm AA}$ significantly, *i.e.*, well beyond both error bands, by nearly a factor of 2 for the central values (somewhat less for semi-central collisions). At low p_T, shadowing is likely to play a role in that, but for $p_T \gtrsim 5\,\text{GeV}$, the studies in Sec. 2 imply that the suppression is largely due to the hot medium effects where the theoretical averages with the pQCD*5 interaction remain well above the data. At lower p_T, the cleaner observable to gauge the interaction strength is the v_2, which should therefore be a major focus for future precision measurements. The calculational average for the pQCD*5 transport coefficient, reaching up to $v_2 \simeq 9\%$ for 30-50% centrality, is well below experimental values, again by about a factor of two over most of the p_T range out to 20 GeV. The shape of the theoretical curves is similar to that of the data, but this might be a coincidence as different (not mutually exclusive) mechanisms could be responsible for the discrepancy (*e.g.*, missing coupling strength to the collective medium at low p_T and elliptic-flow fluctuations at high p_T). The underestimate of the low-momentum v_2 makes the substantial lack of interaction strength of the schematic pQCD*5 model especially apparent, as no mechanisms other than the HQ coupling to the collectively expanding medium are readily conceivable to generate a large anisotropy at low momentum. Even this preliminary data comparison, with a simple HQ interaction in the QGP, demonstrates that the HQ diffusion coefficient, $\mathcal{D}_s(2\pi T)$, in QCD matter must be *significantly* smaller than 6 as underlying the calculations in Sec. 3.2, at least for some temperature region, preferentially where the v_2 of the bulk medium is large. The results also indicate that the theoretical error is controllable and ultimately quantifiable.

The experimental handle on the recombination mechanisms of heavy quarks is likely to be augmented by the measurement of heavy-strange mesons [71, 72], *i.e.*, $D_s = (c\bar{s})$ and $B_s = (b\bar{s})$ (or even more elusive multi-HQ hadrons, *e.g.*, B_c [73] or Ξ^{++} [74]). The main idea is [60, 75, 76] that the well-established enhancement of strange quarks in URHICs, relative to pp collisions, will increase the yields and quantitatively affect the p_T spectra and elliptic flow of the charm-strange mesons in the presence of recombination of charm quarks within a heat bath of strange quarks. To render this a quantiative probe, good control over the recombination mechanism, including the equilibrium limit and deviations from it, is required. In the following two section, we scrutinize some of recombination models which have been used in the HF sector to date.

4.2 Recombination in Thermal Medium

In this section we carry out two comparisons to provide more explicit insights into (some of) the recombination schemes that are being employed in the approaches discussed above. Specifically, we compare the "standard" implementation of the ICM with the RRM using the c-quark spectra from the pQCD*5 Langevin simulation in the TAMU hydro background, where, for simplicity, we neglect space-momentum correlations inherent in the RRM.

Early applications of quark coalescence processes in heavy-ion collisions have been carried out with a spatially uniform ("global") distribution functions in 3-momentum space, amounting to an instantaneous approximation (see Ref. [77] for a review). This allowed for a successful description of the hadron-v_2 and baryon-over-meson ratios in the light- and strange-quark sector in the intermediate-p_T

was made based on the higher precision of these data than available ones for 2.76 TeV, and the fact that both calculations and experimental data show little variations in v_2 and $R_{\rm AA}$ observables when going from 2.76 to 5.02 TeV. Quantitative comparisons in the future will of course have to be made at the same energy for theory and data, while the current experimental accuracy attained for the D-meson v_2 at 5.02 TeV can already give an indication of its constraining power.

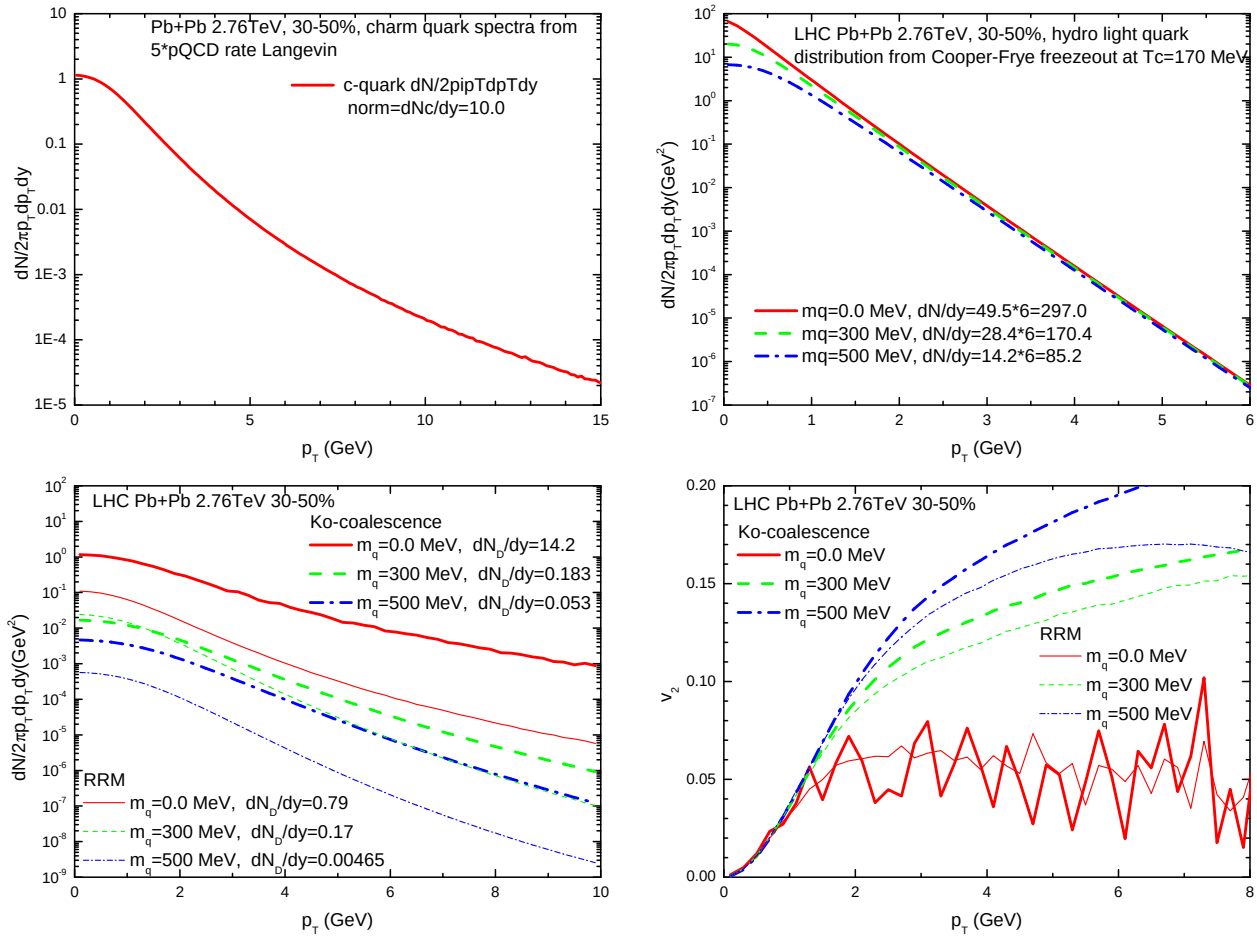

Figure 16: Upper panels: charm- (left) and light-quark (right) p_t spectra from Langevin simulations and hydro-freezeout at $T_{\rm pc}$ = 170 MeV, respectively. Lower panels: comparison of the D-meson p_T spectra (left panel) and elliptic flow (right panel) produced through recombination processes at $T_{\rm pc}$=170 MeV when using the resonance recombination model (RRM, dashed lines) [61, 62] and an ICM (solid lines) [78, 79] in 30-50% Pb-Pb(2.76 TeV) collisions. The input charm-quark spectra are taken from the Langevin simulations with the pQCD*5 interactions (within the TAMU hydro evolution) discussed in Sec. 3.2.

region at RHIC. However, this approximation does not conserve energy in the 2→1 hadron formation process and thus cannot recover the equilibrium limit of the hadron distributions. In Ref. [61] a resonance recombination model (RRM) has been developed, where resonant quark-anti-quark scattering amplitudes are used within a Boltzmann equation, which remedies both energy conservation and the equilibrium limit. It has been implemented in the heavy-quark context on a hydrodynamic hypersurface in Ref. [62].

Here, we will compare results for D-meson spectra from the ICM with the RRM using the same input c-quark spectra and thermal light-quark distributions, which are shown in the two upper panels of Fig. 16. For definiteness, we employ the c-quark spectrum (normalized to $dN/dy = 10.0$) obtained from the Langevin simulations with the pQCD*5 interaction at the end of the QGP phase within the TAMU hydro model (as described in Sec. 3.2), and the light-quark spectra are obtained from Cooper-

Frye freezeout within the same hydro, but for three different parton masses, with correspondingly different total (integrated) yields as indicated in the figure.

Using these quark momentum distributions, the coalescence calculations are performed via a multi-dimensional integration in momentum space without explicit account of the space-momentum correlations. The resulting D-meson p_T spectra and v_2 from the ICM [78, 79] (thick curves) and from RRM (thin curves) are compared in the two lower panels of Fig. 16 for the different light-quark masses. The absolute yields of D mesons per unit rapidity are also indicated in each case (the volume parameter in the coalescence model affects the yields; here it is consistently determined from the hydrodynamic hypersurface; *e.g.*, for the present 30-50% Pb-Pb 2.76 TeV collisions, the fireball volume per unit rapidity is 673.5 fm^3).[4] The yields of D mesons produced in RRM are comparable to the those produced in the ICM for $m_q = 300$ MeV, but substantially smaller for massless and $m_q = 500$ MeV light quarks. The D-meson p_T spectra from the former are significantly softer than those in the latter. This is likely a consequence of satisfying the equilibrium limit within RRM, which was shown to *soften* the high-p_T spectra as to approach the thermal limit, while in the ICM the collinearity of the coalescing quarks tends to strictly *add* 3-momentum in the conversion from c quarks to D mesons. The D-meson v_2 obtained from RRM is a bit smaller than that obtained from the ICM. This may be due to the fact that the latter tends to recombine charm quarks with light quarks for essentially comoving kinematics (parallel momenta), while the RRM allows for significant momentum smearing via the isotropic Breit-Wigner cross section, thereby reducing the D-meson v_2 to some degree.

4.3 In-Medium Fragmentation

In this section we discuss the in-medium hadronization scheme implemented in the most recent version of the POWLANG model. The procedure adopted in Refs. [66, 67] to model the hadronization of heavy quarks in the medium at the end of their propagation in the QGP is the following. Once a heavy quark Q, during its stochastic propagation in the fireball, has reached a fluid cell with a temperature below the decoupling temperature, $T_{\rm dec}$, it is forced to hadronize. One then extracts a light antiquark $\overline{q}$ (up, down or strange, with relative thermal abundancies dictated by the ratio $m/T_{\rm dec}$) from a thermal momentum distribution corresponding to the temperature $T_{\rm dec}$ in the local rest frame (LRF) of the fluid; information on the local fluid four-velocity $u^\mu_{\rm fluid}$ provided by hydrodynamics allows one to boost the momentum of $\overline{q}_{\rm light}$ from the LRF to the laboratory frame. A string is then constructed joining the endpoints given by Q and $\overline{q}$ and passed to PYTHIA 6.4 [80] to simulate its fragmentation into hadrons (and their final decays). This is done as follows: the particle type, energy, polar and azimuthal angle of each endpoint are provided to PYTHIA through the PY1ENT subroutine; the PYJOIN subroutine allows one to construct the corresponding string; finally a PYEXEC call starts the simulation of its fragmentation and the final decays of unstable particles. In case the invariant mass of the string is not large enough to allow its decay into at least a pair of hadrons the event is resampled, extracting a new thermal parton to associate to the heavy quark. In agreement with PYTHIA, in evaluating their momentum distribution, light quarks are taken as "dressed" particles with the effective masses $m_{u/d} = 0.33$ GeV and $m_s = 0.5$ GeV. Notice that, while the model allows one to take properly into account the momentum boost given to the final hadron by the light quark flowing with the medium,

[4] Note that we do not include any contributions from resonance feeddown nor chemistry effects such as a charm-quark fugacity factor which would be required to properly normalize the inclusive D-meson spectra; as such, the ratio ($H_{\rm AA}$) of the direct D-meson spectra to the input charm-quark spectra is not a meaningful quantity here.

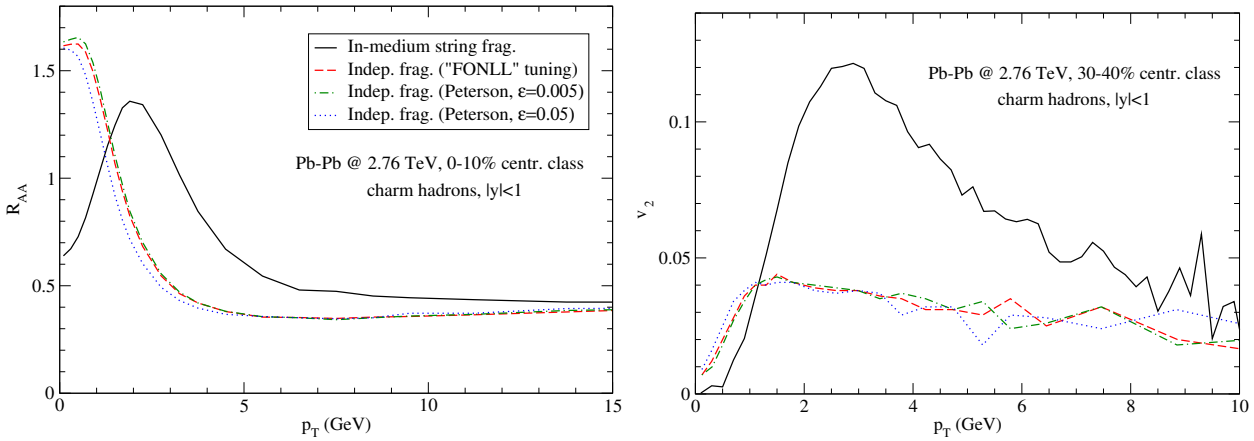

Figure 17: Left panel: the nuclear modification factor of charmed hadrons in 0-10% Pb-Pb collisions. Right panel: the elliptic flow of charmed hadrons in 30-40% Pb-Pb collisions. Results of different hadronization schemes are compared. The fragmentation of strings formed via recombination with light thermal quarks from the medium leads to a bump in the $R_{\rm AA}$ at moderate p_T and to an enhanced v_2 arising from the additional radial and elliptic flow acquired at hadronization. Hadronization via independent vacuum fragmentation functions leads to an $R_{\rm AA}$ reflecting a simple quenching pattern and to a smaller v_2.

we do not get sizable modifications of the heavy-flavour hadrochemistry, *e.g.*, an enhancement of D_s or Λ_c yields which might occur in the collisions and could be instead accommodated by a direct $2 \to 1$ or $3 \to 1$ production mechanism in a coalescence model. Within our framework, a string, once formed, is hadronized as in the vacuum, through the excitation – while stretching – of $q\overline{q}$ pairs (or diquark-antidiquark pairs for the production of a baryon-antibaryon pair) from the vacuum: having a strange quark as an endpoint does not necessarily imply the production of a D_s meson at hadronization.

In order to assess the effect of the in-medium string fragmentation model as described above we also check the results obtained with the standard independent vacuum fragmentation functions (FF's), starting from the same heavy-quark spectrum at the end of the Langevin evolution. We employ the Heavy-Quark Effective Theory (HQET) FF's [11], with parameters referring to the $m_c = 1.5$ GeV case tuned by the authors of FONLL [26]. As a further comparison, we repeat the calculation with Peterson FF's, with parameter $\epsilon = 0.005$ (representing quite a hard FF, very similar to the one of HQET) and $\epsilon = 0.05$ (the default value in PYTHIA, corresponding to a softer FF).

We display the results of our study in Fig. 17. The curves obtained with vacuum FF's are characterized by a rather modest elliptic flow, with maximum value around 0.04, simply reflecting the one of the parent c quarks. Furthermore, the nuclear modification factor of D mesons simply reflects the quenching of the p_T spectrum due to parton energy-loss, the increase at low p_T being due to the conservation of the total number of charm quarks during their evolution in the medium. Notice that the results display a negligible dependence on the particular FF employed. On the other hand, the curves obtained with the in-medium string fragmentation display a shift of the spectrum from low to moderate values of p_T ("flow bump") and a strong enhancement of the elliptic flow. As in the case of coalescence, these features can be qualitatively explained as due to the additional radial and elliptic flow inherited by each charmed hadron from the light thermal partons (carrying the collective velocity

of the medium) picked up through hadronization.

5 Transport Coefficients and Implementation

After having scrutinized the impact of bulk evolution and hadronization models on D-meson observables in nuclear collisions, we now turn to a discussion of HF interactions in QCD matter and their manifestation in the transport through the expanding fireball. In principle, this includes both hadronic and partonic matter, although our focus will mostly be on temperatures above the pseudo-critical one. Since the QCD transition at vanishing chemical potential is a continuous crossover, one should also expect a continuous transition in the heavy-flavor (HF) degrees of freedom as the temperature is lowered. The hadronization mechanisms above are essentially representing the current realization of this transition in phenomenological models, and this issue will also be reiterated in the present section.

As was already mentioned in the introduction, HF phenomenology in heavy-ion collisions provides a unique opportunity to extract a transport coefficient of the QCD medium, *i.e.*, the HF diffusion coefficient, $\mathcal{D}_s$. However, a mere extraction of this number, even including its temperature dependence, remains unsatisfactory from the fundamental point of view of studying the structure of QCD matter. Thus, the goal must be to firmly root HF interactions used in heavy-ion phenomenology in the in-medium QCD dynamics. For a soft quantity like a transport coefficient, this is a tall order; however, this is where the benefits of a large quark mass comes in, by providing opportunities for controlled approximations within suitable theoretical frameworks. On the one hand, this leads to an effective theory known as heavy-quark effective theory (HQET), which, roughly speaking, reduces the 4-component Dirac spinors to 2-component Pauli spinors and utilizes a power counting in $\Lambda_{\rm QCD}/m_Q$ and T/m_Q. On the other hand, ample information on in-medium HF properties is available from lattice-QCD (lQCD) computations, including HQ free energies, which, while not directly identifiable with an in-medium potential, can provide strong constraints on the latter. Ultimately, one should relate back the insights gained from the HF sector to the bulk properties of QCD matter.

We start this section by a brief comparison of results of several approaches for calculating HQ transport coefficients in the QGP (Sec. 5.1), and then reverse the strategy of Sec. 3 by using a common hydrodynamic medium to perform charm-quark Langevin simulations for a few of these interaction models (Sec. 5.2). We assess in-medium HQ interactions from perturbative-QCD (pQCD), functional-renormalization-group (FRG) and lattice-QCD (lQCD) perspectives (Secs. 5.3, 5.4 and 5.5, respectively), followed by a study of Boltzmann and Langevin approaches for carrying out HF transport in heavy-ion collisions (Sec. 5.6).

5.1 Comparison of Existing Coefficients

A rather wide variety of microscopic approaches to compute HQ diffusion coefficients has been adopted in the literature with applications to heavy-ion phenomenology. These include perturbatively inspired approaches, which usually include amendments to the Born diagrams for HQ scattering off light quarks from the medium to augment the the coupling strength in the medium. For example, in the SUBATECH approach a running coupling constant in momentum transfer is implemented reaching close to one at soft momentum transfers [81, 82], while in the quasi-particle model (QPM) of the CATANIA group [83] the "running" essentially occurs in temperature reaching large values near $T_{\rm c}$ to reproduce the QGP EoS with large masses gT for the bulk-medium partons [84] (similarly also

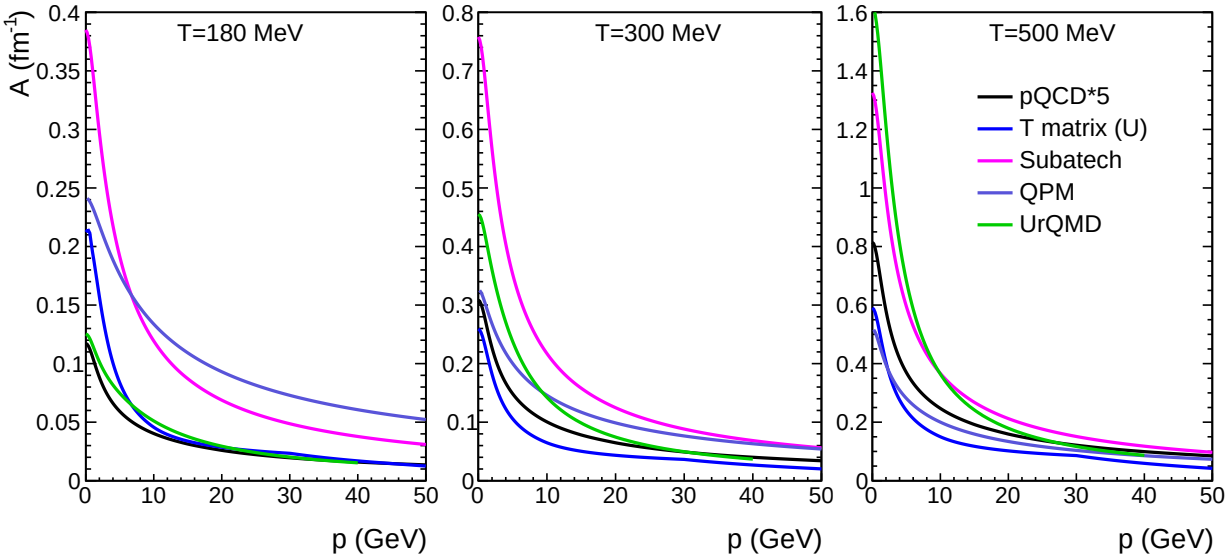

Figure 18: Comparison of charm-quark friction coefficients within different models used in phenomenological applications to heavy-ion data: pQCD*5 interaction as used in Sec. 3 (black lines), T-matrix model with internal-energy potential as used by the TAMU group (light-blue lines), Q^2-running coupling model of the SUBATECH group as used in the Nantes transport approach (pink lines), quasiparticle model as used by the CATANIA group (dark-blue lines) and D-meson resonance model as used by the UrQMD group (green lines). The inverse of the friction coefficient essentially corresponds to the thermal relaxation time, $\tau_c = 1/A$.

in the PHSD approach). Nonperturbative approaches, on the other hand, usually involve a ladder resummation of the interaction kernel including not only Color-Coulomb but also nonperturbative forces. For example, within the T-matrix framework [85–87] employed by the TAMU group remnants of the confining force above T_c are implemented through potential kernels constrained by lQCD results for the free energy. In connection with the ladder resummation the nonperturbative forces lead to the formation of resonance correlations ("pre-hadrons") which in turn induce a marked increase in the HQ interaction strength when approaching T_c from above. In the same spirit, the resonance model [88] used by the UrQMD group is based on resummed D-meson s- and u-channel polegraph interactions resummed to all orders.

In Fig. 18 we compare the charm-quark friction coefficient, $A(p,T)$ (a repository of A, B_0 and B_1 as function of T=160-600 MeV in steps of 20 MeV and p=0-40 GeV/c in steps 0.2 GeV/c can be found at the website [7]) for several of the above scenarios, as a function of 3-momentum for 3 temperatures spaced by a factor of 5/3. All models show a marked fall-off with 3-momentum. The fall-off is most pronounced in the SUBATECH model, mostly due to the Q^2 running of α_s, and in the resonance model (especially at higher temperatures) where the interaction strength is also concentrated at low relative momenta of the charm quark and the medium partons, required to excite a D-meson resonance. Even in the pQCD*5 interaction (underlying the transport calculations carried out in Sec. 3), which does not include a running coupling constant, a significant fall-off with 3-momentum is found, comparable also to the quasiparticle model (QPM). The fall-off is somewhat stronger in the T-matrix calculations at low temperatures, where the force nature changes from a long-range linear

potential at low momenta to a color-Coulomb potential at high momenta; consequently, at higher temperatures, where the remnant confining force is essentially screened, the momentum dependence and magnitude of the transport coefficient becomes comparable to pQCD*5 and QPM interactions. The strongest increase in temperature is found in the pQCD*5 and resonance model, both of which in essence do not include a reduction in interaction strength with temperature and thus fully pick up on the increase in parton densities, resulting in an approximately T^2 dependence of the low-momentum friction coefficient (somewhat weaker in the pQCD*5 case due to the increasing screening mass). In the SUBATECH running-coupling model the increase is roughly linear in T (the screening of the relatively small Debye mass has a stronger effect), while in the QPM (with a rather pronounced decrease of α_s with T) and the T-matrix approach (with a rather pronounced screening of the confining force) there is little temperature variation from T=180 MeV to 300 MeV, while it increases appreciably thereafter once color-Coulomb interactions with little temperature dependence in the coupling take over.

5.2 Different Transport Coefficients in a Common Hydrodynamic Medium

In this section, we implement HQ transport coefficients from different microscopic interactions into a common hydrodynamic medium within the same Langevin scheme. Three sets of model calculations of transport coefficients are used and compared: (1) a leading-order pQCD calculation multiplied by a K factor of 5 (pQCD*5), as utilized in Sec. 3.2 (cf. black curves in Fig. 18); (2) a pQCD-motivated one-gluon exchange model developed by the Nantes group [81, 89] which includes the effects of a running coupling constant and reduced Debye mass, with a fixed c-quark mass of m_c=1.5 GeV (cf. pink curves in Fig. 18); and (3) an in-medium T-matrix formalism developed by the TAMU group [85, 86], with c-quark mass varying as $m_c \simeq 1.4 \to 1.8$ GeV for $T \simeq 500 \to 170$ MeV (cf. blue curves in Fig. 18). The latter two models for the HQ interactions in the QCD medium have had some success in describing open HF data from RHIC and the LHC using different bulk matter evolution models. Therefore, applying them within a common hydrodynamic evolution here not only provides a direct comparison between the different HQ interactions, but, in turn, also helps understand possible differences in the bulk matter and hadronization models that the different groups use.

The common hydrodynamic medium we apply in this section is the (2+1)-dimensional viscous hydrodynamic model VISHNU developed in Refs. [41–43], labelled as "OSU hydro" in Figs. 8 and 9. We employ the code version and parameter tuning provided by Ref. [43] in the present study. The QGP fireballs are initialized using the Monte-Carlo Glauber model for the initial-entropy density distribution. The starting time of the QGP evolution is set at $\tau_0 = 0.6$ fm and a constant shear-viscosity-to-entropy-density ratio of η/s=0.08 is determined to describe the spectra of soft hadrons emitted from the fireballs at both RHIC and the LHC. For the HQ transport through this medium evolution a Langevin process with the pre-point scheme of Refs. [90, 91] is adopted, together with a leading-order pQCD calculation for the initial HQ p_t spectrum (without CNM effects). The transport coefficients of the three microscopic models employed in this study (see above) are suitably converted for use within the pre-point discretization scheme (and with the Einstein relation enforced for the momentum diffusion coefficient starting from the friction coefficient).

In Fig. 19 we summarize the results for the charm-quark $R_{\rm AA}$ and v_2 in two different centrality bins of Pb-Pb collisions at $\sqrt{s_{\rm NN}}$=2.76 TeV, at the end of the QGP evolution at T=165 MeV. The pQCD*5 and the T-matrix interactions result in a rather similar charm-quark $R_{\rm AA}$ over a large range in transverse momentum; a slight difference from the stronger 3-momentum dependence in the latter,

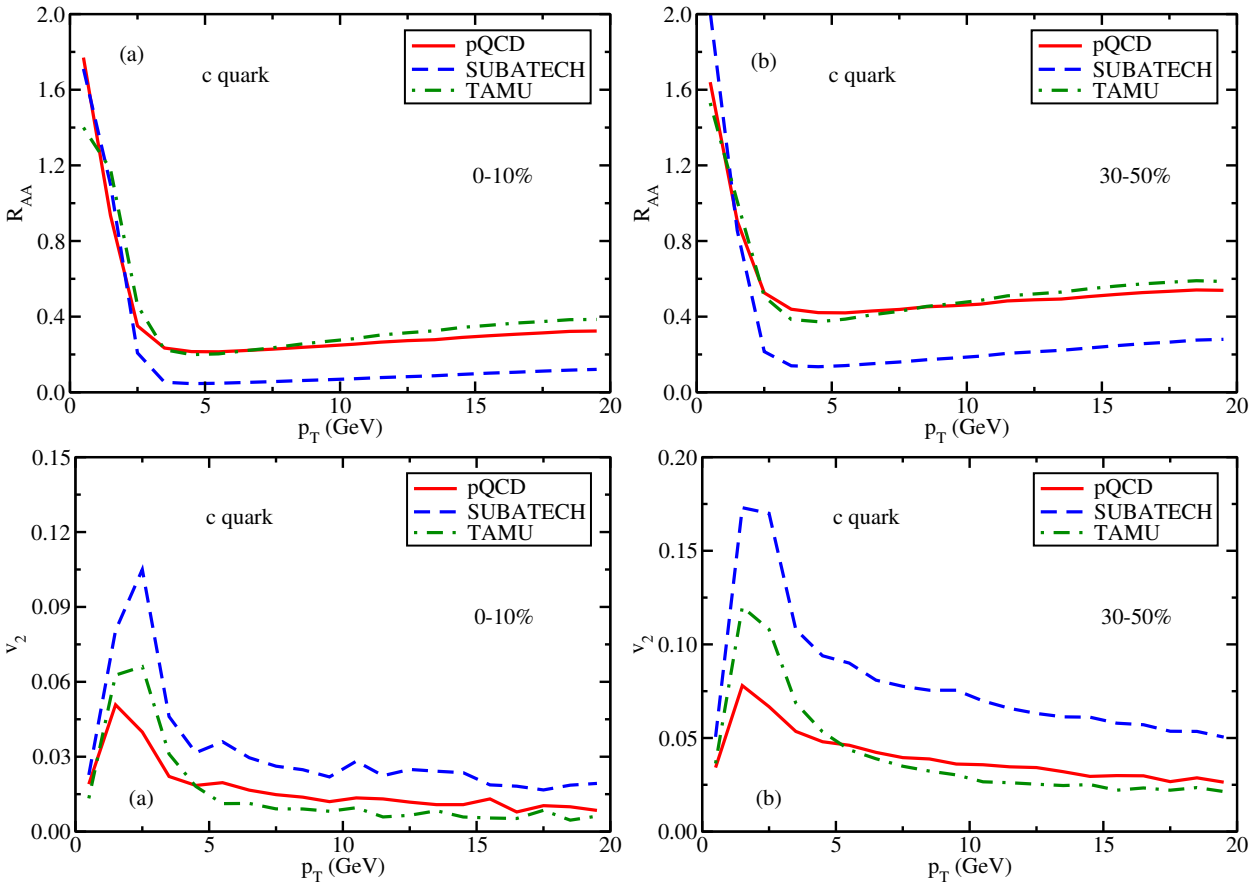

Figure 19: (Color online) Results from Langevin simulation for the charm-quark $R_{\rm AA}$ (upper panels) and v_2 (lower panels) central (left column) and semi-peripheral (right column) 2.76 TeV Pb-Pb collisions using a common viscous hydrodynamic evolution with 3 different transport coefficient (solid lines: pQCD*5; dash-dotted lines: nonperturbative T-matrix approach, dashed lines: pQCD with running coupling).

implying a smaller friction coefficient at large 3-momentum, is still apparent in form of slightly weaker suppression at high p_t (cf. the two upper panels of Fig. 19). On the other hand, the stronger coupling of the T-matrix interaction at low momentum generates a more pronounced collective behavior of the c-quarks as signalled by the elliptic flow coefficient (cf. the two lower panels of Fig. 19): the peak value of the v_2 is up to $\sim$60% larger for the T-matrix interactions than for the pQCD*5 model; at the same time, the high-p_t v_2 from the T-matrix is slightly lower, consistent with the behavior in the $R_{\rm AA}$. The much larger transport coefficient in the Nantes-pQCD calculation, relative to the other two interactions, leads to a much smaller $R_{\rm AA}$ of charm quarks at p_t's down to about 2.5 GeV, accompanied by a larger enhancement below (dictated by charm number conservation). At the same time, the v_2 is also much larger than in the pQCD*5 and T-matrix approach, by about a factor of 2 across all p_t. This factor approximately reflects the difference at the level of the friction coefficient, $A(p)$.

As mentioned earlier, both TAMU and Nantes groups are able to describe experimental observations of HF $R_{\rm AA}$ and v_2 with some success using the pertinent transport coefficients within their respective bulk evolution models (although the T-matrix model tends to underestimate the observed high-p_T suppression), within their respective bulk evolution and hadronization models. The differ-

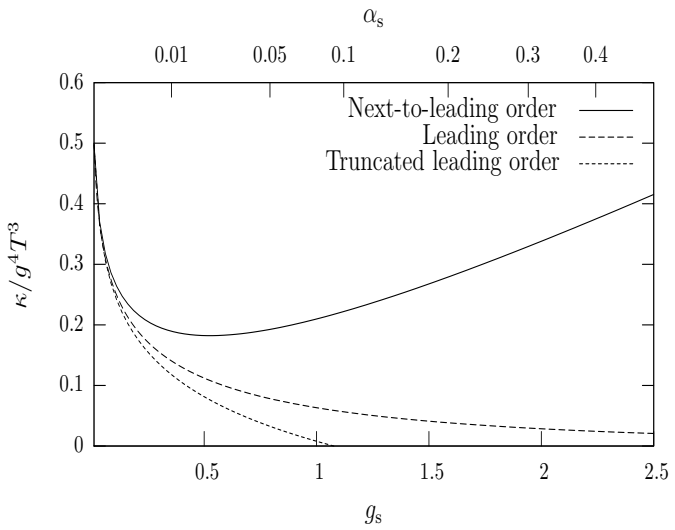

Figure 20: Comparison of leading and next-to-leading order inverse heavy-quark diffusion coefficient, $\kappa/T^3 = 2/(\mathcal{D}_s T)$, scaled by the leading-order coupling constant dependence. The subleading corrections are large even at coupling values usually considered to be very small.

ence in their results for the same bulk evolution thus implies significant differences in other modeling components, most notably in the coalescence part (as discussed in Secs. 4.1 and 4.2), and, to a lesser extent, in the evolution profiles from the different hydrodynamic models used by the two groups (as discussed in Sec. 3.2).

5.3 Perturbative Analysis

In this section we discuss perturbative treatments of the momentum diffusion of heavy quarks in a thermal medium. In doing so, we assume that $T \gg \Lambda_{QCD}$ so that the QCD coupling α_s is small. It is not clear that this approximation is useful at physically achievable temperatures. This issue can be resolved by working beyond leading order (LO), to see the size of next-to-leading order (NLO) corrections.

A perturbative calculation of heavy quark transport is not as simple as a low-order diagrammatic evaluation. Since the diffusion constant is defined in terms of low frequency, long-distance behavior, the evaluation requires diagrammatic resummations, similar to the evaluation of shear viscosity [92]. The situation simplifies if one uses the large quark mass $m^2 \gg T^2$, which ensures that the typical momentum carried in equilibrium is also large, $p^2 \sim mT \gg T^2$. Therefore one can instead compute the momentum diffusion coefficient, and convert it to a spatial momentum diffusion coefficient using Einstein relations.

Benjamin Svetitsky provided the first complete leading-order perturbative treatment of heavy-quark diffusion [3], finding [3, 93–95]

$$\mathcal{D}_s = \frac{27}{16\pi\alpha_s^2 T}\left[3\left(\ln\frac{2T}{m_D}+\frac{1}{2}-\gamma_E+\frac{\zeta'(2)}{\zeta(2)}\right)+\frac{N_f}{2}\left(\ln\frac{4T}{m_D}+\frac{1}{2}-\gamma_E+\frac{\zeta'(2)}{\zeta(2)}\right)\right]^{-1}, \tag{5}$$

where $m_D = T\sqrt{6\pi\alpha_s}$ and N_f is the number of light-quark flavors (3 in most applications). This was extended to finite quark velocity by Moore and Teaney [95].

In a pioneering work, Caron-Huot and Moore extended the calculation of the heavy quark diffusion coefficient to NLO in the strong coupling [96]. The first corrections arise from the soft sector ($p \sim m_{\rm D}$), at order $\mathcal{O}(\sqrt{\alpha_{\rm s}})$, that is, they are non-analytic in the strong coupling $\alpha_{\rm s}$. Rather than discuss the very technical calculation, we will skip to providing the result, which is

$$\mathcal{D}_s^{\rm NLO} = \frac{27}{16\pi\alpha_{\rm s}^2 T}\left(\left[3+\frac{N_{\rm f}}{2}\right]\left[\ln\frac{2T}{m_{\rm D}} - 0.64718\right] + \frac{N_{\rm f}\ln(2)}{2} + 2.3302\frac{3m_{\rm D}}{T}\right)^{-1}, \tag{6}$$

where the last expression, with numerical coefficient 2.3302, represents the NLO corrections.

We illustrate this result in Fig. 20. As the figure shows, for realistic couplings $\alpha_{\rm s} \simeq 0.3$, the "subleading" corrections are several times larger than the leading order behavior. It appears that the perturbative expansion for this quantity is especially poorly behaved. A key reason for this is that the LO of the HQ thermalization rate is already $\mathcal{O}(\alpha_s^2)$, implying that higher orders come in with a larger uncertainty as compared to quantities whose LO is $\mathcal{O}(1)$ (such as the QGP pressure or dilepton rate). This makes it difficult to make much progress in computing the medium's effects on heavy quarks purely with perturbative tools.

5.4 Functional Renormalization Group

A continuum approach for non-perturbative computations of transport coefficients on the basis of single-particle spectral functions of quarks and gluons, ρ_A and ρ_q, has been put forward in Ref. [97]. It has been used for the shear viscosity in in quenched QCD [97, 98], with in-medium gluon propagators obtained with functional renormalization group (FRG) techniques. For high temperatures the results compare well with hard-thermal-loop (HTL) results. This agreement extends to surprisingly low temperatures, $T \gtrsim 2T_c$, and is supported by diagrammatic similarities of the (resummed) perturbative approach to the fully non-perturbative setting. At temperatures below T_c the result is compatible with the viscosity in a glueball resonance gas. Within this approach the diagrammatic similarities of standard perturbative resummation schemes with the fully non-perturbative diagrammatics is apparent. In the case of two-point correlation functions of the energy momentum tensor it leads to a seven-loop exact formula that can be reduced to three-loop resummed expressions in terms of full vertices and propagators [97, 98].

For the computation of the heavy-quark diffusion coefficient, an analogous starting point is the relation of the momentum diffusion coefficient, κ, to the force-force correlator,

$$\kappa = \int dt \langle F(t)F(0)\rangle\,, \qquad \text{with} \qquad F[q,A](t) = \int d^3\bar{q}(t,\vec{x})t^a E_y^a(t,\vec{x})q(t,\vec{x})\,, \tag{7}$$

see, *e.g.* [3, 99]. This correlation can be approximated by that of two chromo-electric fields connected by Wilson lines. In the present approach it is more convenient to directly compute the correlation function, eq. (7). The latter has a seven-loop exact representation given by

$$\kappa = \int dt F[\hat{q},\hat{A}](t)\,F[\hat{q},\hat{A}](0)\,, \qquad \text{with} \qquad \hat{A}_\mu = \langle A_\mu\phi\rangle_c\frac{\delta}{\delta\phi} + \phi\,, \qquad \phi = (A_\mu, q, \bar{q})\,, \tag{8}$$

where the subscript $_c$ indicates the connected part. The real-time two-point functions, $\langle\phi_1\phi_2\rangle_c$, can be expressed through the respective single-particle spectral functions of quarks and gluons in QCD. These can be either computed directly or with the help of MEM-type methods from Euclidean correlation functions. In the latter approach the largest systematic error arises from the low-frequency tail of the

reconstructed real-time correlation functions. In the present diagrammatic approach this systematic error is averaged over via the frequency loop-integrals [97, 98]. Both methods, the direct computation and the reconstruction, have been applied in QCD and low-energy effective models [97, 98, 100–104], and the respective results can be used for the computation of the diffusion coefficient.

As mentioned above, this approach bears diagrammatic similarities to the standard perturbative approach described in Sec. 5.3. For example, the lowest order contribution in eq. (8) arises from diagrams with two quark and one gluon spectral function (lines) between the F's. In particular, this similarity can be used to discuss the convergence of the perturbative approach as well as its regime of validity. A particularly simple example for this structure is the Debye mass which agrees in next-to-leading order with the full non-perturbative result for temperatures $T \gtrsim 2T_c$ [105]. The failure for temperatures $T \lesssim 2T_c$ can be readily explained by the influence of the non-perturbative confinement physics and scale at these temperatures.

In future the combination of these approaches will also allow for functionally assisted analytic computations: the perturbative setting allows for analytic computations while the non-perturbative approach is used to access and determine the validity regime of the (resummed) perturbative approach.

5.5 Information and Constraints from Lattice QCD

QCD calculations can contribute to understanding of heavy-flavor production in hot medium in several different ways. Lattice-QCD can provide some information on the heavy quark diffusion coefficient. These calculations can be compared to the calculations based on a weak-coupling expansion, which are valid are sufficiently high temperature. Diagonal and off-diagonal charm susceptibilities can provide information on the charm degrees of freedom across the QCD transition. Finally, spatial and temporal correlators provide information on in-medium properties of charm hadrons and/or about their dissolution in hot medium. Below we will discuss the status of these calculations in more detail.

5.5.1 Heavy-quark diffusion coefficient

The spatial HQ diffusion coefficient can be defined in terms of spectral functions corresponding to current-current correlators of heavy quarks

$$\sigma(\omega,\vec{p}) = \frac{1}{\pi}\int dt e^{i\omega t}\int d^3x e^{i\vec{x}\cdot\vec{p}}\langle[J_i(t,\vec{x}),J_i(0,0)]\rangle, \tag{9}$$

where $J_i = \bar{\psi}_h\gamma_i\psi$ with ψ_h being the heavy quark field. The spatial diffusion coefficient is defined as

$$\mathcal{D}_s = \lim_{\omega\to 0}\sigma(\omega,\vec{p}=0)/(\omega\chi_q\pi). \tag{10}$$

Here χ_q is the quark number susceptibility for heavy quarks. In the case of a large quark mass, $M \gg T$, the structure of the spectral function has a simple form for $\vec{p}=0$:

$$\sigma(\omega,0) = \frac{1}{\pi}\chi_q\frac{\omega\eta}{\omega^2+\eta^2}\frac{T}{M}, \tag{11}$$

where $\eta = T/(M\mathcal{D}_s)$ is drag coefficient entering the Langevin equation [106] ($\tau_Q = 1/\eta$ is the thermal HQ relaxation time). In other words, for zero spatial momentum the spectral function has a transport peak at $\omega \simeq 0$. For $p \ll T$ the structure of the spectral function can be worked out and it is determined by the same constant η [106], *i.e.*, for small momenta there is no dependence of the drag

coefficient on the momentum. As one can see from Eq. (11) the width of the transport peak is very small for large quark mass. This makes the lattice determination of the HQ diffusion coefficient very challenging [106, 107]. However, the difficulty associated with the large quark mass can be turned into an advantage. Namely, one can integrate out the HQ degrees of freedom in the spirit of HQ effective theory and reduce the current-current correlator to the correlator of the chromo-electric field strength [108]. The corresponding spectral function in the $\omega \to 0$ limit gives the momentum diffusion coefficient $\kappa = 2MT\eta$ [108]. Furthermore, this spectral function does not have a peak around $\omega = 0$, instead the high-ω and the low-ω regions are smoothly connected [108, 109]. From the point of view of reconstructing the spectral function from the lattice data this has a clear advantage since for determination of κ one has to determine the intercept rather than the width of the transport peak, and therefore the lattice determination of κ may be more easily feasible. Lattice determinations of κ in quenched QCD have been reported in Refs. [110, 111]. A prerequisite for the determination of the transport coefficient κ is sufficiently accurate data for the electric field strength correlator. Due to gluonic nature of the correlation functions the lattice data are very noisy and the use of noise reduction techniques is mandatory [110, 111]. In addition one has to perform calculations at several lattice spacings and perform a continuum extrapolation. This step has so far been performed only in Ref. [111]. Given the lattice data one relies on a fit ansatz that smoothly connects the known high-ω asymptotics of the spectral function with the form $\kappa\omega$ for small ω. This ansatz is not unique and the use of different ansätze translates into systematic errors in the determination of κ. The detailed analysis of Ref. [111] results in a value of

$$\kappa/T^3 = 1.8 - 3.4. \tag{12}$$

for $T = 1.5\,T_c$ (where $T_c \simeq 270\,\mathrm{MeV}$ for quenched QCD). This corresponds to a range of values for $2\pi T\mathcal{D}_s$ of 3.7-7.0. This result agrees with findings presented in Ref. [110] at fixed lattice spacing within errors. It is also comparable to the value of ∼6 from the "pQCD*5" interaction employed in the various bulk and hadronization models discussed in Secs. 3 and 4.

Attempts to determine the spatial HQ diffusion coefficient from current-current correlators have been presented in Ref. [112] in quenched QCD:

$$2\pi T\mathcal{D}_s = 1.8 \pm 0.5(stat.)^{+1.3}_{-0.5}(syst.), T = 1.46T_c. \tag{13}$$

This is significantly smaller than the value of $\mathcal{D}_s$ reported above. Note, however, that not all systematic effects have been taken into account in this analysis. As discussed before it is difficult to determine reliably the width of the transport peak.

For phenomenological applications it would be important to perform calculations in full QCD. With the current technology this is not possible since the noise reduction techniques are only available for quenched QCD. One possible way to deal with noise in full QCD would be to use a gradient-flow method [113–116].

The formulation of the HQ diffusion in terms of electric field strength correlators, or equivalently in terms of force-force correlators acting on the heavy quark, turned out to be very useful when calculating the momentum diffusion coefficient in the weak coupling expansion [96] or in AdS/CFT [99]. The value of κ from the lattice calculation given by Eq. (12) is in the range of the NLO weak coupling result of Ref. [96] shown in Fig. 20 if the value of $\alpha_s \simeq 0.26$ is used; however, as emphasized in Sec. 5.3, the perturbative series is badly convergent at even smaller values of the coupling. Weak-coupling

techniques could still be useful to better constrain the shape of the spectral function of the chromo-electric field strength at intermediate frequencies. Since these do not involve the $\omega \to 0$ limit they could be useful to guide analyses of lattice calculations.

5.5.2 Charm fluctuations and correlations and charm degrees of freedom in hot matter

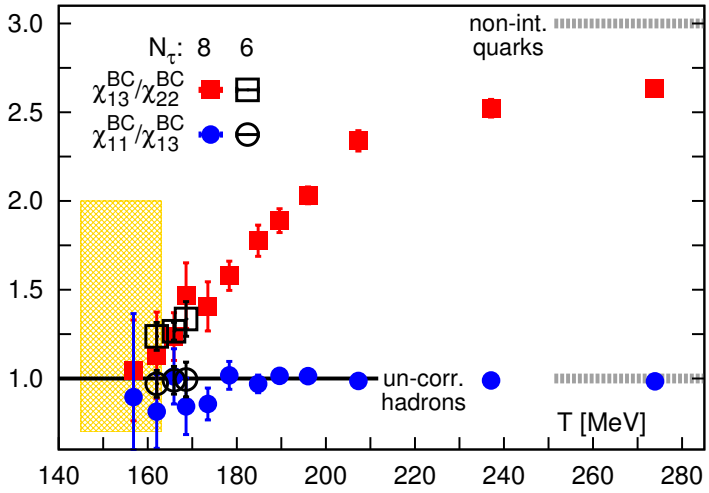

Figure 21: Ratio of baryon number charm correlations as functions of temperatures. The horizontal lines correspond to HRG and to quark gas. The ratio of correlations involving the same number of derivatives in baryon chemical potential but same number of derivatives with respect to charm chemical potential are always one because sectors with $|C| = 2, 3$ do not contribute because of the large charm-quark mass [117].

Derivatives of the QCD pressure with respect to the chemical potential,

$$\chi_n^X = T^n \frac{\partial^n (p(T, \mu_X, \mu_Y)/T^4)}{\partial \mu_X^n} \tag{14}$$

$$\chi_{nm}^{XY} = T^{n+m} \frac{\partial^{n+m} (p(T, \mu_X, \mu_Y)/T^4)}{\partial \mu_X^n \partial \mu_Y^m} \ , \tag{15}$$

define fluctuations of a conserved charge X or correlations between conserved charge X and conserved charge Y. These have been calculated on the lattice including the case of charm $X = C$ [117]. Fluctuations and correlation of conserved charges are sensitive to deconfinement and provide information on the relevant degrees of freedom. At low temperature the fluctuations and correlations can be understood in terms of hadron resonance gas (HRG) model [117–119], while at high temperatures they can be understood in terms of quark degrees of freedom [117, 120–122]. This is demonstrated in Fig. 21 in terms of baryon number charm correlations. In fact these correlations together with charm fluctuations χ_2^C can clarify the nature of charm degrees of freedom. Below T_c charm fluctuations and correlations can be described in terms of HRG (cf. Fig. 21). Above T_c the partial pressure of the charm degrees of freedom can be written as sum of partial pressures of charm mesons, charm baryons and charm quarks [123]. Using lattice data on χ_2^C, χ_{22}^{BC} and χ_{13}^{BC} one can obtain the partial pressures of charm quarks, $p_q(T)$, charm mesons, $p_M(T)$, and charm baryons, $p_B(T)$, which are shown in Fig. 22. At T_c the partial baryon and meson pressures agree with HRG prediction, while the partial charm-quark pressure is consistent with zero within errors. As the temperature increases the partial meson pressure

and baryon pressure decrease and become very small for $T > 200$ MeV. This can be interpreted as gradual melting of charm hadrons above T_c. The important point here, however, is that hadron like excitations in the open charm sector may exist above T_c. Quarks dominate the charm pressure only for $T > 200$ MeV. At these temperatures charm quark properties, like in-medium mass and width can be extracted from charm fluctuations, χ_2^C, see Ref. [124]. As shown there the quasi-particle model with T-dependent effective charm-quark mass works well [124].

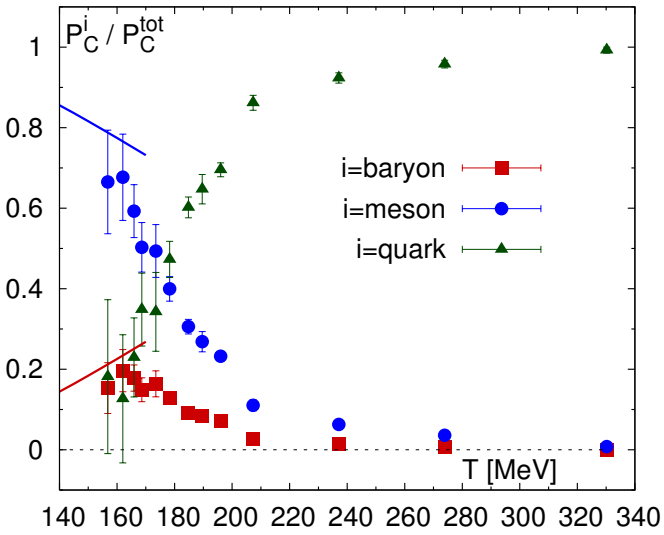

Figure 22: The partial pressure of charm quarks, charm mesons and charm baryons, normalized by the total charm pressure, as function of the temperature [123].

5.5.3 Charm meson correlators

Properties of charm hadrons are encoded in the spectral functions. Temporal and spatial correlators that can be calculated in lattice QCD are related to the spectral functions. The temporal correlators are simple periodic Laplace transformations of the spectral functions. Therefore, many attempts to reconstruct the spectral functions by using a Bayesian approach have been presented in the literature, mostly focusing on hidden heavy-flavor mesons (see, *e.g.*,, Ref. [125]). Due to the fact the the temporal meson correlators are defined only for Euclidean time separation $\tau < 1/(2T)$ there is a limited sensitivity to the in-medium modification of the spectral functions [86, 107, 126].

Alternatively, one can consider spatial meson correlation functions, which seem to be much more sensitive to the in-medium modifications of the spectral functions [127]. However, the relation of the spatial meson correlators to the spectral functions is more complicated. It is given by a double integral transformation [127]. Nevertheless, some qualitative information on the in-medium modifications of the open-charm mesons can be obtained. It turns out that open-charm meson spectral functions are modified already below T_c [127]. The in-medium modifications are large above T_c, and for $T > 250$ MeV the spatial meson correlators are compatible with the propagation of an uncorrelated quark anti-quark pair, *i.e.*, with the dissolution of D-meson states. This is consistent with the findings of the previous section based on baryon charm correlations.

First attempts to study D-meson spectral functions have been presented in Ref. [128] and the findings are in agreement with the study of spatial correlators.

5.6 Boltzmann vs. Langevin

In this section we compare the two transport implementations for HF propagation through QCD matter that have been most widely employed at low and intermediate momenta, *i.e.*, Boltzmann (BM) and Langevin (LV) approaches. In particular, we will elaborate on both benefits and drawbacks of both schemes.

5.6.1 Fokker-Planck and Boltzmann transport equations

The Boltzmann equation for the HQ distribution function can be written in a compact form as:

$$p^\mu \partial_\mu f_Q(x,p) = \mathcal{C}[f_q, f_g, f_Q](x,p) \tag{16}$$

where $\mathcal{C}[f_q, f_g, f_Q](x,p)$ is the relativistic Boltzmann-like collision integral where the phase-space distribution function of the bulk medium f_q, f_g can be evaluated solving the Boltzmann-equation also for quarks and gluons [129, 130].

It is well known that the relativistic collision integral for two-body collisions can be written in a simplified form [3, 6] in the following way:

$$\mathcal{C}[f_Q] = \int d^3q \, [\, w(\mathbf{p}{+}\mathbf{q}, \mathbf{q}) f_Q(x, p+q) - w(\mathbf{p}, \mathbf{q}) f_Q(x,p)] \tag{17}$$

where $w(\mathbf{p}, \mathbf{q})$ is the rate of collisions of a heavy quark per unit of momentum phase space which changes the its momentum from **p** to **p-q**. It is directly related to the scattering matrix $\mathcal{M}_{(q,g)+Q\to(q,g)+Q}$:

$$w(\mathbf{p}, \mathbf{q}) = \frac{1}{128\,\pi^2} \int \frac{d^3k}{(2\pi)^3} \, f_{q,g}(x,p) \, \frac{|\mathcal{M}_{(q,g)Q}|^2}{E_p \, E_k \, E_{p-q} \, E_{k+q}} \, \delta^0(E_p + E_k - E_{p-q} - E_{k+q}) \tag{18}$$

we recall that the scattering matrix is the real kernel of the dynamical evolution for both the Boltzmann approach and the Fokker-Planck one. Of course all the calculations discussed in the following will originate from the same scattering matrix for both cases.

The non-linear integer-differential Boltzmann equation can be significantly simplified employing the Landau approximation whose physical relevance can be associated to the dominance of soft scatterings with momentum transfers, $q = |\mathbf{q}|$, which are small compared to the particle momentum, p. Namely, one expands $w(\mathbf{p}{+}\mathbf{q}, \mathbf{q}) f(x, p+q)$ around q,

$$w(\mathbf{p}+\mathbf{q}, \mathbf{q}) f_Q(\mathbf{x}, \mathbf{p}{+}\mathbf{q}) \approx w(\mathbf{p}, \mathbf{q}) f(\mathbf{x}, \mathbf{p}) + q_i \frac{\partial}{\partial p_i}(\omega f) + \frac{1}{2} q_i q_j \frac{\partial^2}{\partial p_i \partial p_j}(\omega f) \tag{19}$$

and inserts this into the Boltzmann collision integral, Eq.(17), to obtain the Fokker-Planck Equation:

$$\frac{\partial f}{\partial t} = \frac{\partial}{\partial p_i} \left[A_i(\mathbf{p}) f + \frac{\partial}{\partial p_j} [B_{ij}(\mathbf{p})] \right] \, . \tag{20}$$

The transport coefficients defined by $A_i = \int d^3q \, w(\mathbf{p}, \mathbf{q}) q_i = A(\mathbf{p}) p_i$ and $B_{ij} = \int d^3q \, w(\mathbf{p}, \mathbf{q}) q_i q_j$ are directly related to the so-called drag (γ) and momentum diffusion coefficient (D_p) that are determined by the underlying scattering matrix figuring in the transition probabilities, $w(\mathbf{p}, \mathbf{q})$.

In a locally isotropic medium, the diffusion tensor B_{ij} can be reduced to two independent components that determine the diffusion in the directions transverse and longitudinal relative to the HQ momentum, B_0 and B_1, respectively:

$$B_0 = (\delta_{ij} - \frac{p_i p_j}{p^2}) \, B_{ij} \quad , \quad B_1 = \frac{p_i p_j}{p^2} \, B_{ij} \tag{21}$$

In principle, the 3 transport coefficients are related to each other through the dissipation fluctuation theorem (DFT), leaving two independent ones. In practice, especially at high momenta, this is not readily satisfied which limits the applicability of the Fokker-Planck approximation. Therefore, to ensure the HQ distribution to converge to the correct the equilibrium distribution, $f_{eq}(p) = e^{-E/T}$, most of the groups have enforced the Einstein relation by expressing B_1 through $A(p)$. The deviations from using the explicitly calculated coefficients can serve as a quality check of the approximation [88]. For the following study, we adopt the same implementation as in the calculations reported in Secs. 3 and 4, *i.e.*, the drag (A) and transverse diffusion (B_0) coefficients are calculated from the pQCD*5 matrix elements and the longitudinal one is adjusted to $B_1 = TEA$ within the post-point Ito scheme of realizing the Langevin process.[5] The Boltzmann equation is solved numerically by dividing coordinate space into a three-dimensional lattice and using the test particle method to sample the distributions functions. The collision integral is solved by mean of a stochastic implementation of the collision probability [129–131].

Before turning to the numerical results in the following section, we recall that the semi-classical nature of the Boltzmann equation implies that the surrounding medium consists of well-defined quasi-particles, *i.e.*, quantum effects inducing a finite energy resolution for a given momentum state are neglected. However, the Fokker-Planck equation, realized via a more general Langevin process, does not rely on this assumption; the underlying transport coefficients can be evaluated with the full off-shell effects included in the medium's spectral function [87, 132–134]. This situation may be relevant for a strongly coupled QGP where strong quantum effects due to intense rescattering among the medium particles could render the Langevin approach preferrable over the Boltzmann one, provided the HQ mass is large enough to warrant a soft-interaction approximation while maintaining the heavy quark a good quasi-particle.

5.6.2 Numerical Results Comparing Boltzmann and Langevin Simulations

To investigate the differences that arise from the two different transport implementations, we report test calculations performed with simple LO pQCD HQ scattering matrix elements in two versions (a) with a constant coupling $\alpha_s = 0.4$ and K factor, similar to what was done for the comparisons in Sec. 3, as well as for a quasiparticle model (QPM) [84]. We will consider four values for the HQ mass, corresponding to values for charm (M_Q=1.3 GeV) and bottom quarks (M_Q=5 GeV), and two intermediate values (M_Q=2 and 3 GeV). We expect that the differences between the Boltzmann and the Langevin dynamics are regulated by the ratio M_Q/T, but a key role is also played also by the differential cross section that determines the momentum transfer per collision [135] as well as the masses of the medium particles (assumed to be massless for the pQCD case (which differs from the studies in Sec. 3) and massive for the QPM).

During the expansion of the QGP matter in AA collisions, M_Q/T increases by about a factor of three due to the wide range of temperatures explored by the expanding QGP matter (*e.g.*, $T\simeq$160-500 MeV at the LHC), and an additional amount due to a variation of the in-medium HQ masses,

[5] The BM vs. LV comparison can, in fact, help to assess different implementations of the Einstein relation (or DFT) which is usually not automatically satisfied for a given model calculation of the different transport coefficients. It turns out that employing the friction coefficient, A, from the model calculation to enforce the DFT for the longitudinal diffusion coefficient (as done here) results in better agreement with the BM results than, *e.g.*, using the calculated B_1 and readjust A (and B_0); typically, the calculated A and B_0 are better compatible with the DFT than B_1 in relation to A or B_0.

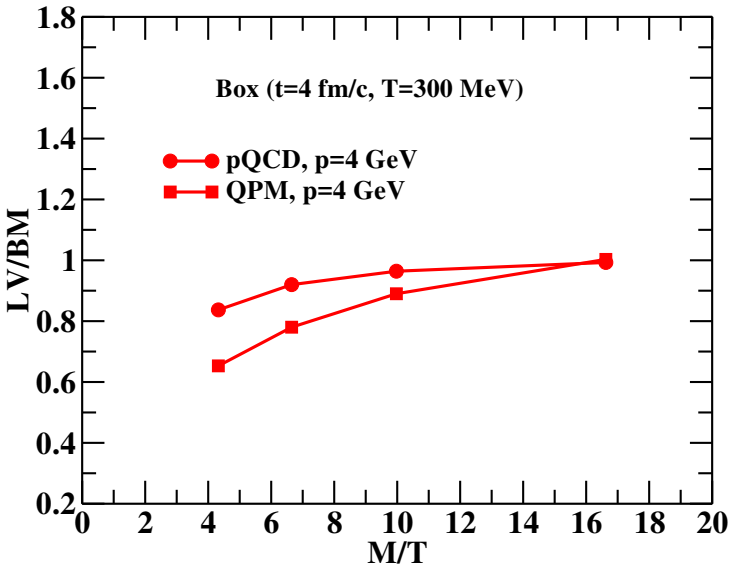

Figure 23: Ratio of the HQ $R_{\rm AA}$ in a Langevin simulation over that in a Boltzmann simulation for HQ transport in a massless QGP in a box at fixed temperature, T=300 MeV, recorded after an evolution time of t=4 fm for a value of p=4 GeV of the HQ momentum. The results are plotted as a function of the HQ mass scaled by temperature, and the different symbols correspond to different underlying HQ interactions with medium partons.

usually leading to an increase of the mass as $T_{\rm c}$ is approached from above (*e.g.*, from m_c=1.3 GeV to 1.8 GeV [86]), which augments the range of the M_Q/T values to ∼3-11). A study as a function of M_Q/T is therefore most transparent if carried out in a box of bulk matter at fixed T with periodic boundary conditions. Toward this end we have performed a calculation in a box at T=300 MeV for different M_Q/T values for the case of an underlying scattering matrix in the HQ scattering off the medium partons from (a) a "pQCD*3" scenario (similar to Sec. 3.2 with $\alpha_s = 0.4$ and $m_D = gT$ (corresponding to $m_D \simeq 0.67$ GeV), but with massless medium partons and a K-factor of 3 to reproduce the same charm-quark diffusion coefficient as in the pQCD*5 scenario (which uses massive partons), and (b) a QPM with $\alpha_s \simeq 0.62$ and m_D=0.85 GeV in a medium of massive partons with m_g=0.69 GeV and m_q=0.46 GeV. In Fig. 23 we show the ratio of the momentum distribution, $LV/BM = f_{LV}(p,t_f)/f_{BM}(p,t_f)$, at a time t_f=4 fm, determined such that $R_{AA} \approx 0.4$ for the BM case, in the range of what has been found in Sec. 3.2, recall. Fig. 12. This condition is chosen with the aim of comparing BM and LV dynamics under conditions that mimic the one observed experimentally, even if we are considering a bulk matter at fixed T.

For both HQ interactions, the b-quark case leads to negligible deviations in the HQ R_{AA} between Boltzmann and Langevin simulations. For the pQCD*3 case (filled circles in Fig. 23), also the lower M_Q/T values, in the range of possible c-quark masses near T_c, only lead to small to moderate deviations, in the 5-20% range. The filled squares, corresponding to the LV/BM ratio in the QPM model are larger, leading to a deviation of up to 35% for the smallest M_Q/T ratio of 4 (or ∼25% for M_Q/T=6.7 applicable for c quarks at lower temperatures, $T \leq$250 MeV). Here, the larger Debye

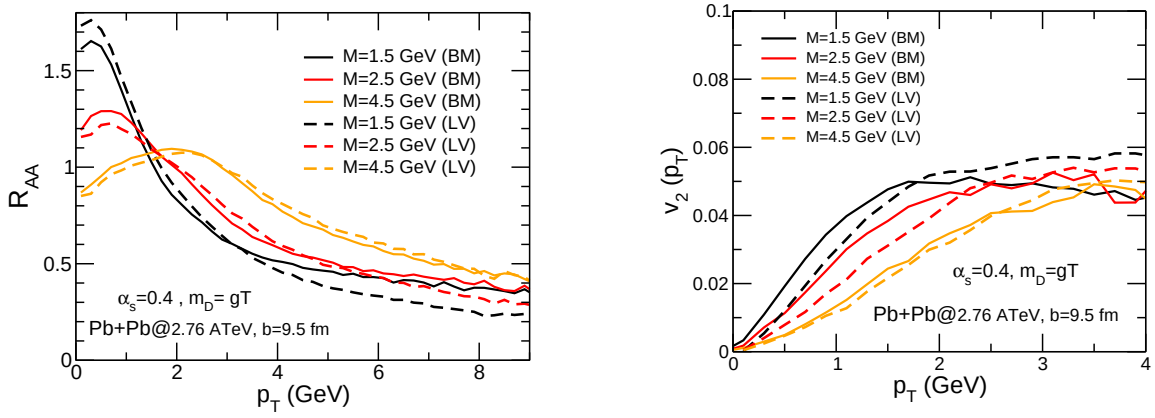

Figure 24: Nuclear modification factor (left panel) and elliptic flow (right panel) for heavy quarks in semi-central Pb+Pb($\sqrt{s_{NN}} = 2.76\,\mathrm{TeV}$) collisions (at $b = 9.5\,\mathrm{fm}$) for different values of the HQ mass, M_Q (indicated by the different line colors), in a Boltzmann (solid lines) and in a Langevin approach (dashed lines).

mass, m_D, and the heavier medium scattering centers in the QPM, relative to the (massless) pQCD*3 scenario, lead to a differential scattering cross section which is more isotropic which affects the small-momentum transfer approximation in the Langevin process. We also note that the differences are expected to become smaller again at lower momenta and larger times as the HQ distributions get closer to the universal equilibrium limit which is of course realized in both BM and LV approaches.

Finally, a comparison has been made under conditions of a more realistic simulation for Pb+Pb($\sqrt{s_{NN}}$=2.76 TeV) collisions at impact parameter b=9.5 fm, as were considered in Sec. 3 for the 30-50% centrality class, using the same underlying scattering matrix as employed there, *i.e.*, LO pQCD with $\alpha_s = 0.4$. In Fig. 24 the pertinent nuclear modification factor and elliptic flow are plotted for heavy quarks of varying mass at the end of the QGP phase. Boltzmann transport generally leads to a larger R_{AA} relative to Langevin dynamics. For a mass of $M_Q = 1.5\,\mathrm{GeV}$ corresponding to charm quarks, the R_{AA} from BM is about 25-30% larger in the intermediate p_t region where it tends to saturate. On the other hand, the elliptic flow is slightly larger for BM dynamics at low p_t but smaller at high p_t. For bottom quarks, both $R_{AA}(p_t)$ and $v_2(p_t)$ are nearly identical in the two approaches. In general, the deviations become larger with increasing p_t as the Gaussian distribution in the energy loss underlying the Langevin approximation becomes less accurate while the BM approach captures the full differential distribution following from the microscopic scattering matrix element. In addition, one expects radiative contributions to become relevant, whose interferences effects are not easily captured in either BM or LV descriptions. The differences increase slightly for more central collisions, as can be expected for a longer duration of the QGP medium. While there are no significant differences of R_{AA} and v_2 for bottom quarks, some difference can arise for more exclusive observables, *e.g.*, angular correlations between B and $\bar{B}$ [136].

6 High-p_T Energy Loss and $\hat{q}$

In this section we discuss various aspects pertaining to the description of high-p_T heavy quarks propagating through the QGP. While the previous sections focused on elastic interactions which are parametrically dominant at low p_T, radiative processes are expected to become dominant at high p_T. The understanding of the transition between the two regimes is an important ingredient for quantifying the temperature and momentum dependence of HQ transport coefficients. In Secs. 6.1 and 6.2 we discuss basic ingredients to, and definitions of, high-p_T transport coefficients, most commonly quantified via the average transverse-momentum transfer per mean-free-path, $\hat{q}$. In Secs. 6.3 and 6.4 we discuss two different state-of-the-art approaches to high-energy HQ energy loss (which include radiative contributions and their coherence), and in Sec. 6.5 we compare their results for the path length dependence of the fractional energy loss to other implementations used in HF phenomenology.

6.1 Transverse momentum broadening and QGP properties

Different approaches to calculating the non-abelian parton energy loss are available in the literature [137–141]. The medium-induced radiative spectrum generally depends on the multiple scattering of the propagating parton in the medium and the transverse-momentum transfer distribution in the scatterings. These can be schematically expressed as $\int d\Delta z \;\; 1/\lambda_g(z) \cdots$ and $\int d^2\mathbf{q}_\perp \;\; 1/\sigma_{el} d\sigma_{el}^{\rm med}/d^2\mathbf{q}_\perp \cdots$, respectively. Note that for soft gluon emission in the eikonal limit only the gluon scattering length enters the expression for the medium-induced radiative spectrum. It is obvious that without further approximations this spectrum depends on $\lambda_g(z)$ and the typical inverse range of the interaction, $m_D \sim 1/r_D$.

There are several possibilities for relations between the interaction length and the momentum transfer from the QCD medium.

- The interaction length and momentum transfer are largely independent, providing a 2D parameter space. Such a scenario would require rather involved multi-parameter fits to data and has not been explored so far in the literature.

- Assuming local thermal equilibrium, density and temperature can be related at any space time point. The range of the interaction and parton scattering cross section can be estimated and depend on the typical coupling between the jet and the medium gluon. The interaction length is then obtained form the QGP density and the scattering cross section [139].

- One can use thermal field theory to relate the relevant medium parameters to the temperature T. This is similar to the situation described in the previous item, but without explicitly evaluating the scattering cross sections and densities [141].

- An approach to energy loss in the limit of infinite energies and infinite number of scatterings assumes that at *any scale* the transverse-momentum broadening of any size is given by a 2D Gaussian random walk [137, 138]. By discarding the detailed kinematic information that pertains to parton scattering one can relate the radiative intensity spectra to the transport parameter as $\hat{q} \sim m_D^2/\lambda_g$.

- In deep inelastic scattering the radiative spectrum can be related to higher-twist matrix elements of field operators [140]. The interaction length can be thought of as the inter-nucleon distance.

The application to the QGP case is by analogy.

The momentum broadening of a parton that propagates in dense QCD mater is often discussed in relation to parton energy loss. An impact parameter space resummation is used together with a small-impact parameter approximation of the Fourier transform of the differential scattering cross section. Although such an approach is analytically appealing, it gives jet distributions that may differ substantially from the exact formula [142]. Let us elaborate on this in more detail. The normalized elastic cross section (triggering a gluon emission) in Fourier space can be written as

$$\frac{d\tilde{\sigma}_{el}}{d^2\mathbf{q}}(\mathbf{b}) = \int \frac{d^2\mathbf{q}}{(2\pi)^2}\, e^{-i\mathbf{q}\cdot\mathbf{b}} \frac{1}{\pi}\frac{m_D^2}{(\mathbf{q}^2+m_D^2)^2} = \frac{m_D\, b}{4\pi^2} K_1(m_D\, b) \approx \frac{1}{4\pi^2}\left(1 - \frac{\xi\, m_D^2\, b^2}{2} + \mathcal{O}(b^3)\right) \,, \qquad (22)$$

where $b = |\mathbf{b}|$ is the magnitude of the impact parameter vector; in the quadratic term in Eq. (22) a factor $\log[2/(1.08\, m_D\, b)]$ has been absorbed into a b-independent constant, ξ, which is the source of the leading logarithmic energy dependence in momentum space. Starting from a jet propagating in the "$\hat{z}$" direction, $dN^{(0)}/d^2\mathbf{p} = \delta^2(\mathbf{p})$, the approximation of large-number, small-impact parameter scatterings reduces the momentum space distribution to a classic Moliere form,

$$dN(\mathbf{p}) = \int d^2\mathbf{b}\; e^{i\mathbf{p}\cdot\mathbf{b}} \frac{1}{(2\pi)^2} \frac{e^{-\frac{\chi\, m_D^2\, \xi\, b^2}{2}}}{\chi\, m_D^2\, \xi} = \frac{1}{2\pi} \frac{e^{-\frac{p^2}{2\,\chi\, m_D^2\, \xi}}}{\chi\, m_D^2\, \xi} \,. \qquad (23)$$

The resulting distribution is of Gaussian form with a width of $\chi\, m_D^2\, \xi$. Within this Gaussian approximation the average broadening is

$$\langle \mathbf{p}^2 \rangle = 2\chi\, m_D^2\, \xi \,, \qquad \xi \sim O(1) \,.$$

The factor of 2 arises from the two-dimensional random walk. The opacity χ is the number of scatterings. With these caveats, for a non-expanding homogeneous medium a transport coefficient $\hat{q} = 2m_D^2/\lambda$ can characterize the typical *soft* momentum transfer between the jet and the medium.

In heavy-ion collisions it is not possible to define a model-independent length, as the medium has a varying density as a function of position and time. The Gaussian broadening result can be rewritten as

$$\langle \mathbf{p}^2 \rangle = \int \hat{q}(z)\, d\Delta z \,, \qquad \hat{q}(z) = 2\frac{m_D^2(z)}{\lambda_g(z)}.$$

Even though the transport parameter $\hat{q}$ alone does not even describe the simpler problem of transverse momentum broadening, the above definition captures properties of the medium without mixing in large logarithms of the jet energy. It should be noted that presently there exists no derivation of the strong-coupling constant renormalization in the presence of a medium. Therefore, the coupling constant in the above formulas is kept fixed.

One should not overrate the meaning of the quantitative values for $\hat{q}$ since they are rather model dependent. These values will differ at different space-time points $(x_\perp, \tau)$, as the density, temperature and transport properties depend on both the geometry and evolution of the medium. If averages are performed, the way in which different space-time points are weighted must be explicitly specified. The same applies to the temperature, Debye screening scale, interaction length and combinations thereof. Even in this case there will be residual dependences on the type of thermal QCD medium that is assumed, *e.g.*, a gluon-dominated plasma vs. a quark-gluon plasma, or the number of active quark flavors.

6.2 Energy dependence of the transport coefficient

In this subsection, we concentrate on a dynamical QCD medium, *i.e.*, the thermal motion and recoil of the constituents is accounted for. However, we note that the derivation and subsequent discussion is similar in the static medium case, so this section (with straightforward corrections) is applicable to static QCD medium as well.

In a dynamical QCD medium, the perturbative interactions between a high-energy parton and the QGP can be characterized by the HTL resummed elastic collision rate [143]

$$\frac{d\Gamma_{\rm el}}{d^2\mathbf{q}} = CT^3 \frac{\alpha_s^2}{\mathbf{q}^2(\mathbf{q}^2+m_D^2)} \ , \tag{24}$$

where $C = 4C_A(1+N_f/6)$ is a constant with C_A the value of the Casimir operator for the propagating parton and N_f the number of active light-quark flavors in the QGP.

The transport coefficient, *i.e.*, the average transverse-momentum transfer squared per mean-free-path, is then defined as

$$\hat{q} = \int^{q_{\rm max}} d^2\mathbf{q}\, \mathbf{q}^2 \frac{d\Gamma_{\rm el}}{d^2\mathbf{q}} \tag{25}$$

where $q_{\rm max} \approx 6ET$ is an ultraviolet (UV) cut-off. If coupling constant is assumed to be constant, $\hat{q}$ reduces to [143]

$$\hat{q} \approx CT^3\alpha_s^2 \ln(6ET/m_D^2). \tag{26}$$

As the transport coefficient is a *medium property* [143] that controls the parton energy loss, this parameter should not depend on the energy of the jet. However, from Eq. 26, we see that $\hat{q}$ has a logarithmic jet energy dependence.

A practical prescription to remove the energy dependence from the transport coefficient is to include the running of the strong coupling constant as in vacuum in the jet-medium interaction vertices. That is, if the running coupling is defined as in Ref. [144] (where Λ_{QCD} is the perturbative QCD scale),

$$\alpha_s(Q^2) = \frac{4\pi}{(11-2/3N_f)\ln(Q^2/\Lambda_{QCD}^2)}, \tag{27}$$

then Eq. (25) can be solved similarly to the procedure in Ref. [145], yielding

$$\hat{q} \approx CT^3\, \alpha_s(m_D^2)\, \alpha_s(6ET)\, \ln(6ET/m_D^2) \ , \tag{28}$$

which straightforwardly leads to

$$\hat{q} \approx CT^3\, \frac{4\pi}{(11-2/3N_f)}\, \alpha_s^2(m_D^2) \ . \tag{29}$$

Therefore, to leading logarithmic accuracy, this leads to a cancellation of the logarithmic terms that arise from the power-law tails of Moliere multiple scattering and consequently to a transport coefficient that does not depend on the jet energy.

6.3 Dynamical energy loss formalism

The dynamical energy loss formalism is an approach based on finite-temperature field theory with a hard-thermal loop (HTL) resummation that incorporates that the scattering partners in the QGP are dynamical (*i.e.*, moving) partons. Furthermore, it takes into account finite-size effects

of the medium as relevant for QGP droplets created in URHICs. The main ingredients of this model are: i) radiative [146, 147] and collisional [148] energy loss computed in the same theoretical framework (finite-size dynamical QCD medium), ii) magnetic-mass (non-perturbative) effects [149] in radiative energy loss, consistently included into the energy loss through a sum rule procedure, iv) a running coupling [150]. The model is implemented within a numerical procedure that takes into account parton production and fragmentation functions, as well as path length and multi-gluon fluctuations [150]. Additionally, the dynamical energy loss uses no fit parameters and is able to treat both light and heavy partons, so that it can provide predictions for an extensive set of observables. The details of the framework are briefly outlined below.

General framework

To calculate the quenched spectra of final hadrons, the formalism uses the generic pQCD convolution

$$\frac{E_f d^3\sigma}{dp_f^3} = \frac{E_i d^3\sigma(q)}{dp_i^3} \otimes P(E_i \to E_f) \otimes D(q \to H_q) \otimes f(H_q \to e, J/\psi) \; ; \tag{30}$$

the subscripts "i" and "f" correspond, respectively, to "initial" and "final", q denotes both quarks and gluons, while the different factors on the *rhs* mean the following:

(i) $E_i d^3\sigma(Q)/dp_i^3$ denotes the initial parton spectrum. The spectrum is extracted from Ref. [151] for gluons and light quarks, and from Ref. [9, 10] for charm and bottom quarks.

(ii) $P(E_i \to E_f)$ is the energy loss probability, generalized to include both collisional and radiative energy loss in a realistic finite-size dynamical QCD medium (a short review on the energy loss mechanism is given in the following subsection), as well as multi-gluon [142] and path length fluctuations [152].

(iii) $D(q \to H_q)$ is the fragmentation function of quark/gluon q to hadron H_q. We use DSS [153], BCFY [11] and KLP [154] fragmentation functions for light hadrons, D mesons and B mesons, respectively.

(iv) In the case of heavy quarks, there can also be a decay of hadron H_q into single electrons or J/ψ. This is represented by the functions $f(H_q \to e, J/\psi)$. The decays of D and B mesons to non-photonic single electrons, and decays of B mesons to non-prompt J/ψ are obtained according to Ref. [10].

In the dynamical energy loss calculations, the four steps outlined by Eq. (30) are treated separately, in the order defined by the above expression.

Assumptions

The following assumptions are used in the dynamical energy loss approach:

(i) The final quenched energy is sufficiently large so that the Eikonal approximation can be employed.

(ii) The radiative and collisional energy loss can be treated separately, so that the change of the spectrum can be first calculated due to radiative, and then due to collisional energy loss. This approximation is reasonable when collisional and radiative energy loss processes can be decoupled

from each other (which follows from the HTL approach [155] that is used in dynamical energy loss calculations) and when the radiative/collisional energy losses are sufficiently small (which is the essence of the soft-gluon, soft-rescattering approximation).

(iii) The parton-to-hadron fragmentation functions are the same for Pb+Pb and e^+e^- collisions; this is expected to be valid for hadronization outside the QGP.

(iv) Multiple gluon emissions can be independently treated in multi-gluon fluctuations. This is a reasonable assumption [156, 157] within (the above mentioned) soft-gluon approximation.

Energy loss calculations

The expression for the radiative energy loss in a finite-size dynamical QCD medium [146, 147], obtained within the HTL approximation, at 1^{st} order in opacity is given by:

$$\frac{\Delta E_{rad}}{E} = \frac{C_R\alpha_s}{\pi}\frac{L}{\lambda_{\rm dyn}}\int dx\frac{d^2k}{\pi}\frac{d^2q}{\pi}\,v(\mathbf{q})\left(1-\frac{\sin\frac{(\mathbf{k}+\mathbf{q})^2+\chi}{xE^+}L}{\frac{(\mathbf{k}+\mathbf{q})^2+\chi}{xE^+}L}\right)\frac{2(\mathbf{k}+\mathbf{q})}{(\mathbf{k}+\mathbf{q})^2+\chi}\left(\frac{(\mathbf{k}+\mathbf{q})}{(\mathbf{k}+\mathbf{q})^2+\chi}-\frac{\mathbf{k}}{\mathbf{k}^2+\chi}\right)\,. \quad (31)$$

Here, E is initial parton energy, L is the length of the QGP fireball, $C_R=\frac{4}{3}$ and $C_2(G)=3$; $\mathbf{k}$ and $\mathbf{q}$ denote transverse momenta of radiated and exchanged (virtual) gluons, respectively, $\chi\equiv M_q^2x^2+m_g^2$ where M_q is the bare quark mass and x is the longitudinal momentum fraction of the quark carried away by the emitted gluon; $m_g=m_D/\sqrt{2}$ is the effective (asymptotic) thermal mass for gluons with hard momenta $k\gtrsim T$ [158]; $\lambda_{\rm dyn}=(3\alpha_T)^{-1}$ is the mean-free-path in the dynamical QCD medium; $v(\mathbf{q})$ corresponds to the effective cross section, which for the case of finite magnetic mass [149], m_M, is given by:

$$v(\mathbf{q}) = \frac{m_D^2-m_M^2}{(\mathbf{q}^2+m_D^2)(\mathbf{q}^2+m_M^2)}\,, \quad (32)$$

reducing to a well-known HTL effective cross section [141, 146] in the case of zero magnetic mass:

$$v(\mathbf{q}) = \frac{m_D^2}{\mathbf{q}^2(\mathbf{q}^2+m_D^2)}\,. \quad (33)$$

In dynamical energy loss approach, Eq. (32) is dominantly used, since several non-perturbative approaches [159, 160], suggest that at RHIC and the LHC magnetic mass is different from zero, $0.4<m_M/m_D<0.6$.

Collisional energy loss, calculated in the finite-size dynamical QCD medium (*i.e.*, in a framework consistent with the radiative energy loss) is discussed in detail in Ref. [148]. For collisional energy loss, Eq. (14) from this reference is used (not spelled out here since it is rather lengthy).

Running coupling

The running coupling is defined as in Ref. [144]:

$$\alpha_s(Q^2) = \frac{4\pi}{(11-2/3N_f)\ln(Q^2/\Lambda^2_{QCD})}. \quad (34)$$

Here, N_f=2.5(3) is used at RHIC (LHC) and $\Lambda_{QCD}=0.2$ GeV as the perturbative QCD scale.

In the case of the running coupling, the Debye mass m_D [161] is obtained by selfconsistently solving the equation:

$$\frac{m_D^2}{\Lambda_{QCD}^2} \ln\left(\frac{m_D^2}{\Lambda_{QCD}^2}\right) = \frac{1+N_f/6}{11-2/3N_f}\left(\frac{4\pi T}{\Lambda_{QCD}}\right)^2 . \tag{35}$$

For the collisional energy loss, the coupling was introduced according to Ref. [145], while for the radiative energy loss the coupling was introduced according to Ref. [150].

Path length and multi-gluon fluctuations

Path length fluctuations take into account that partons can traverse different paths through the QGP fireball, while multi-gluon fluctuations take into account that the energy loss is a distribution.

For the radiative energy loss, the numerical method for including multi-gluon fluctuations is based on the approach developed in Ref. [142]. A generalization of this approach is developed for the dynamical energy loss case [150], which includes energy loss in a finite-size dynamical QCD medium, together with magnetic-mass and running-coupling effects.

For collisional energy loss, the full fluctuation spectrum is approximated by a Gaussian [95, 152]. The mean of the Gaussian is determined by the average energy loss and the variance by $\sigma_{coll}^2 = 2T\langle \Delta E^{coll}(E_i, L)\rangle$, where $\Delta E^{coll}(E_i, L)$ is given by Eq. (14) in Ref. [148].

Path length fluctuations are included in the energy loss probability according to [152]:

$$P(E_i \to E_f = E_i - \Delta_{rad} - \Delta_{coll}) = \int dL\, P(L)\, P_{rad}(\Delta_{rad}; L) \otimes P_{coll}(\Delta_{coll}; L) . \tag{36}$$

Here, $P(L)$ is the path length distribution extracted from Ref. [162] assumed to be the same for all parton varieties, as it corresponds to a geometric quantity.

6.4 Next-to-leading order calculation of heavy-flavor spectra in heavy-ion collisions

In the past several years new theoretical developments in the description of hard probes in heavy-ion collisions were enabled by the introduction of an effective theory of jet propagation in matter, the so-called Soft Collinear Effective Theory with Glauber Gluons, SCET$_{\rm G}$ [163, 164]. The collinear in-medium splitting functions, the building blocks in parton shower formation [165, 166], were obtained to first order in opacity. This allows for a unified description of vacuum and medium-induced branching. Applications so far, beyond the traditional energy loss approach, have been limited to light hadrons [167], jets [168] and jet substructure [168, 169].

An important step toward generalizing such a unified description to heavy flavor is to include quark masses into SCET$_{\rm G}$. The SCET$_{\rm M}$ Lagrangian with quark masses in the vacuum was obtained in Ref. [170]. The introduction of HQ masses requires a specific power counting, where $M_Q/p^+ \sim \lambda$ is of the order of the small power counting parameter in SCET. This is also consistent with the power counting for the dominant transverse-momentum component of the Glauber gluon exchange $\sim (\lambda^2, \lambda^2, \lambda)$. Hence, to lowest order, the new effective theory of HQ propagation in matter [171] is denoted as SCET$_{\rm M,G}$ =SCET$_{\rm M}\otimes$SCET$_{\rm G}$.

The three splitting processes where the heavy quark mass plays a role are $Q \to Qg$, $Q \to gQ$ and $g \to Q\bar{Q}$. Going beyond the energy loss limit of soft-gluon emission, a more careful consideration of

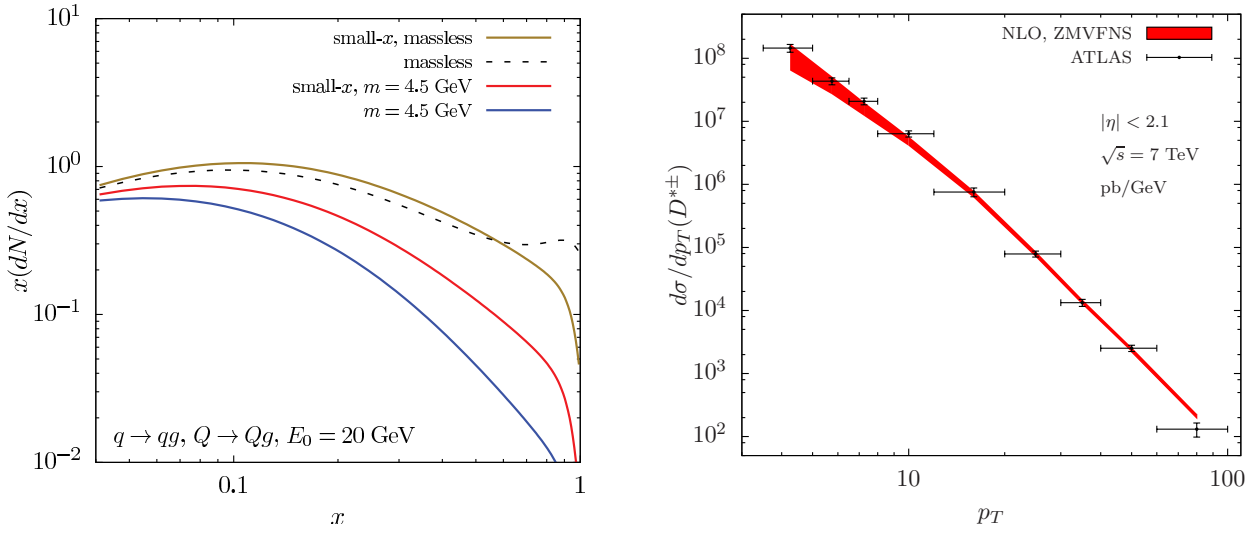

Figure 25: Left panel: comparison of the intensity spectra, $x(dN/dx)$, for the heavy-quark → quark splitting process. The massive results for the full splitting, $Q \to Qg$, are in blue, the corresponding small-x results are in red. We have chosen the mass $m_b = 4.5$ GeV. We also plot the massless results $q \to qg$ for both the full splitting in dashed black and the small-x limit in green. Right panel: differential cross sections for $pp \to D^{*\pm}X$ at $\sqrt{s}$=7 TeV. Data are from ATLAS [17].

parton splitting and deflection kinematics is necessary which was also achieved in Ref. [171]. The full expressions for the splitting functions, $\mathcal{P}^{\rm med}_{i\to jk}(z,\mu)$, are lengthy and not reproduced here. However, we emphasize again the main idea of separating the perturbative splitting processes induced by Glauber gluon interactions from the medium, which themselves can be non-perturbative. As such, the expressions derived in Ref. [171] are applicable for both the QGP and cold nuclear matter but one has to take into account the different transport properties of these strongly-interacting systems.

The soft-gluon emission limit, *i.e.*, the limit when $x = k^+/p^+ \ll 1$, is the only limit where a radiative energy loss interpretation of the general splitting processes described above can be given. It is easy to see that the $Q \to gQ$ and $g \to Q\bar{Q}$ splittings are formally suppressed. Taking the small-x limit in $Q \to Qg$ yields

$$x\left(\frac{dN^{\rm SGA}}{dxd^2\mathbf{k}_\perp}\right)_{Q\to Qg} = \frac{\alpha_s}{\pi^2}C_F\int d\Delta z\frac{1}{\lambda_g(z)}\int d^2\mathbf{q}_\perp\frac{1}{\sigma_{el}}\frac{d\sigma^{\rm med}_{el}}{d^2\mathbf{q}_\perp} \times\frac{2\mathbf{k}_\perp\cdot\mathbf{q}_\perp}{[k_\perp^2+x^2m^2][(\mathbf{k}_\perp-\mathbf{q}_\perp)^2+x^2M_Q^2]}\left[1-\cos\frac{(\mathbf{k}_\perp-\mathbf{q}_\perp)^2+x^2M_Q^2}{xp_0^+}\Delta z\right], \tag{37}$$

a much simpler result, see also Ref. [172]. The comparison of the full splitting kernels with the soft-gluon limit results and the comparison of massless and finite-mass partons is given in Fig. 25. We show results for splitting functions averaged over the binary-collision distributed jet production in central Pb+Pb collisions at $\sqrt{s_{\rm NN}} = 5.02$ TeV at the LHC in a gluon-dominated plasma. Note the pronounced differences between the massless and massive cases. It is also important to observe that in the energy region where mass effects are most important the differences between the full splitting functions and the soft-gluon approximation are large.

Traditionally, energy loss calculations have focused on a scenario where only heavy quarks fragment into heavy mesons. This leads to simple arguments about mass and color charge ordering of light hadron, D-meson and B-meson suppression. The splitting functions above imply that both light partons and heavy quarks can fragment into heavy mesons. This will, of course, have implications for their quenching pattern. It is important to identify the regions where the uncertainty due to the possibly different production mechanisms is minimal. In pp collisions a good description of heavy-meson production can be achieved using the fragmentation functions of Refs. [173–176] in which light parton fragmentation into heavy mesons is included. The calculation combines the zero-mass variable-flavor number scheme (ZMVFNS) [177, 178] and the $pp \to HX$ NLO framework [179, 180], to obtain

$$\frac{d\sigma^H_{pp}}{dp_T d\eta} = \frac{2p_T}{s}\sum_{a,b,c}\int_{x_a^{\min}}^1 \frac{dx_a}{x_a} f_a(x_a,\mu)\int_{x_b^{\min}}^1 \frac{dx_b}{x_b} f_b(x_b,\mu)\int_{z_c^{\min}}^1 \frac{dz_c}{z_c^2}\frac{d\hat{\sigma}^c_{ab}(\hat{s},\hat{p}_T,\hat{\eta},\mu)}{dvdz} D_c^H(z_c,\mu). \tag{38}$$

One example of D-meson production at the LHC is shown in the right panel of Fig. 25. It is important to note that the contributions of HQ and gluon fragmentation to D mesons are approximately equal, and similarly for B mesons. Recent global analysis of D^* production, which includes novel open heavy flavor-in-jet measurements favors even larger gluon fragmentation contribution [181].

Going beyond the soft-gluon approximation requires a new treatment of the medium-induced parton shower. Incorporating this contribution consistent with NLO calculations can be schematically expressed as

$$d\sigma^H_{\rm PbPb} = d\sigma^{H,\rm NLO}_{pp} + d\sigma^{H,\rm med}_{\rm PbPb}, \tag{39}$$

where $d\sigma^{H,\rm NLO}_{pp}$ is the NLO cross section in the vacuum, and $d\sigma^{H,\rm med}_{\rm PbPb} = \hat{\sigma}_i^{(0)} \otimes D_i^{H,\rm med}$ is the one-loop medium correction. Using the medium-induced splitting functions, $\mathcal{P}^{\rm med}_{i\to jk}(z,\mu)$, we find for the medium-modified quark and gluon fragmentation functions, $D_i^{H,\rm med}$,

$$\begin{aligned} D_q^{H,\rm med}(z,\mu) = {} & \int_z^1 \tfrac{dz'}{z'} D_q^H\left(\tfrac{z}{z'},\mu\right)\mathcal{P}^{\rm med}_{q\to qg}(z',\mu) - D_q^H(z,\mu)\int_0^1 dz' \mathcal{P}^{\rm med}_{q\to qg}(z',\mu) \\ & + \int_z^1 \tfrac{dz'}{z'} D_g^H\left(\tfrac{z}{z'},\mu\right)\mathcal{P}^{\rm med}_{q\to gq}(z',\mu), \end{aligned} \tag{40}$$

$$\begin{aligned} D_g^{H,\rm med}(z,\mu) = {} & \int_z^1 \tfrac{dz'}{z'} D_g^H\left(\tfrac{z}{z'},\mu\right)\mathcal{P}^{\rm med}_{g\to gg}(z',\mu) - \tfrac{D_g^H(z,\mu)}{2}\int_0^1 dz' \left[\mathcal{P}^{\rm med}_{g\to gg}(z',\mu)\right. \\ & \left. + 2N_f \mathcal{P}^{\rm med}_{g\to q\bar{q}}(z',\mu)\right] + \int_z^1 \tfrac{dz'}{z'}\textstyle\sum_{i=q,\bar{q}} D_i^H\left(\tfrac{z}{z'},\mu\right)\mathcal{P}^{\rm med}_{g\to q\bar{q}}(z',\mu). \end{aligned} \tag{41}$$

The suppression of heavy mesons that originate from gluon fragmentation can be considerably stronger than the suppression of heavy mesons that originate from heavy-quark fragmentation. The nuclear modification factors become equal only at very high p_T, where the larger "energy loss" of gluons is offset by its softer fragmentation function. A practical way, however, of determining the region where the perturbative calculations can be used to probe the properties of the medium is to compare the $R_{\rm AA}(p_T)$ from the energy loss and the full NLO calculation. Results are presented in Fig. 26. For D mesons the results are fairly comparable within uncertainties; a comparison to recent CMS data in 0-10% central Pb+Pb collisions at the LHC is shown in the right panel of Fig. 26. For B mesons there is significant deviation below $p_T \sim 20$ GeV. At those transverse momenta collisional energy loss [152], described elsewhere in this document, and/or heavy-meson dissociation [182–184] is expected to play a role. However, it is important to realize that there is uncertainty in the absolute magnitude of the suppression based on medium-induced splitting/radiative processes that has not been discussed in the literature until very recently [171]. For the purpose of presenting results in this

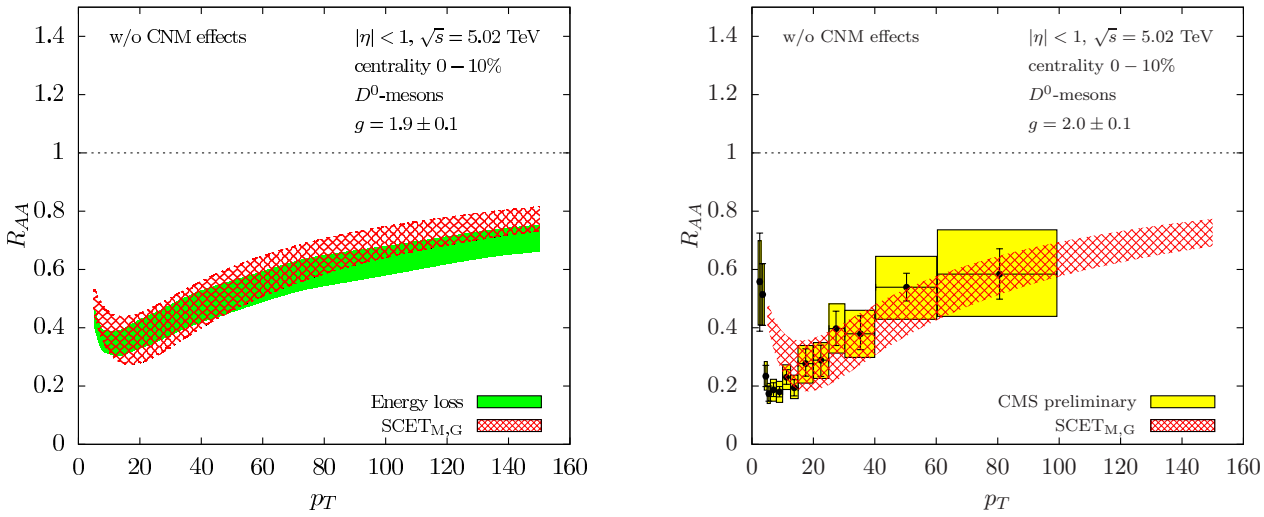

Figure 26: The nuclear modification factor, $R_{\rm AA}$, for D^0 mesons as a function of transverse momentum in 0-10% central Pb+Pb(5.02 TeV) collisions at the LHC. Left panel: comparison of the results obtained within the traditional approach to energy loss (green band) to those based on SCET$_{\rm M,G}$ (hatched red band); the bands reflect the range of the strong coupling constant, g=1.9±0.1. Right panel: a SCET$_{\rm M,G}$ calculation of D^0-meson suppression (with a slightly readjusted coupling of g=2.0±0.1) compared to preliminary CMS data.

report we take the soft-gluon emission, heavy-quark energy loss limit. Theoretical model assumptions are listed in a separate section.

Theoretical model assumptions

We describe below the theoretical model assumptions that go into the SCET$_{\rm M,G}$ calculation of open heavy flavor.

- Most of the model dependence comes form the treatment of the background QGP medium adopted here. Jet production, being rare such that $\sigma(E_T > E_{T\ \rm min})T_{AA}(b) \ll 1$, follows binary collision scaling $\sim d^2N_{\rm bin.}/d^2\mathbf{x}_\perp$. In contrast, the medium is assumed to be distributed according to the participant number density, $\sim d^2N_{\rm part.}/d^2\mathbf{x}_\perp$. We take into account longitudinal Bjorken expansion. It was shown that transverse expansion does not affect the overall cross section suppression much, however it leads to a smaller high-p_T elliptic flow v_2. This is the reason for which the elliptic flow at high p_T in the numerical results section turns out to be quite large.

- We assume local thermal equilibrium and a gluon-dominated plasma. The medium formation time is taken to be $\tau_0 = 0.3$ fm at the LHC. The local density of the medium then reads

$$\rho = \frac{1}{\tau}\frac{d^2(dN^g/dy)}{d^2\mathbf{x}_\perp} \approx \frac{1}{\tau}\frac{3}{2}\left|\frac{d\eta}{dy}\right|\frac{d^2(dN_{\rm ch}/d\eta)}{d^2\mathbf{x}_\perp}\ . \tag{42}$$

  Here, $dN_{\rm ch}/d\eta = \kappa N_{\rm part}/2$ with $\kappa \approx 8.25$ for Pb+Pb collisions at $\sqrt{s_{NN}} = 2.76$ TeV at the LHC. The parameter κ can be constrained by experimentally measured charged-particle rapidity density. Since a gluon-dominated plasma has fewer degrees of freedom than a QGP, it is hotter at equal space-time points.

- The temperature at any space-time position can be obtained from the density as

$$T(\tau, \mathbf{x}_\perp) = \sqrt[3]{\pi^2 \rho(\tau, \mathbf{x}_\perp)/16\zeta(3)}\ , \tau > \tau_0\ . \tag{43}$$

  The Debye screening scale is given by $m_D = gT$, recalling that we work in the approximation of a gluon-dominated plasma, *i.e.*, $N_f = 0$. The relevant gluon mean free path is easily evaluated: $\lambda_g = 1/\sigma^{gg}\rho$ with $\sigma^{gg} = (9/2)\pi\alpha_s^2/m_D^2$.

- We assume an effective fixed coupling g between the jet and the medium. At present, there are no reliable results for the renormalization of the strong coupling in the presence of a medium. Typical values at the LHC are in the range g=1.9-2.2, typical values at the RHIC are in the range g=2.0-2.3. The value of this coupling is adjusted for comparison to other calculations in the numerical section. For parton splitting processes an additional α_s associated with the splitting vertex occurs. In fixed-order calculations, such as NLO [171, 185], we evaluate α_s at the hard scale, Q^2, in the process. If multiple gluon emission in the energy loss limit [186] or full QCD evolution for parton showers [167, 187] are considered, α_s runs with the transverse mass of the emitted parton relative to the jet axis.

6.5 Reference Results in an Infinite and Finite QGP

In this section we provide reference results in a QGP at fixed temperature for radiative energy loss models for high-p_t heavy quarks, as well as an application to the D-meson nuclear modification factor and elliptic flow for the models discussed in Secs. 6.3 (dynamical energy loss) and 6.4 (SCET) which were not included in the comparisons using the pQCD*5 elastic interaction conducted in Secs. 3 and 4.

In Figs. 27 and 28, the relative energy loss, $\Delta E/E$, for c- and b-quarks, respectively, is displayed as a function of the path length L for four model calculations. In practice, the most relevant range for HF phenomenology in heavy-ion collisions turns out to be about $L \lesssim 5\,\text{fm}$. We recall that in the SCET NLO approach of Vitev et al. (as described in Sec. 6.4), multi-gluon radiation is included with $\alpha_s = 0.4$ resulting in $\hat{q} = 2m_D^2/\lambda_g = 0.36(1.20)\,\text{GeV}^2/\text{fm}$ for $T = 0.2(0.3)\,\text{GeV}$. The Djordjevic et al. calculations correspond to the radiative part evaluated within the DGLV formalism (as described in Sec. 6.3), which also includes multi-gluon emission, but differs, *e.g.*, in the choice of the gluon propagators (HTL vs. Debye-screened vacuum in SCET, which, however, in practice are quite similar) and the prescription for the cutoff in transverse momentum, and includes the Ter-Mikayelian effect. Nevertheless, the two approaches show good agreement for c-quark energy loss, with some deviation developing only for relatively large path lengths, especially at higher temperature and lower c-quark energy, where the Vitev et al. calculation tends to level off in a more pronounced way (the Djordjevic et al. calculations for the energy loss, ΔE, do not include multi-gluon emission fluctuations). For small path lengths, $L \lesssim$3-4 fm (somewhat decreasing with temperature), we observe a hierarchy where the more energetic c-quarks lose a smaller fraction of their energy, while the effective path length dependence is $\propto L^\gamma$ with $\gamma > 1$ (also found in the BDMPSZ approach not shown here). At later times, the exponent for the effective path length dependence reduces, first becoming linear (γ) and then turning over ($\gamma < 1$) well before the expected saturation for values of $\Delta E/E$ close to unity is reached. The change in γ is more pronounced for smaller initial parton energies. In the LBL-CCNU approach [188, 189] the number of emitted gluons per time step is computed from a radiation

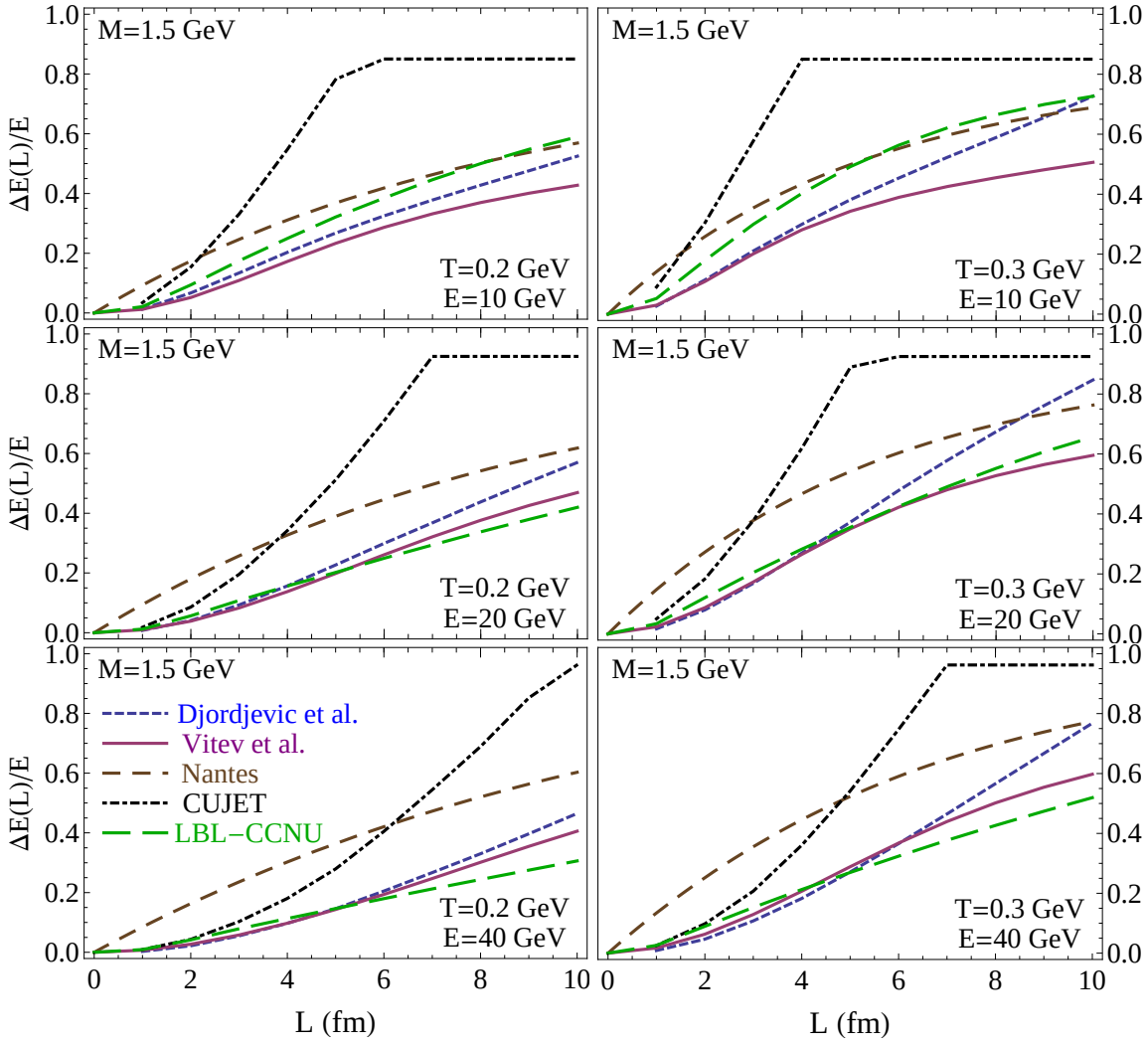

Figure 27: Fractional *radiative* energy loss, $\Delta E/E$, of c-quarks as a function of their path length in a fixed-temperature QGP for various model calculations (SCET NLO energy loss limit [Vitev et al.], DGLV [Djordjevic et al.], higher-twist [LBL-CCNU], running-coupling elastic [Nantes] and internal-energy elastic [CUJET] formalisms), for two temperatures (T=0.2 and 0,3 GeV in the left and right columns, respectively) and three initial quark energies (E=10, 20, 40 GeV in the upper, middle and lower panels, respectively).

spectrum obtained from the higher-twist energy loss formalism. The radiation rate is proportional to $\alpha_s\hat{q}$ where $\hat{q}$ is based on pQCD elastic scattering [188], with a running coupling constant at scale Q^2=$2ET$ for the HQ-gluon vertices and a constant α_s=0.15 for the gluon's Debye mass and coupling to thermal partons (assumed to be massless). The resulting $\hat{q}$ amounts to 0.16(0.41) GeV^2/fm for T=0.2(0.3) GeV. Effects from both finite formation times and multi-gluon emission are accounted for. The fractional energy loss of charm quarks obtained from this model turns out to be comparable to the other pQCD-based calculations displayed in Fig. 27, with, however, different values for α_s (and $\hat{q}$). The Nantes calculation [190, 191] is characterized by a running α_s, reaching rather large values, and a reduced Debye mass in the elastic HQ scattering that triggers the radiation; it has been constructed to be primarily applicable at intermediate p_t and therefore neglects finite-path length effects due to gluon formation outside the QGP. These two features are presumably responsible for

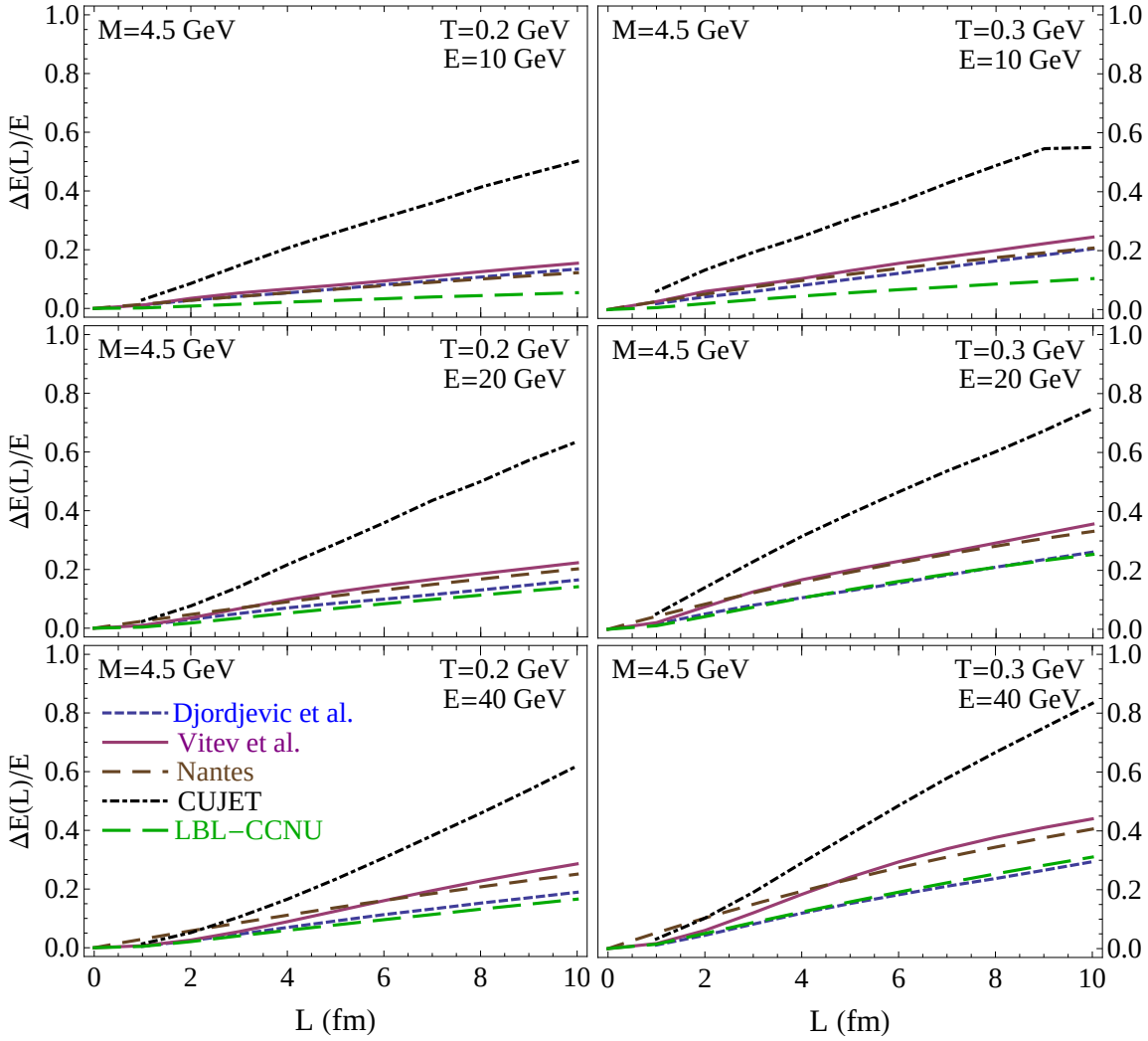

Figure 28: Same as Fig. 27 but for b-quarks.

the significantly larger energy loss at small path lengths compared to the other approaches. In the CUJET3 framework [45, 46, 192], the medium contains non-perturbative chromo-magnetic degrees of freedom which interact strongly with a jet parton, leading to a potential akin to the heavy-quark internal energy. This also includes a strong running of the coupling at nonperturbative energy scales. When the parton energy becomes small at large path lengths, $L \gtrsim 4\,\mathrm{fm}$, the radiative energy loss becomes about a factor of 2 larger than in the Vitev et al. and Djordjevic et al. approaches. However, since such path lengths are often smaller than the typical ones in non-central heavy-ion collisions, this difference may not have marked phenomenological consequences. A stronger-than-linear increase in the CUJET energy loss remains until saturation is reached when all kinetic energy of the original quark is radiated. Further work is required to better understand the relations between the different approaches and their results.

In Fig. 28, we display the corresponding fractional energy loss for b quarks. As expected, it is substantially smaller than for c quarks, especially at the lower energies (E=10 and 20 GeV) due to the well-known dead-cone effect. This implies that collisional energy loss play a more important role than for c quarks. In addition, interference effects are much less pronounced as formation times are generally reduced to due the larger quark mass. Together, these features create an overall much closer

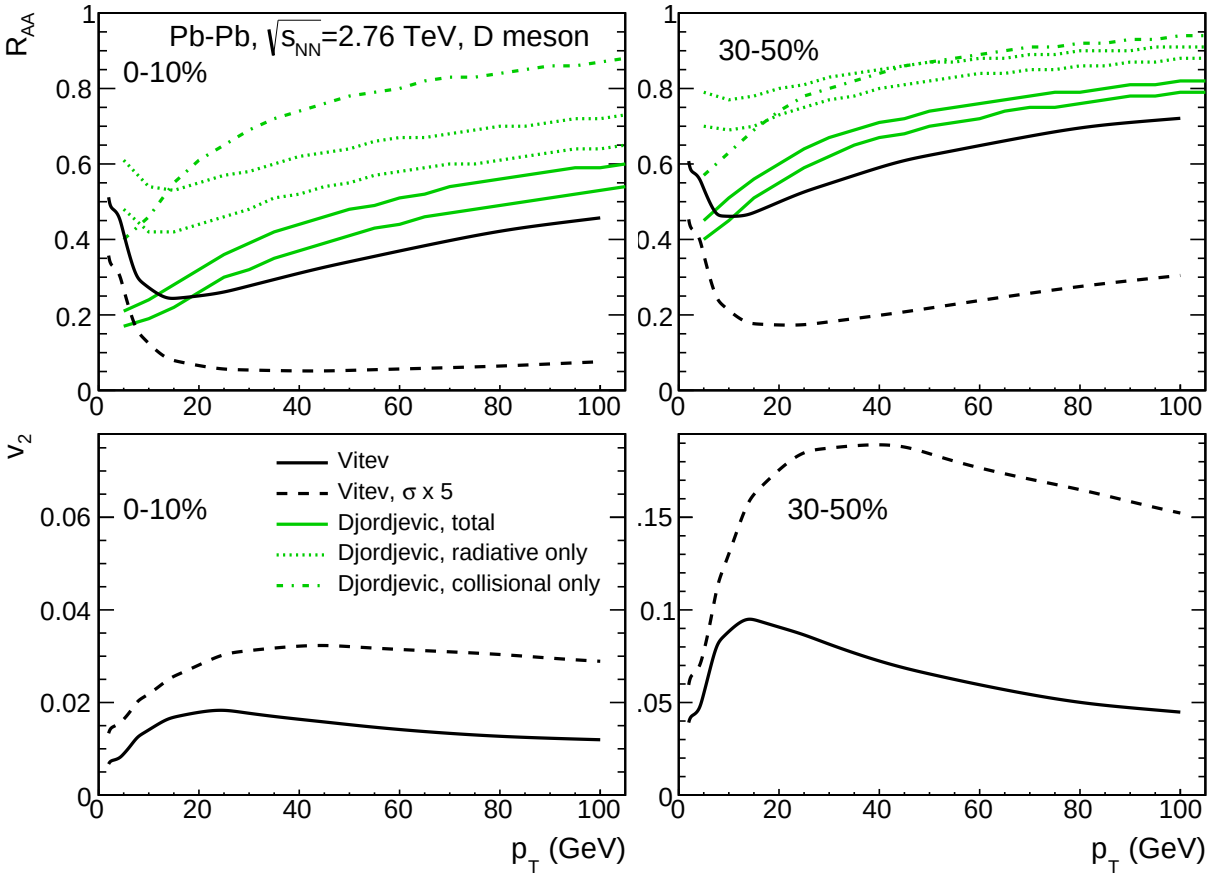

Figure 29: Comparison of the nuclear modification factor (upper row) and elliptic flow (lower row) of D-mesons in 0-10% (left column) and 30-50% (right column) Pb-Pb(2.76 TeV) collisions from two energy loss models (black lines: Vitev et al., green lines: Djordjevic et al.) within the QGP phase in these reactions. The theoretical uncertainty band for the radiative-only (green dotted lines) and total (solid green lines) results is due to a range of 0.4-0.6 in the ratio of magnetic to electric screening masses.

to linear dependence of the energy loss on path length out to values of 10 fm. The Nantes results are now in better agreement with the Vitev et al. and Djordjevic et al. calculations, while the non-perturbative interaction encoded in the internal-energy potential used in CUJET still leads to larger energy loss by a factor of 2-3 (leading to near saturation at $\Delta E = m_b$ around L=10 fm for a 10 GeV initial b quark). Even for b-quark energies as large as 40 GeV, the deviations from a linear behavior are relatively small.

Finally, we illustrate for a few cases how the energy loss calculations compare at the level of the nuclear modification factor and elliptic flow in Pb-Pb collisions at the LHC, cf. Fig. 29. This requires the additional input of a bulk medium evolution model. For the Vitev et al. calculations, the QGP fireball has been modelled by 1-D Bjorken expansion with Glauber geometry in the transverse plane, while for the Djordjevic et al. calculations a static spherically symmetric fireball has been employed. The baseline calculations in both approaches, including both radiative and collisional energy loss for Djordjevic et al. and only radiative for Vitev et al., agree within 20% for $p_T >$ 10 GeV (and generally do a good job in describing experimental data at high p_T). For the former, we also show results when only accounting for either radiative or collisional energy loss. For semi-central collisions, both contributions

are comparable for most of the considered p_T range out to 100 GeV, while for central collision the radiative one becomes dominant for $p_T \gtrsim 20$ GeV. This can be attributed to the stronger than linear rise in the radiative energy loss of charm quarks at high p_T, recall the lower panels in Fig. 27. On the other hand, the radiative-only result for the $R_{\rm AA}$ from the Djordjevic et al. calculation shows a factor of ∼2 less suppression than the result from Vitev et al. which one would not have expected from the charm-quark energy loss results displayed in Fig. 27. This suggests a marked difference in the underlying bulk evolution models. Finally, including a K-factor of 5 in the HQ scattering cross section in the Vitev et al. calculation leads to a much stronger suppression in the $R_{\rm AA}$ which is well beyond what is found in experimental data.

7 Summary and Perspectives

The characterization of heavy-flavor diffusion in QCD matter remains one of the most powerful approaches to investigate, both qualitatively and quantitatively, the properties of the medium created in high-energy heavy-ion collisions. On the one hand, this pertains to determining the temperature and momentum dependence of relevant transport coefficients (such as diffusion and energy-loss coefficients), but, maybe more importantly, gives the opportunity to unravel underlying microscopic processes which reveal the structure of the QCD medium in the strongly coupled regime. Similarly to other probes, the progress of HF probes hinges on a close connection between theory, phenomenology and experimental data, further fueled by dedicated future plans [193, 194] to improve and extend the current data set. The present report is a first attempt to systematically break down the HF probe of QCD matter into its main modeling components, with the ultimate goal of understanding and quantifying the uncertainties that each component imprints on the final extraction of the transport coefficients. These components are the initial heavy-quark spectra and their modifications due to nuclear shadowing, the bulk evolution of the fireball medium, the microscopic description of heavy-quark transport in the QGP and through hadronization[6]. Another important objective has been the identification of baseline criteria and standard inputs that can be broadly agreed upon and channeled into future refinements of the majority of the transport approaches.

As for the initial conditions, a best-fit of state-of-the-art D-meson spectra in pp collisions at LHC energies has been carried out within the FONLL framework (and associated BCFY fragmentation functions), including a systematic error band. The comparison with initial c-quark p_t spectra currently in use in 6 different approaches showed good agreement within this band (with the largest uncertainty at low $p_t \lesssim 2$ GeV). The implementation of shadowing is more uncertain, especially if more conservative error bands from recent EPPS16 nPDF fits are employed. This uncertainty is larger in the low-p_t region, as verified in an explicit transport study for Pb-Pb collisions. The extraction of shadowing effects from pA data is further complicated by the possible occurence of final-state interactions of HF particles.

To test the role of different bulk evolution models, the participating research groups delivered the p_T spectra and v_2 of direct pions and protons in central and semicentral Pb-Pb collisions at $\sqrt{s_{\rm NN}} = 2.76$ TeV at the end of the QGP phase in their hydrodynamic or transport model, to

[6] In the present report we have neither explicitely addressed the impact of a pre-equilibrium evolution, bridging the (short) time between the initial production and the formation of a locally thermalized medium, nor diffusion through the hadronic phase.

benchmark the environment for testing c-quark diffusion. For the integrated direct-pion yields at T_c a rather large spread of about $\pm 25\%$ for central collisions was found within the hydrodynamic models (further augmented by transport models and in semicentral collisions); the situation improved (with a couple of outliers) when comparing inclusive spectra (*i.e.*, including resonance feeddown), presumably because inclusive pion numbers are closer to observables that the models are tuned to in the first place. Remaining discrepancies should be resolvable in a next iteration through closer inspection of, *e.g.*, the hadro-chemistry and more uniform choices of the centrality classes and chemical freezeout temperature. The pion and proton radial and elliptic (v_2) flow at T_c exhibited better agreement. Within their evolution models the groups carried out charm-quark transport calculations using a *common* (predefined) c-quark interaction with QGP partons (pQCD elastic Born scattering with a K factor of 5). Except for 2 outliers, an encouraging degree of agreement of the c-quark spectra and v_2 emerged, with an extracted "systematic" error of 10-15%. This suggests that the diagnosed spread in the bulk evolution models is in reality smaller (presumably because the evolution models are, in principle calibrated to final-state hadron spectra), and/or that the results for the c-quark observables are more robust than light-hadron spectra against details of the medium evolution.

Concerning the hadronization of heavy quarks at the end of the QGP phase, all approaches feature some type of recombination with constituent quarks from the surrounding medium, supplemented with independent fragmentation for quarks that are not recombining. The employed mechanisms include instantaneous coalescence (both local and global in coordinate space), in-medium fragmentation, or heavy-light resonance formation. The ensuing spread in the resulting D-meson R_{AA} and v_2 is appreciably increased over the one found at the charm-quark level. We have quantified this by introducing a new quantity, H_{AA}, the ratio of D-meson to c-quark spectra right after and before hadronization, respectively. The treatment of hadronization has therefore been identified as a prime area of future improvements. Quantitative criteria will have to be applied to benchmark the various approaches, *e.g.*, the compatability with the equilibrium limit (both chemical and thermal) in the conversion from heavy quarks to hadrons.

We have then performed a model average of D-meson R_{AA} and v_2 for semi-/central Pb-Pb collisions at $\sqrt{s_{NN}} = 2.76$ TeV which, without further attempts of narrowing down uncertainties, resulted in encouragingly moderate error bands. Not withstanding remaining caveats (such as neglecting pre-equilibrium effects and hadronic transport), an initial comparison to existing data showed that the pQCD*5 interaction does not provide enough interaction strength by an appreciable margin, implying that the HF diffusion coefficient, as a measure of low-momentum transport through the QCD medium, must be well below $\mathcal{D}_s(2\pi T)$=6, at least for some temperature range (preferentially where the v_2 of the fireball is large).

Let us briefly comment on the role of hadronic diffusion, which has not been explicitly addressed in the present effort. Using different versions of effective hadronic lagrangians, the interactions of D-mesons with light and strange hadrons have been ultilized to evaluate D-meson relaxation time in hot hadronic matter [195–200]. After initially rather widely varying results, there is now emerging consensus that the (scaled) hadronic diffusion coefficient becomes rather small near T_{pc}, reaching down to near 5 or less. This suggests a minimum structure, as well as a possible continuity with the values for charm quarks in the QGP (as discussed above), in the vicinity of T_{pc}. It also implies that hadronic-diffusion effects in URHICs are quantitatively significant. Current estimates of the hadronic contribution to the observed D-meson v_2 are in the range of 10-40% [49, 60] (also depending on p_T)

relative to the QGP contribution, while the $R_{\rm AA}$ tends to be much less affected. These contributions thus have to be accounted for in future precision extractions of heavy-flavor transport coefficients from URHIC data.

We have also discussed the microscopic description of heavy-quark diffusion from several angles. We have emphasized that the convergence of the perturbative series for the diffusion coefficient is ill-behaved even at coupling constants as small as α_s=0.1; a key role in this behavior is played by the fact that the leading contribution already carries a rather large power in the coupling constant, $\mathcal{D}_s \sim \mathcal{O}(1/\alpha_s^2)$. Thus, nonperturbative methods are indispensable to develop a credible microscopic description of heavy-quark diffusion in the QGP. Due to its sensitivity to the coupling strength, one may argue that the heavy-quark diffusion coefficient provides one of the most direct windows on the nonperturbative many-body physics of the strongly-coupled QGP. Constraints from lattice QCD, together with nonperturbative many-body methods, will be necessary to exploit this opportunity. An increasing interaction strength toward $T_{\rm c}$ suggests that the onset of hadronization, expected to be a gradual process, plays an important role in the interactions of heavy quarks in this regime, as can be implemented, for example, in a thermodynamic T-matrix approach. Lattice-QCD calculations of charm-quark susceptibilities, indicative for an onset of hadronic degrees of freedom above $T_{\rm c}$, support such a picture. Some care has to be taken in implementing the transport of heavy quarks in heavy-ion collisions. When the temperature becomes large, the charm-quark mass may no longer be large enough to satisfy the parametric hierarchy, $m_Q/T \gg 1$, which will ultimately limit the ability of the Fokker-Planck/Langevin treatment of charm-quark diffusion at the precision frontier. The Boltzmann approach does not require such an approximation. On the other hand, the Boltzmann approach will run into issues when the collision rates become so large that the medium partons cannot be reliably modeled by an ensemble of (quasiclassical) quasiparticels any more. In his case, the Langevin approach is still viable as long as the heavy quarks remain good quasiparticles (even if the medium partons are not). Bottom quarks, due to their larger mass, thus provide the largest margin for a theoretically accurate implementation of heavy-flavor transport and the extraction of the diffusion coefficient.

While the main focus of the working group activities was on low-momentum interactions where incoherent elastic collisions dominate, we have also discussed heavy-quark interactions at high p_T and radiative energy loss. We have reviewed the definition of the usual transport coefficient, $\hat{q}$, along with subtleties in its evaluation and discussed recent progress by applying effective theory to perform next-to-leading-order calculations. Also in the high-p_T regime, the medium evolution is identified as a significant source of uncertainty in current modeling efforts. We have compared results within 4 different approaches to energy loss and pertinent manifestations in $R_{\rm AA}$ and v_2 observables, illustrating the relative role of radiative and elastic contributions. Inspection of the results in a fixed-temperature QGP revealed that the energy loss for bottom quarks remains essentially linear in the path length, *i.e.*, incoherent, up to energies of 20 GeV, while for charm quarks its magnitude and nonlinearities are significantly more pronounced. Quantitative differences in the magnitude of the radiative energy loss not only emerge from different perturbative treatments but also show appreciable sensitivity to nonperturbative effects of a strongly coupled QGP, both of which deserve further scrutiny.

Based on the insights in this task-force report, and in the interest of a collective progress in the physics of HF probes of QCD matter, we suggest the following set of recommendations for future modeling efforts in heavy-ion collisions:

1. Adopt FONLL baseline HQ spectra with EPS09 shadowing for the initial conditions in transport simulations.

2. Employ publicly available hydrodynamic or transport evolution models which have been tuned to data, with a maximal range of viable initial conditions and model parameters; or even a single one with a pre-specified tune as a single point of contact of all approaches.

3. Use recombination schemes of heavy quarks with light medium partons which satisfy 4-momentum conservation and recover equilibrium distributions in the long-time limit for the resulting hadron distributions.

4. Incorporate nonperturbative interactions in the modeling of heavy-flavor transport in a QGP at moderate temperatures as established and constrained by information from lattice QCD; utilize resummed interactions leading to bound-state formation near T_c to facilitate a seamless transition into coalescence processes.

5. Include diffusion through the hadronic phase of heavy-ion collisions.

Consequently, to address the question which particular future measurements could have the largest impact on improving our knowledge about the in-medium interactions of heavy flavor, we suggest the following observables with associated objectives:

A. Bottom observables as the theoretically cleanest probe of a strongly-coupled QGP, in terms of the implementation of both microscopic interactions and transport, and as a measure of coupling strength without saturation due to thermalization;

B. v_2 peak structures and maximal values for D and B mesons to gauge the heavy-flavor interaction strength and delineate elastic and radiative regimes;

C. Precision $R_{\rm AA}$ and v_2 of D and B mesons at various beam energies to extract temperature and mass dependence of transport coefficients;

D. D_s and Λ_c hadron observables at low and intermediate p_T to unravel the in-medium charm-quark chemistry, specifically its role in hadronization processes and reach in p_T;

E. Heavy-flavor (especially bottom) in jets to disentangle gluon vs. heavy-flavor energy loss and production mechanisms (direct vs. gluon splitting).

F. Correlation measurements of heavy-flavor pairs to delineate collisional from radiative interactions and test Langevin against Boltzmann transport approaches.

Whereas the effort presented here merely constitutes a first step toward a truly systematic and broad investigation of heavy-flavor probes of QCD matter, we believe that we have gained insights and identified criteria that will prove useful in the future and help to match the experimental precision of upcoming measurements with a robust theoretical understanding and quantitative phenomenology. Concerted theory collaborations will play a critical role in achieving this goal.

Acknowledgments

We gratefully acknowledge support of the Heavy-Flavor Rapid Reaction Task Force (RRTF) meetings through the Extreme Matter Institute (EMMI). This work has been supported by the US National Science Foundation (NSF) under grant Nos. PHY-1614484 (SL, RR), PHY-1352368 (JL, SS) and ACI-1550228 (JETSCAPE) (SC, XNW), by the US Department of Energy (DOE) under grant Nos. DE-SC0012704 (PP), DE-AC02-05CH11231 (SC, XNW), DE-SC0013460 (SC) and the Early Career Program (IV), by Région Pays de la Loire (France) under contract no. 2015-08473 (PBG, MN), by NSF China (NSFC) under grant Nos. 11675079 (MH) and 11221504 (XNW), by the European Research Council (ERC) StG under grant No. 259684 (SKD, VG, SP), by the LANL LDRD program under grant Nos. 2012LANL7033 and 20170073DR (IV), by the German Academic Exchange Service (DAAD) (TS), by the Deutsche Forschungsgemeinschaft (DFG) under grant Nos. CRC-TR 211 (EB, HvH, OK, GM, TS) and SFB-1225 (ISOQUANT) (PBM, SM, JMP, JS), and by the Major State Basic Research Development Program in China under grant No. 2014CB845404 (XNW).

A Overview of Model Approaches Employed in this Work

In Table 2 we list the acronyms of the model approaches that were involved in the various studies reported in this paper, including elastic and radiative interactions (both pQCD and non-perturbative) of heavy quarks in the QGP, hadronization mechanisms and a wide variety of bulk evolution models (hydrodynamic and transport) for the expanding fireball in heavy-ion collisions to make contact with observables.

Name of the Approach	References
Catania	[54, 83, 135]
CUJET	[45, 46, 192]
Djordjevic et al.	[146, 149, 150]
Duke	[64, 90]
LBL-CCNU	[188, 189]
Nantes (MC@sHQ+EPOS2)	[33, 63, 190]
POWLANG	[66, 67]
PHSD	[48–50]
SCET	[164, 168, 171]
TAMU	[36, 61, 86]
URQMD	[201, 202]

Table 2: Models of open heavy-flavor "transport" in hot QCD matter applied to ultra-relativistic heavy-ion collisions which participated in the studies reported in the present work, with up to 3 most pertinent publications describing the approach.

References

[1] Y. Akiba *et al.*, "The Hot QCD White Paper: Exploring the Phases of QCD at RHIC and the LHC," arXiv:1502.02730 [nucl-ex].

[2] H. Niemi, K. J. Eskola, and R. Paatelainen, "Event-by-event fluctuations in a perturbative QCD + saturation + hydrodynamics model: Determining QCD matter shear viscosity in ultrarelativistic heavy-ion collisions," *Phys. Rev. C* **93** no. 2, (2016) 024907, arXiv:1505.02677 [hep-ph].

[3] B. Svetitsky, "Diffusion of charmed quarks in the quark-gluon plasma," *Phys. Rev. D* **37** (1988) 2484–2491.

[4] A. Beraudo, "Dynamics of heavy flavor quarks in high energy nuclear collisions," *Nucl. Phys. A* **931** (2014) 145–154, arXiv:1407.5918 [hep-ph].

[5] A. Andronic *et al.*, "Heavy-flavour and quarkonium production in the LHC era: from proton-proton to heavy-ion collisions," *Eur. Phys. J. C* **76** no. 3, (2016) 107, arXiv:1506.03981 [nucl-ex].

[6] F. Prino and R. Rapp, "Open Heavy Flavor in QCD Matter and in Nuclear Collisions," *J. Phys. G* **43** no. 9, (2016) 093002, arXiv:1603.00529 [nucl-ex].

[7] A. Andronic *et al.*, "ExtreMe Matter Institute (EMMI) Rapid Reaction Task Force (RRTF) Meeting on *Extraction of heavy-flavor transport coefficients in QCD matter*,". https://indico.gsi.de/conferenceDisplay.py?confId=5049.

[8] A. Andronic *et al.* http://www-alice.gsi.de/HQ_RRTF_2016/.

[9] M. Cacciari, M. Greco, and P. Nason, "The p_T spectrum in heavy flavor hadroproduction," *JHEP* **05** (1998) 007, arXiv:hep-ph/9803400 [hep-ph].

[10] M. Cacciari, S. Frixione, N. Houdeau, M. L. Mangano, P. Nason, *et al.*, "Theoretical predictions for charm and bottom production at the LHC," *JHEP* **1210** (2012) 137, arXiv:1205.6344 [hep-ph].

[11] E. Braaten, K.-m. Cheung, S. Fleming, and T. C. Yuan, "Perturbative QCD fragmentation functions as a model for heavy quark fragmentation," *Phys. Rev.* **D51** (1995) 4819–4829, arXiv:hep-ph/9409316 [hep-ph].

[12] J. Pumplin, D. R. Stump, J. Huston, H. L. Lai, P. M. Nadolsky, and W. K. Tung, "New generation of parton distributions with uncertainties from global QCD analysis," *JHEP* **07** (2002) 012, arXiv:hep-ph/0201195 [hep-ph].

[13] **ALICE** Collaboration, S. Acharya *et al.*, "Measurement of D-meson production at mid-rapidity in pp collisions at $\sqrt{s} = 7$ TeV," *Eur. Phys. J.* **C77** no. 8, (2017) 550, arXiv:1702.00766 [hep-ex].

[14] **CMS** Collaboration, A. M. Sirunyan *et al.*, "Nuclear modification factor of D0 mesons in PbPb collisions at sqrt(s[NN]) = 5.02 TeV," arXiv:1708.04962 [nucl-ex].

[15] **STAR** Collaboration, L. Adamczyk *et al.*, "Measurements of D^0 and D^* Production in $p+p$ Collisions at $\sqrt{s} = 200$ GeV," *Phys. Rev. D* **86** (2012) 072013, arXiv:1204.4244 [nucl-ex].

[16] **CDF** Collaboration, D. Acosta *et al.*, "Measurement of prompt charm meson production cross sections in $p\bar{p}$ collisions at $\sqrt{s} = 1.96$ TeV," *Phys. Rev. Lett.* **91** (2003) 241804, arXiv:hep-ex/0307080 [hep-ex].

[17] **ATLAS** Collaboration, G. Aad *et al.*, "Measurement of $D^{*\pm}$, $D^{\pm}$ and $D_s^{\pm}$ meson production cross sections in pp collisions at $\sqrt{s} = 7$ TeV with the ATLAS detector," *Nucl. Phys. B* **907** (2016) 717–763, arXiv:1512.02913 [hep-ex].

[18] **ALICE** Collaboration, B. Abelev *et al.*, "Measurement of charm production at central rapidity in proton-proton collisions at $\sqrt{s} = 7$ TeV," *JHEP* **01** (2012) 128, arXiv:1111.1553 [hep-ex].

[19] **ALICE** Collaboration, B. Abelev *et al.*, "Measurement of charm production at central rapidity in proton-proton collisions at $\sqrt{s} = 2.76$ TeV," *JHEP* **07** (2012) 191, arXiv:1205.4007 [hep-ex].

[20] **ALICE** Collaboration, B. Abelev *et al.*, "D_s^+ meson production at central rapidity in proton–proton collisions at $\sqrt{s} = 7$ TeV," *Phys. Lett. B* **718** (2012) 279–294, arXiv:1208.1948 [hep-ex].

[21] **ALICE** Collaboration, J. Adam *et al.*, "D-meson production in p-Pb collisions at $\sqrt{s_{\rm NN}} = 5.02$ TeV and in pp collisions at $\sqrt{s} = 7$ TeV," *Phys. Rev. C* **94** no. 5, (2016) 054908, arXiv:1605.07569 [nucl-ex].

[22] **LHCb** Collaboration, R. Aaij *et al.*, "Prompt charm production in pp collisions at $\sqrt{s} = 7$ TeV," *Nucl. Phys. B* **871** (2013) 1–20, arXiv:1302.2864 [hep-ex].

[23] **LHCb** Collaboration, R. Aaij *et al.*, "Measurements of prompt charm production cross-sections in pp collisions at $\sqrt{s} = 5$ TeV," arXiv:1610.02230 [hep-ex].

[24] **LHCb** Collaboration, R. Aaij *et al.*, "Measurements of prompt charm production cross-sections in pp collisions at $\sqrt{s} = 13$ TeV," *JHEP* **03** (2016) 159, arXiv:1510.01707 [hep-ex]. [Erratum: JHEP09,013(2016)].

[25] K. J. Eskola, H. Paukkunen, and C. A. Salgado, "EPS09: A New Generation of NLO and LO Nuclear Parton Distribution Functions," *JHEP* **04** (2009) 065, arXiv:0902.4154 [hep-ph].

[26] M. Cacciari and P. Nason, "Charm cross-sections for the Tevatron Run II," *JHEP* **09** (2003) 006, arXiv:hep-ph/0306212 [hep-ph].

[27] J. L. Albacete *et al.*, "Predictions for Cold Nuclear Matter Effects in p+Pb Collisions at $\sqrt{s_{NN}}$=8.16 'TeV," *Nucl. Phys.* **A972** (2018) 18–85, arXiv:1707.09973 [hep-ph].

[28] J. L. Albacete *et al.*, "Predictions for p+Pb Collisions at $\sqrt{s_{NN}}$=5 TeV," *Int. J. Mod. Phys.* **E22** (2013) 1330007, arXiv:1301.3395 [hep-ph].

[29] K. J. Eskola, P. Paakkinen, H. Paukkunen, and C. A. Salgado, "EPPS16: Nuclear parton distributions with LHC data," *Eur. Phys. J.* **C77** no. 3, (2017) 163, arXiv:1612.05741 [hep-ph].

[30] M. L. Mangano, P. Nason, and G. Ridolfi, "Heavy quark correlations in hadron collisions at next-to-leading order," *Nucl. Phys. B* **373** (1992) 295–345.

[31] H.-L. Lai, M. Guzzi, J. Huston, Z. Li, P. M. Nadolsky, J. Pumplin, and C. P. Yuan, "New parton distributions for collider physics," *Phys. Rev.* **D82** (2010) 074024, arXiv:1007.2241 [hep-ph].

[32] **LHCb** Collaboration, R. Aaij *et al.*, "Study of prompt D^0 meson production in pPb collisions at $\sqrt{s_{\mathrm{N\,N}}} = 5$ TeV," *JHEP* **10** (2017) 090, arXiv:1707.02750 [hep-ex].

[33] M. Nahrgang, J. Aichelin, P. B. Gossiaux, and K. Werner, "Azimuthal correlations of heavy quarks in Pb + Pb collisions at $\sqrt{s} = 2.76$ TeV at the CERN Large Hadron Collider," *Phys. Rev.* **C90** no. 2, (2014) 024907, arXiv:1305.3823 [hep-ph].

[34] J. Steinheimer, V. Dexheimer, H. Petersen, M. Bleicher, S. Schramm, and H. Stoecker, "Hydrodynamics with a chiral hadronic equation of state including quark degrees of freedom," *Phys. Rev.* **C81** (2010) 044913, arXiv:0905.3099 [hep-ph].

[35] H. Petersen, "Identified Particle Spectra and Anisotropic Flow in an Event-by-Event Hybrid Approach in Pb+Pb collisions at $\sqrt{s_{\mathrm{NN}}} = 2.76$ TeV," *Phys. Rev.* **C84** (2011) 034912, arXiv:1105.1766 [nucl-th].

[36] M. He, R. J. Fries, and R. Rapp, "Ideal Hydrodynamics for Bulk and Multistrange Hadrons in $\sqrt{s_{NN}}$=200 AGeV Au-Au Collisions," *Phys. Rev.* **C85** (2012) 044911, arXiv:1112.5894 [nucl-th].

[37] K. Werner, I. Karpenko, T. Pierog, M. Bleicher, and K. Mikhailov, "Event-by-Event Simulation of the Three-Dimensional Hydrodynamic Evolution from Flux Tube Initial Conditions in Ultrarelativistic Heavy Ion Collisions," *Phys. Rev.* **C82** (2010) 044904, arXiv:1004.0805 [nucl-th].

[38] T. Pierog, I. Karpenko, S. Porteboeuf, and K. Werner, "New Developments of EPOS 2," arXiv:1011.3748 [astro-ph.HE].

[39] S. Plumari, A. Puglisi, F. Scardina, and V. Greco, "Shear Viscosity of a strongly interacting system: Green-Kubo vs. Chapman-Enskog and Relaxation Time Approximation," *Phys. Rev.* **C86** (2012) 054902, arXiv:1208.0481 [nucl-th].

[40] P. Huovinen and P. Petreczky, "QCD Equation of State and Hadron Resonance Gas," *Nucl. Phys.* **A837** (2010) 26–53, arXiv:0912.2541 [hep-ph].

[41] H. Song and U. W. Heinz, "Suppression of elliptic flow in a minimally viscous quark-gluon plasma," *Phys. Lett.* **B658** (2008) 279–283, arXiv:0709.0742 [nucl-th].

[42] H. Song and U. W. Heinz, "Causal viscous hydrodynamics in 2+1 dimensions for relativistic heavy-ion collisions," *Phys. Rev.* **C77** (2008) 064901, arXiv:0712.3715 [nucl-th].

[43] Z. Qiu, C. Shen, and U. Heinz, "Hydrodynamic elliptic and triangular flow in Pb-Pb collisions at $\sqrt{s} = 2.76$ATeV," *Phys. Lett.* **B707** (2012) 151–155, arXiv:1110.3033 [nucl-th].

[44] J. Liao and E. Shuryak, "Angular Dependence of Jet Quenching Indicates Its Strong Enhancement Near the QCD Phase Transition," *Phys. Rev. Lett.* **102** (2009) 202302, arXiv:0810.4116 [nucl-th].

[45] J. Xu, J. Liao, and M. Gyulassy, "Consistency of Perfect Fluidity and Jet Quenching in semi-Quark-Gluon Monopole Plasmas," *Chin. Phys. Lett.* **32** no. 9, (2015) 092501, arXiv:1411.3673 [hep-ph].

[46] J. Xu, J. Liao, and M. Gyulassy, "Bridging Soft-Hard Transport Properties of Quark-Gluon Plasmas with CUJET3.0," *JHEP* **02** (2016) 169, arXiv:1508.00552 [hep-ph].

[47] L. Del Zanna, V. Chandra, G. Inghirami, V. Rolando, A. Beraudo, A. De Pace, G. Pagliara, A. Drago, and F. Becattini, "Relativistic viscous hydrodynamics for heavy-ion collisions with ECHO-QGP," *Eur. Phys. J.* **C73** (2013) 2524, arXiv:1305.7052 [nucl-th].

[48] E. L. Bratkovskaya, W. Cassing, V. P. Konchakovski, and O. Linnyk, "Parton-Hadron-String Dynamics at Relativistic Collider Energies," *Nucl. Phys.* **A856** (2011) 162–182, arXiv:1101.5793 [nucl-th].

[49] T. Song, H. Berrehrah, D. Cabrera, J. M. Torres-Rincon, L. Tolos, W. Cassing, and E. Bratkovskaya, "Tomography of the Quark-Gluon-Plasma by Charm Quarks," *Phys. Rev.* **C92** no. 1, (2015) 014910, arXiv:1503.03039 [nucl-th].

[50] T. Song, H. Berrehrah, D. Cabrera, W. Cassing, and E. Bratkovskaya, "Charm production in Pb + Pb collisions at energies available at the CERN Large Hadron Collider," *Phys. Rev.* **C93** no. 3, (2016) 034906, arXiv:1512.00891 [nucl-th].

[51] **ALICE** Collaboration, B. Abelev *et al.*, "Centrality dependence of π, K, p production in Pb-Pb collisions at $\sqrt{s_{NN}} = 2.76$ TeV," *Phys. Rev.* **C88** (2013) 044910, arXiv:1303.0737 [hep-ex].

[52] Y. Xu, P. Moreau, T. Song, M. Nahrgang, S. A. Bass, and E. Bratkovskaya, "Traces of nonequilibrium dynamics in relativistic heavy-ion collisions," *Phys. Rev.* **C96** no. 2, (2017) 024902, arXiv:1703.09178 [nucl-th].

[53] R. Rapp, "Theory and Phenomenology of Heavy Flavor at RHIC," *J. Phys.* **G36** (2009) 064014, arXiv:0812.3850 [hep-ph].

[54] S. K. Das, F. Scardina, S. Plumari, and V. Greco, "Toward a solution to the R_{AA} and v_2 puzzle for heavy quarks," *Phys. Lett.* **B747** (2015) 260–264, arXiv:1502.03757 [nucl-th].

[55] **PHENIX** Collaboration, A. Adare *et al.*, "Energy Loss and Flow of Heavy Quarks in Au+Au Collisions at $\sqrt{s_{\rm NN}} = 200$ GeV," *Phys. Rev. Lett.* **98** (2007) 172301, arXiv:nucl-ex/0611018 [nucl-ex].

[56] H. van Hees, V. Greco, and R. Rapp, "Heavy-quark probes of the quark-gluon plasma at RHIC," *Phys. Rev. C* **73** (2006) 034913, arXiv:nucl-th/0508055 [nucl-th].

[57] Z.-w. Lin and D. Molnar, "Quark coalescence and elliptic flow of charm hadrons," *Phys. Rev. C* **68** (2003) 044901, arXiv:nucl-th/0304045 [nucl-th].

[58] V. Greco, C. Ko, and R. Rapp, "Quark coalescence for charmed mesons in ultrarelativistic heavy ion collisions," *Phys. Lett. B* **595** (2004) 202–208, arXiv:nucl-th/0312100 [nucl-th].

[59] **ALICE** Collaboration, B. B. Abelev *et al.*, "Azimuthal anisotropy of D meson production in Pb-Pb collisions at $\sqrt{s_{\rm NN}} = 2.76$ TeV," *Phys. Rev. C* **90** no. 3, (2014) 034904, arXiv:1405.2001 [nucl-ex].

[60] M. He, R. J. Fries, and R. Rapp, "$\mathbf{D_s}$-Meson as Quantitative Probe of Diffusion and Hadronization in Nuclear Collisions," *Phys. Rev. Lett.* **110** no. 11, (2013) 112301, arXiv:1204.4442 [nucl-th].

[61] L. Ravagli and R. Rapp, "Quark Coalescence based on a Transport Equation," *Phys. Lett. B* **655** (2007) 126–131, arXiv:0705.0021 [hep-ph].

[62] M. He, R. J. Fries, and R. Rapp, "Heavy-Quark Diffusion and Hadronization in Quark-Gluon Plasma," *Phys. Rev. C* **86** (2012) 014903, arXiv:1106.6006 [nucl-th].

[63] P. B. Gossiaux, R. Bierkandt, and J. Aichelin, "Tomography of a quark gluon plasma at RHIC and LHC energies," *Phys. Rev.* **C79** (2009) 044906, arXiv:0901.0946 [hep-ph].

[64] S. Cao, G.-Y. Qin, and S. A. Bass, "Heavy-quark dynamics and hadronization in ultrarelativistic heavy-ion collisions: Collisional versus radiative energy loss," *Phys. Rev.* **C88** (2013) 044907, arXiv:1308.0617 [nucl-th].

[65] R. E. Nelson, R. Vogt, and A. D. Frawley, "Narrowing the uncertainty on the total charm cross section and its effect on the J/? cross section," *Phys. Rev.* **C87** no. 1, (2013) 014908, arXiv:1210.4610 [hep-ph].

[66] A. Beraudo, A. De Pace, M. Monteno, M. Nardi, and F. Prino, "Heavy flavors in heavy-ion collisions: quenching, flow and correlations," *Eur. Phys. J.* **C75** no. 3, (2015) 121, arXiv:1410.6082 [hep-ph].

[67] A. Beraudo, A. De Pace, M. Monteno, M. Nardi, and F. Prino, "Heavy-flavour production in high-energy d-Au and p-Pb collisions," *JHEP* **03** (2016) 123, arXiv:1512.05186 [hep-ph].

[68] T. Song and H. Berrehrah, "Hadronization time of heavy quarks in nuclear matter," *Phys. Rev.* **C94** no. 3, (2016) 034901, arXiv:1601.04449 [nucl-th].

[69] **ALICE** Collaboration, J. Adam *et al.*, "Transverse momentum dependence of D-meson production in Pb-Pb collisions at $\sqrt{\rm s_{NN}} = 2.76$ TeV," *JHEP* **03** (2016) 081, arXiv:1509.06888 [nucl-ex].

[70] **CMS** Collaboration, A. M. Sirunyan *et al.*, "Measurement of prompt D^0 meson azimuthal anisotropy in PbPb collisions at $\sqrt{s_{NN}} = 5.02$ TeV," arXiv:1708.03497 [nucl-ex].

[71] **ALICE** Collaboration, J. Adam *et al.*, "Measurement of $\rm D_s^+$ production and nuclear modification factor in Pb-Pb collisions at $\sqrt{\rm s_{NN}} = 2.76$ TeV," *JHEP* **03** (2016) 082, arXiv:1509.07287 [nucl-ex].

[72] **STAR** Collaboration, M. Nasim, "Production of D_s meson in Au+Au collision at $\sqrt{s_{NN}} = 200$ GeV," *PoS* **CPOD2017** (2018) 089, arXiv:1801.04164 [nucl-ex].

[73] M. Schroedter, R. L. Thews, and J. Rafelski, "B_c meson production in nuclear collisions at RHIC," *Phys. Rev.* **C62** (2000) 024905, arXiv:hep-ph/0004041 [hep-ph].

[74] J. Zhao, H. He, and P. Zhuang, "Searching for Ξ_{cc}^+ in Relativistic Heavy Ion Collisions," *Phys. Lett.* **B771** (2017) 349–353, arXiv:1603.04524 [nucl-th].

[75] I. Kuznetsova and J. Rafelski, "Heavy flavor hadrons in statistical hadronization of strangeness-rich QGP," *Eur. Phys. J.* **C51** (2007) 113–133, arXiv:hep-ph/0607203 [hep-ph].

[76] A. Andronic, P. Braun-Munzinger, K. Redlich, and J. Stachel, "Statistical hadronization of heavy quarks in ultra-relativistic nucleus-nucleus collisions," *Nucl. Phys.* **A789** (2007) 334–356, arXiv:nucl-th/0611023 [nucl-th].

[77] R. J. Fries, V. Greco, and P. Sorensen, "Coalescence Models For Hadron Formation From Quark Gluon Plasma," *Ann. Rev. Nucl. Part. Sci.* **58** (2008) 177–205, arXiv:0807.4939 [nucl-th].

[78] V. Greco, C. M. Ko, and P. Levai, "Parton coalescence at RHIC," *Phys. Rev. C* **68** (2003) 034904, arXiv:nucl-th/0305024 [nucl-th].

[79] Y. Oh, C. M. Ko, S. H. Lee, and S. Yasui, "Heavy baryon/meson ratios in relativistic heavy ion collisions," *Phys. Rev.* **C79** (2009) 044905, arXiv:0901.1382 [nucl-th].

[80] T. Sjostrand, S. Mrenna, and P. Z. Skands, "PYTHIA 6.4 Physics and Manual," *JHEP* **05** (2006) 026, arXiv:hep-ph/0603175 [hep-ph].

[81] P. B. Gossiaux and J. Aichelin, "Towards an understanding of the RHIC single electron data," *Phys. Rev.* **C78** (2008) 014904, arXiv:0802.2525 [hep-ph].

[82] A. Peshier, "Turning on the Charm," *Nucl. Phys.* **A888** (2012) 7–22, arXiv:0801.0595 [hep-ph].

[83] F. Scardina, S. K. Das, V. Minissale, S. Plumari, and V. Greco, "Estimating the charm quark diffusion coefficient and thermalization time from D meson spectra at energies available at the BNL Relativistic Heavy Ion Collider and the CERN Large Hadron Collider," *Phys. Rev.* **C96** no. 4, (2017) 044905, arXiv:1707.05452 [nucl-th].

[84] S. Plumari, W. M. Alberico, V. Greco, and C. Ratti, "Recent thermodynamic results from lattice QCD analyzed within a quasi-particle model," *Phys. Rev.* **D84** (2011) 094004, arXiv:1103.5611 [hep-ph].

[85] H. van Hees, M. Mannarelli, V. Greco, and R. Rapp, "Nonperturbative heavy-quark diffusion in the quark-gluon plasma," *Phys. Rev. Lett.* **100** (2008) 192301, arXiv:0709.2884 [hep-ph].

[86] F. Riek and R. Rapp, "Quarkonia and Heavy-Quark Relaxation Times in the Quark-Gluon Plasma," *Phys. Rev. C* **82** (2010) 035201, arXiv:1005.0769 [hep-ph].

[87] S. Y. F. Liu and R. Rapp, "Spectral and Transport Properties of a Non-Perturbative Quark-Gluon Plasma," arXiv:1612.09138 [nucl-th].

[88] H. van Hees and R. Rapp, "Thermalization of heavy quarks in the quark-gluon plasma," *Phys. Rev. C* **71** (2005) 034907, arXiv:nucl-th/0412015 [nucl-th].

[89] P. B. Gossiaux and J. Aichelin, "Energy Loss of Heavy Quarks in a QGP with a Running Coupling Constant Approach," *Nucl. Phys.* **A830** (2009) 203C–206C, arXiv:0907.4329 [hep-ph].

[90] S. Cao and S. A. Bass, "Thermalization of charm quarks in infinite and finite QGP matter," *Phys. Rev.* **C84** (2011) 064902, arXiv:1108.5101 [nucl-th].

[91] S. Cao, G.-Y. Qin, and S. A. Bass, "Model and parameter dependence of heavy quark energy loss in a hot and dense medium," *J. Phys.* **G40** (2013) 085103, arXiv:1205.2396 [nucl-th].

[92] S. Jeon, "Hydrodynamic transport coefficients in relativistic scalar field theory," *Phys. Rev.* **D52** (1995) 3591–3642, arXiv:hep-ph/9409250 [hep-ph].

[93] E. Braaten and M. H. Thoma, "Energy loss of a heavy fermion in a hot plasma," *Phys. Rev.* **D44** (1991) 1298–1310.

[94] E. Braaten and M. H. Thoma, "Energy loss of a heavy quark in the quark - gluon plasma," *Phys. Rev.* **D44** no. 9, (1991) R2625.

[95] G. D. Moore and D. Teaney, "How much do heavy quarks thermalize in a heavy ion collision?," *Phys. Rev. C* **71** (2005) 064904, arXiv:hep-ph/0412346 [hep-ph].

[96] S. Caron-Huot and G. D. Moore, "Heavy quark diffusion in QCD and N=4 SYM at next-to-leading order," *JHEP* **02** (2008) 081, arXiv:0801.2173 [hep-ph].

[97] M. Haas, L. Fister, and J. M. Pawlowski, "Gluon spectral functions and transport coefficients in Yang–Mills theory," *Phys. Rev.* **D90** (2014) 091501, arXiv:1308.4960 [hep-ph].

[98] N. Christiansen, M. Haas, J. M. Pawlowski, and N. Strodthoff, "Transport Coefficients in Yang–Mills Theory and QCD," *Phys. Rev. Lett.* **115** no. 11, (2015) 112002, arXiv:1411.7986 [hep-ph].

[99] J. Casalderrey-Solana and D. Teaney, "Heavy quark diffusion in strongly coupled N=4 Yang-Mills," *Phys. Rev. D* **74** (2006) 085012, arXiv:hep-ph/0605199 [hep-ph].

[100] J. M. Pawlowski and N. Strodthoff, "Real time correlation functions and the functional renormalization group," *Phys. Rev.* **D92** no. 9, (2015) 094009, arXiv:1508.01160 [hep-ph].

[101] S. Strauss, C. S. Fischer, and C. Kellermann, "Analytic structure of the Landau gauge gluon propagator," *Phys.Rev.Lett.* **109** (2012) 252001, arXiv:1208.6239 [hep-ph].

[102] K. Kamikado, N. Strodthoff, L. von Smekal, and J. Wambach, "Real-Time Correlation Functions in the O(N) Model from the Functional Renormalization Group," *Eur.Phys.J.* **C74** (2014) 2806, arXiv:1302.6199 [hep-ph].

[103] R.-A. Tripolt, N. Strodthoff, L. von Smekal, and J. Wambach, "Spectral Functions for the Quark-Meson Model Phase Diagram from the Functional Renormalization Group," *Phys. Rev.* **D89** no. 3, (2014) 034010, arXiv:1311.0630 [hep-ph].

[104] T. Yokota, T. Kunihiro, and K. Morita, "Functional renormalization group analysis of the soft mode at the QCD critical point," *PTEP* **2016** no. 7, (2016) 073D01, arXiv:1603.02147 [hep-ph].

[105] A. K. Cyrol, M. Mitter, J. M. Pawlowski, and N. Strodthoff, "Non-perturbative finite-temperature Yang-Mills theory," arXiv:1708.03482 [hep-ph].

[106] P. Petreczky and D. Teaney, "Heavy quark diffusion from the lattice," *Phys. Rev. D* **73** (2006) 014508, arXiv:hep-ph/0507318 [hep-ph].

[107] P. Petreczky, "On temperature dependence of quarkonium correlators," *Eur. Phys. J. C* **62** (2009) 85–93, arXiv:0810.0258 [hep-lat].

[108] S. Caron-Huot, M. Laine, and G. D. Moore, "A Way to estimate the heavy quark thermalization rate from the lattice," *JHEP* **04** (2009) 053, arXiv:0901.1195 [hep-lat].

[109] Y. Burnier, M. Laine, J. Langelage, and L. Mether, "Colour-electric spectral function at next-to-leading order," *JHEP* **08** (2010) 094, arXiv:1006.0867 [hep-ph].

[110] D. Banerjee, S. Datta, R. Gavai, and P. Majumdar, "Heavy quark momentum diffusion coefficient from Lattice QCD," *Phys. Rev. D* **85** (2012) 014510, arXiv:1109.5738 [hep-lat].

[111] A. Francis, O. Kaczmarek, M. Laine, T. Neuhaus, and H. Ohno, "Nonperturbative estimate of the heavy quark momentum diffusion coefficient," *Phys. Rev. D* **92** no. 11, (2015) 116003, arXiv:1508.04543 [hep-lat].

[112] H. Ding, A. Francis, O. Kaczmarek, F. Karsch, H. Satz, *et al.*, "Charmonium properties in hot quenched lattice QCD," *Phys. Rev. D* **86** (2012) 014509, arXiv:1204.4945 [hep-lat].

[113] M. Kitazawa, T. Iritani, M. Asakawa, and T. Hatsuda, "Correlations of Energy-Momentum Tensor via Gradient Flow in SU(3) Yang-Mills Theory at Finite Temperature," arXiv:1708.01415 [hep-lat].

[114] M. Kitazawa, T. Iritani, M. Asakawa, T. Hatsuda, and H. Suzuki, "Equation of State for SU(3) Gauge Theory via the Energy-Momentum Tensor under Gradient Flow," *Phys. Rev.* **D94** no. 11, (2016) 114512, arXiv:1610.07810 [hep-lat].

[115] S. Datta, S. Gupta, and A. Lytle, "Using Wilson flow to study the SU(3) deconfinement transition," *Phys. Rev.* **D94** no. 9, (2016) 094502, arXiv:1512.04892 [hep-lat].

[116] P. Petreczky and H. P. Schadler, "Renormalization of the Polyakov loop with gradient flow," *Phys. Rev.* **D92** no. 9, (2015) 094517, arXiv:1509.07874 [hep-lat].

[117] A. Bazavov, H. T. Ding, P. Hegde, O. Kaczmarek, F. Karsch, *et al.*, "The melting and abundance of open charm hadrons," *Phys. Lett. B* **737** (2014) 210, arXiv:1404.4043 [hep-lat].

[118] **HotQCD** Collaboration, A. Bazavov *et al.*, "Fluctuations and Correlations of net baryon number, electric charge, and strangeness: A comparison of lattice QCD results with the hadron resonance gas model," *Phys. Rev. D* **86** (2012) 034509, arXiv:1203.0784 [hep-lat].

[119] S. Borsanyi, Z. Fodor, S. D. Katz, S. Krieg, C. Ratti, *et al.*, "Fluctuations of conserved charges at finite temperature from lattice QCD," *JHEP* **1201** (2012) 138, arXiv:1112.4416 [hep-lat].

[120] R. Bellwied, S. Borsanyi, Z. Fodor, S. D. Katz, A. Pasztor, C. Ratti, and K. K. Szabo, "Fluctuations and correlations in high temperature QCD," *Phys. Rev. D* **92** no. 11, (2015) 114505, arXiv:1507.04627 [hep-lat].

[121] H. T. Ding, S. Mukherjee, H. Ohno, P. Petreczky, and H. P. Schadler, "Diagonal and off-diagonal quark number susceptibilities at high temperatures," *Phys. Rev. D* **92** no. 7, (2015) 074043, arXiv:1507.06637 [hep-lat].

[122] A. Bazavov, H. T. Ding, P. Hegde, F. Karsch, C. Miao, S. Mukherjee, P. Petreczky, C. Schmidt, and A. Velytsky, "Quark number susceptibilities at high temperatures," *Phys. Rev. D* **88** no. 9, (2013) 094021, arXiv:1309.2317 [hep-lat].

[123] S. Mukherjee, P. Petreczky, and S. Sharma, "Charm degrees of freedom in the quark gluon plasma," *Phys. Rev. D* **93** no. 1, (2016) 014502, arXiv:1509.08887 [hep-lat].

[124] **RBC-Bielefeld** Collaboration, P. Petreczky, P. Hegde, and A. Velytsky, "Quark number fluctuations at high temperatures," *PoS* **LAT2009** (2009) 159, arXiv:0911.0196 [hep-lat].

[125] A. Mocsy, P. Petreczky, and M. Strickland, "Quarkonia in the quark gluon plasma," *Int. J. Mod. Phys. A* **28** (2013) 1340012, arXiv:1302.2180 [hep-ph].

[126] A. Mocsy and P. Petreczky, "Can quarkonia survive deconfinement?," *Phys. Rev. D* **77** (2008) 014501, arXiv:0705.2559 [hep-ph].

[127] A. Bazavov, F. Karsch, Y. Maezawa, S. Mukherjee, and P. Petreczky, "In-medium modifications of open and hidden strange-charm mesons from spatial correlation functions," *Phys. Rev. D* **91** no. 5, (2015) 054503, arXiv:1411.3018 [hep-lat].

[128] A. Kelly and J.-I. Skullerud, "Thermal D mesons from anisotropic lattice QCD," arXiv:1701.09005 [hep-lat]. [EPJ Web Conf.137,07025(2017)].

[129] G. Ferini, M. Colonna, M. Di Toro, and V. Greco, "Scalings of Elliptic Flow for a Fluid at Finite Shear Viscosity," *Phys. Lett.* **B670** (2009) 325–329, arXiv:0805.4814 [nucl-th].

[130] M. Ruggieri, F. Scardina, S. Plumari, and V. Greco, "Thermalization, Isotropization and Elliptic Flow from Nonequilibrium Initial Conditions with a Saturation Scale," *Phys. Rev.* **C89** no. 5, (2014) 054914, arXiv:1312.6060 [nucl-th].

[131] Z. Xu and C. Greiner, "Thermalization of gluons in ultrarelativistic heavy ion collisions by including three-body interactions in a parton cascade," *Phys. Rev.* **C71** (2005) 064901, arXiv:hep-ph/0406278 [hep-ph].

[132] L. Kadanoff and G. Baym, "Quantum Statistical Mechanics," *Benjamin, Inc., New York* (1962) .

[133] P. Danielewicz, "Quantum Theory of Nonequilibrium Processes. 1.," *Annals Phys.* **152** (1984) 239–304.

[134] H. Berrehrah, P.-B. Gossiaux, J. Aichelin, W. Cassing, and E. Bratkovskaya, "Dynamical collisional energy loss and transport properties of on- and off-shell heavy quarks in vacuum and in the Quark Gluon Plasma," *Phys. Rev.* **C90** no. 6, (2014) 064906, arXiv:1405.3243 [hep-ph].

[135] S. K. Das, F. Scardina, S. Plumari, and V. Greco, "Heavy-flavor in-medium momentum evolution: Langevin versus Boltzmann approach," *Phys. Rev.* **C90** (2014) 044901, arXiv:1312.6857 [nucl-th].

[136] J. I. B. F. Scardina, S. K. Das and V. Greco, "in preparation,".

[137] B. G. Zakharov, "On the energy loss of high-energy quarks in a finite size quark - gluon plasma," *JETP Lett.* **73** (2001) 49–52, arXiv:hep-ph/0012360 [hep-ph]. [Pisma Zh. Eksp. Teor. Fiz.73,55(2001)].

[138] R. Baier, Y. L. Dokshitzer, A. H. Mueller, S. Peigne, and D. Schiff, "Radiative energy loss and p(T) broadening of high-energy partons in nuclei," *Nucl. Phys.* **B484** (1997) 265–282, arXiv:hep-ph/9608322 [hep-ph].

[139] M. Gyulassy, P. Levai, and I. Vitev, "Reaction operator approach to nonAbelian energy loss," *Nucl. Phys.* **B594** (2001) 371–419, arXiv:nucl-th/0006010 [nucl-th].

[140] X.-N. Wang and X.-f. Guo, "Multiple parton scattering in nuclei: Parton energy loss," *Nucl. Phys.* **A696** (2001) 788–832, arXiv:hep-ph/0102230 [hep-ph].

[141] P. B. Arnold, G. D. Moore, and L. G. Yaffe, "Photon and gluon emission in relativistic plasmas," *JHEP* **06** (2002) 030, arXiv:hep-ph/0204343 [hep-ph].

[142] M. Gyulassy, P. Levai, and I. Vitev, "Reaction operator approach to multiple elastic scatterings," *Phys. Rev.* **D66** (2002) 014005, arXiv:nucl-th/0201078 [nucl-th].

[143] **JET** Collaboration, K. M. Burke *et al.*, "Extracting the jet transport coefficient from jet quenching in high-energy heavy-ion collisions," *Phys. Rev.* **C90** no. 1, (2014) 014909, arXiv:1312.5003 [nucl-th].

[144] R. Field, "Applications of perturbative qcd," *Perseus Books, Cambridge, Massachussetts* (1995) .

[145] S. Peigne and A. Peshier, "Collisional energy loss of a fast heavy quark in a quark-gluon plasma," *Phys. Rev.* **D77** (2008) 114017, arXiv:0802.4364 [hep-ph].

[146] M. Djordjevic, "Theoretical formalism of radiative jet energy loss in a finite size dynamical QCD medium," *Phys. Rev.* **C80** (2009) 064909, arXiv:0903.4591 [nucl-th].

[147] M. Djordjevic and U. W. Heinz, "Radiative energy loss in a finite dynamical QCD medium," *Phys. Rev. Lett.* **101** (2008) 022302, arXiv:0802.1230 [nucl-th].

[148] M. Djordjevic, "Collisional energy loss in a finite size QCD matter," *Phys. Rev.* **C74** (2006) 064907, arXiv:nucl-th/0603066 [nucl-th].

[149] M. Djordjevic and M. Djordjevic, "Generalization of radiative jet energy loss to non-zero magnetic mass," *Phys. Lett.* **B709** (2012) 229–233, arXiv:1105.4359 [nucl-th].

[150] M. Djordjevic and M. Djordjevic, "LHC jet suppression of light and heavy flavor observables," *Phys. Lett.* **B734** (2014) 286–289, arXiv:1307.4098 [hep-ph].

[151] Z.-B. Kang, I. Vitev, and H. Xing, "Nuclear modification of high transverse momentum particle production in p+A collisions at RHIC and LHC," *Phys. Lett.* **B718** (2012) 482–487, arXiv:1209.6030 [hep-ph].

[152] S. Wicks, W. Horowitz, M. Djordjevic, and M. Gyulassy, "Elastic, inelastic, and path length fluctuations in jet tomography," *Nucl. Phys.* **A784** (2007) 426–442, arXiv:nucl-th/0512076 [nucl-th].

[153] D. de Florian, R. Sassot, and M. Stratmann, "Global analysis of fragmentation functions for pions and kaons and their uncertainties," *Phys. Rev.* **D75** (2007) 114010, arXiv:hep-ph/0703242 [HEP-PH].

[154] V. G. Kartvelishvili, A. K. Likhoded, and V. A. Petrov, "On the Fragmentation Functions of Heavy Quarks Into Hadrons," *Phys. Lett.* **B78** (1978) 615–617.

[155] M. Djordjevic, "Heavy quark energy loss: Collisional vs radiative," *Nucl. Phys.* **A783** (2007) 197–204.

[156] J.-P. Blaizot, F. Dominguez, E. Iancu, and Y. Mehtar-Tani, "Medium-induced gluon branching," *JHEP* **01** (2013) 143, arXiv:1209.4585 [hep-ph].

[157] M. Fickinger, G. Ovanesyan, and I. Vitev, "Angular distributions of higher order splitting functions in the vacuum and in dense QCD matter," *JHEP* **07** (2013) 059, arXiv:1304.3497 [hep-ph].

[158] M. Djordjevic and M. Gyulassy, "The Ter-Mikayelian effect on QCD radiative energy loss," *Phys. Rev.* **C68** (2003) 034914, arXiv:nucl-th/0305062 [nucl-th].

[159] **WHOT-QCD** Collaboration, Y. Maezawa, S. Aoki, S. Ejiri, T. Hatsuda, N. Ishii, K. Kanaya, N. Ukita, and T. Umeda, "Electric and Magnetic Screening Masses at Finite Temperature from Generalized Polyakov-Line Correlations in Two-flavor Lattice QCD," *Phys. Rev.* **D81** (2010) 091501, arXiv:1003.1361 [hep-lat].

[160] A. Nakamura, T. Saito, and S. Sakai, "Lattice calculation of gluon screening masses," *Phys. Rev.* **D69** (2004) 014506, arXiv:hep-lat/0311024 [hep-lat].

[161] A. Peshier, "Running coupling and screening in the (s)QGP," arXiv:hep-ph/0601119 [hep-ph].

[162] **ALICE** Collaboration, A. Dainese, "Perspectives for the study of charm in-medium quenching at the LHC with ALICE," *Eur. Phys. J.* **C33** (2004) 495–503, arXiv:nucl-ex/0312005 [nucl-ex].

[163] A. Idilbi and A. Majumder, "Extending Soft-Collinear-Effective-Theory to describe hard jets in dense QCD media," *Phys. Rev. D* **80** (2009) 054022, arXiv:0808.1087 [hep-ph].

[164] G. Ovanesyan and I. Vitev, "An effective theory for jet propagation in dense QCD matter: jet broadening and medium-induced bremsstrahlung," *JHEP* **06** (2011) 080, arXiv:1103.1074 [hep-ph].

[165] G. Ovanesyan and I. Vitev, "Medium-induced parton splitting kernels from Soft Collinear Effective Theory with Glauber gluons," *Phys. Lett. B* **706** (2012) 371–378, arXiv:1109.5619 [hep-ph].

[166] G. Ovanesyan, F. Ringer, and I. Vitev, "Initial-state splitting kernels in cold nuclear matter," *Phys. Lett. B* **760** (2016) 706–712, arXiv:1512.00006 [hep-ph].

[167] Z.-B. Kang, R. Lashof-Regas, G. Ovanesyan, P. Saad, and I. Vitev, "Jet quenching phenomenology from soft-collinear effective theory with Glauber gluons," *Phys. Rev. Lett.* **114** no. 9, (2015) 092002, arXiv:1405.2612 [hep-ph].

[168] Y.-T. Chien and I. Vitev, "Towards the understanding of jet shapes and cross sections in heavy ion collisions using soft-collinear effective theory," *JHEP* **05** (2016) 023, arXiv:1509.07257 [hep-ph].

[169] Y.-T. Chien and I. Vitev, "Probing the hardest branching of jets in heavy ion collisions," arXiv:1608.07283 [hep-ph].

[170] A. K. Leibovich, Z. Ligeti, and M. B. Wise, "Comment on quark masses in SCET," *Phys. Lett. B* **564** (2003) 231–234, arXiv:hep-ph/0303099 [hep-ph].

[171] Z.-B. Kang, F. Ringer, and I. Vitev, "Effective field theory approach to open heavy flavor production in heavy-ion collisions," *JHEP* **03** (2017) 146, arXiv:1610.02043 [hep-ph].

[172] M. Djordjevic and M. Gyulassy, "Heavy quark radiative energy loss in QCD matter," *Nucl. Phys.* **A733** (2004) 265–298, arXiv:nucl-th/0310076 [nucl-th].

[173] T. Kneesch, B. A. Kniehl, G. Kramer, and I. Schienbein, "Charmed-meson fragmentation functions with finite-mass corrections," *Nucl. Phys. B* **799** (2008) 34–59, arXiv:0712.0481 [hep-ph].

[174] B. A. Kniehl, G. Kramer, I. Schienbein, and H. Spiesberger, "Open charm hadroproduction and the charm content of the proton," *Phys. Rev. D* **79** (2009) 094009, arXiv:0901.4130 [hep-ph].

[175] B. A. Kniehl, G. Kramer, I. Schienbein, and H. Spiesberger, "Inclusive photoproduction of D*+- mesons at next-to-leading order in the General-Mass Variable-Flavor-Number Scheme," *Eur. Phys. J. C* **62** (2009) 365–374, arXiv:0902.3166 [hep-ph].

[176] B. A. Kniehl, G. Kramer, I. Schienbein, and H. Spiesberger, "Inclusive Charmed-Meson Production at the CERN LHC," *Eur. Phys. J. C* **72** (2012) 2082, arXiv:1202.0439 [hep-ph].

[177] J. C. Collins and W.-K. Tung, "Calculating Heavy Quark Distributions," *Nucl. Phys. B* **278** (1986) 934.

[178] T. P. Stavreva and J. F. Owens, "Direct Photon Production in Association With A Heavy Quark At Hadron Colliders," *Phys. Rev. D* **79** (2009) 054017, arXiv:0901.3791 [hep-ph].

[179] F. Aversa, P. Chiappetta, M. Greco, and J. P. Guillet, "QCD Corrections to Parton-Parton Scattering Processes," *Nucl. Phys. B* **327** (1989) 105.

[180] B. Jager, A. Schafer, M. Stratmann, and W. Vogelsang, "Next-to-leading order QCD corrections to high p(T) pion production in longitudinally polarized pp collisions," *Phys. Rev. D* **67** (2003) 054005, arXiv:hep-ph/0211007 [hep-ph].

[181] D. P. Anderle, T. Kaufmann, M. Stratmann, F. Ringer, and I. Vitev, "Using hadron-in-jet data in a global analysis of D^* fragmentation functions," *Phys. Rev.* **D96** no. 3, (2017) 034028, arXiv:1706.09857 [hep-ph].

[182] A. Adil and I. Vitev, "Collisional dissociation of heavy mesons in dense QCD matter," *Phys. Lett. B* **649** (2007) 139–146, arXiv:hep-ph/0611109 [hep-ph].

[183] R. Sharma, I. Vitev, and B.-W. Zhang, "Light-cone wave function approach to open heavy flavor dynamics in QCD matter," *Phys. Rev. C* **80** (2009) 054902, arXiv:0904.0032 [hep-ph].

[184] R. Sharma and I. Vitev, "High transverse momentum quarkonium production and dissociation in heavy ion collisions," *Phys. Rev. C* **87** no. 4, (2013) 044905, arXiv:1203.0329 [hep-ph].

[185] Z.-B. Kang, F. Ringer, and I. Vitev, "Inclusive production of small radius jets in heavy-ion collisions," *Phys. Lett.* **B769** (2017) 242–248, arXiv:1701.05839 [hep-ph].

[186] I. Vitev and M. Gyulassy, "High p_T tomography of d + Au and Au+Au at SPS, RHIC, and LHC," *Phys. Rev. Lett.* **89** (2002) 252301, arXiv:hep-ph/0209161 [hep-ph].

[187] Y.-T. Chien, A. Emerman, Z.-B. Kang, G. Ovanesyan, and I. Vitev, "Jet Quenching from QCD Evolution," *Phys. Rev.* **D93** no. 7, (2016) 074030, arXiv:1509.02936 [hep-ph].

[188] S. Cao, T. Luo, G.-Y. Qin, and X.-N. Wang, "Linearized Boltzmann transport model for jet propagation in the quark-gluon plasma: Heavy quark evolution," *Phys. Rev.* **C94** no. 1, (2016) 014909, arXiv:1605.06447 [nucl-th].

[189] S. Cao, T. Luo, G.-Y. Qin, and X.-N. Wang, "Heavy and light flavor jet quenching at RHIC and LHC energies," *Phys. Lett.* **B777** (2018) 255–259, arXiv:1703.00822 [nucl-th].

[190] J. Aichelin, P. B. Gossiaux, and T. Gousset, "Gluon radiation by heavy quarks at intermediate energies," *Phys. Rev.* **D89** no. 7, (2014) 074018, arXiv:1307.5270 [hep-ph].

[191] P. B. Gossiaux, "Recent results on heavy quark quenching in ultrarelativistic heavy ion collisions: the impact of coherent gluon radiation," *Nucl. Phys.* **A910-911** (2013) 301–305, arXiv:1209.0844 [hep-ph].

[192] S. Shi, J. Xu, J. Liao, and M. Gyulassy, "A Unified Description for Comprehensive Sets of Jet Energy Loss Observables with CUJET3," *Nucl. Phys.* **A967** (2017) 648–651, arXiv:1704.04577 [hep-ph].

[193] **ALICE** Collaboration, B. Abelev *et al.*, "Upgrade of the ALICE Experiment: Letter Of Intent," *J. Phys.* **G41** (2014) 087001.

[194] **CMS** Collaboration, "Projected Heavy Ion Physics Performance at the High Luminosity LHC Era with the CMS Detector," https://cds.cern.ch/record/2291105/files/FTR-17-002-pas.pdf.

[195] M. Laine, "Heavy flavour kinetic equilibration in the confined phase," *JHEP* **04** (2011) 124, arXiv:1103.0372 [hep-ph].

[196] M. He, R. J. Fries, and R. Rapp, "Thermal Relaxation of Charm in Hadronic Matter," *Phys. Lett.* **B701** (2011) 445–450, arXiv:1103.6279 [nucl-th].

[197] S. Ghosh, S. K. Das, S. Sarkar, and J.-e. Alam, "Dragging D mesons by hot hadrons," *Phys. Rev.* **D84** (2011) 011503, arXiv:1104.0163 [nucl-th].

[198] L. M. Abreu, D. Cabrera, F. J. Llanes-Estrada, and J. M. Torres-Rincon, "Charm diffusion in a pion gas implementing unitarity, chiral and heavy quark symmetries," *Annals Phys.* **326** (2011) 2737–2772, arXiv:1104.3815 [hep-ph].

[199] J. M. Torres-Rincon, L. Tolos, and O. Romanets, "Open bottom states and the $\bar{B}$-meson propagation in hadronic matter," *Phys. Rev.* **D89** no. 7, (2014) 074042, arXiv:1403.1371 [hep-ph].

[200] V. Ozvenchuk, J. M. Torres-Rincon, P. B. Gossiaux, L. Tolos, and J. Aichelin, "D-meson propagation in hadronic matter and consequences for heavy-flavor observables in ultrarelativistic heavy-ion collisions," *Phys. Rev.* **C90** (2014) 054909, arXiv:1408.4938 [hep-ph].

[201] T. Lang, H. van Hees, J. Steinheimer, and M. Bleicher, "Charm quark transport in Pb+Pb reactions at $\sqrt{s_{NN}} = 2.76$ TeV from a $(3+1)$ dimensional hybrid approach," arXiv:1208.1643 [hep-ph].

[202] T. Lang, H. van Hees, J. Steinheimer, G. Inghirami, and M. Bleicher, "Heavy quark transport in heavy ion collisions at energies available at the BNL Relativistic Heavy Ion Collider and at the CERN Large Hadron Collider within the UrQMD hybrid model," *Phys. Rev.* **C93** no. 1, (2016) 014901, arXiv:1211.6912 [hep-ph].